LABEL FREE AND MULTIPLEXED IMMUNOSENSOR CHIPS FOR DETECTION OF MACROMOLECULAR AND CELLULAR BIOMARKERS

A Dissertation

Presented to

The Graduate Faculty of The University of Akron

In Partial Fulfillment

of the Requirements for the Degree

Doctor of Philosophy

Yu Han

December, 2015

LABEL FREE AND MULTIPLEXED IMMUNOSENSOR CHIPS FOR DETECTION OF MACROMOLECULAR AND CELLULAR BIOMARKERS

Yu Han

Dissertation

Approved:	Accepted:
_____	_____
Advisor Dr. Jiang Zhe	Department Chair Dr. Sergio Felicelli
_____	_____
Committee Member Dr. Gang Cheng	Dean of the College Dr. Mario R. Garzia
_____	_____
Committee Member Dr. Qin Liu	Dean of the Graduate School Dr. Chand K. Midha
_____	_____
Committee Member Dr. Francis Loth	Date
_____	
Committee Member Dr. Chang Ye	

ABSTRACT

Biomarker detection represents an important task for many scientific fields such as disease diagnosis, biodefense, environmental monitoring and biological research. In this research, micro resistive pulse immunoaggregation sensors were studied to quantitatively detect macromolecular and cellular biomarker concentrations. First, to prove the concept of the immunoaggregation assay and resistive pulse sensing, goat anti-rabbit IgG, used as a model biomarker, was detected by the micro resistive pulse immunoaggregation sensor. A detection range from 16.0 to 160 ng/mL was achieved. The human ferritin in 10% fetal bovine serum was then detected to prove the device's performance in a complex media. A detection range from 0.104 to 208 ng/mL was achieved. In addition, the studies showed that the detection range can be shifted to lower and higher concentrations by decreasing and increasing MP concentrations, respectively.

Second, the multiplexed immunoaggregation assay was also studied in this research to achieve multiple biomarker detection in a single test. A mixture consisting of multiple types of MPs functionalized by different antibody with different sizes and magnetic properties was used for testing the multiplexed assay. 2.00 μm non-magnetic MPs coated with rabbit anti-mouse IgG antibody and 2.80 μm magnetic MPs coated with goat anti-human ferritin antibody were used to detect the concentration of mouse anti-rabbit IgG and

human ferritin, respectively. Detection ranges from 5.20 to 208 ng/mL and 3.10 to 51.2 × 10^3 ng/mL were achieved for human ferritin and mouse anti-rabbit IgG detection.

Next, a two-stage resistive pulse sensor was invented to detect target cells in a mixed cell population. *S. cerevisiae* and *Chlorella* were used as target cells and control cells, respectively. The specific capture efficiency of *S. cerevisiae* was greater than 94.8%, while the nonspecific capture efficiency was less than 3.4%. *S. cerevisiae* ratio measurements in a mixture with *Chlorella* showed that for *S. cerevisiae* to *Chlorella* ratios ranging from 1.0 to 2.0, the measurement errors were less than 7%, while the errors were 20% to 32% for lower ratios, ranging from 0.1 to 0.5, caused by nonspecific attachment.

The testing results demonstrated that the immunoaggregation biomarker sensor and MP cellular sensor enable reliable detection of target macromolecular and cellular biomarkers in samples at very low concentrations, without the fluorescence and enzyme labeling of biomarker. These innovative biosensors will lead to a fast and cost-effective bioassay instrument for disease diagnosis, environmental monitoring and homeland security.

DEDICATION

This dissertation is dedicated to my parents

Tianyun Fu and Zhaoqi Han

who made all this possible,

for their endless love, support, encouragement and patience.

ACKNOWLEDGEMENTS

It would not have been possible to write this doctoral dissertation without the help and support of the kind people around me, to only some of whom it is possible to give particular mention here. First, this dissertation would not have been possible without the help, support and patience of my advisor and mentor Dr. Jiang Zhe. His good advice and support has been invaluable on both an academic and a personal level, for which I am extremely grateful.

I would also like to thank Dr. Gang Cheng for his continuing advice with my research. In addition, I must extend my gratitude towards my committee members Dr. Gang Cheng, Dr. Qin Liu, Dr. Francis Loth and Dr. Chang Ye.

The research journey at The University of Akron would not be possible without the support of all my colleagues and friends in the lab: Ms. Haiyan Wu, Dr. Li Du, Mr. Zhuochen Wang, Mr. Xiaoliang Zhu, Mr. Fan Liu, Dr. Ashish V. Jagtiani, Dr. Liangliang Fan, and Mr. Mingxian Ma. I would also like to extend my gratitude to the staff in the Mechanical Engineering: Mrs Christina Christian, Mrs Stacy Meier, Ms. Cortney Castleman and Mr. Cliff Bailey for their assistance and technical support since the start of my graduate work in The University of Akron.

I would also like thank my friends that I made over the years at The University of Akron, Li Du, Haiyan Wu, Zhuochen Wang, YanFeng Lu, Feixiang Huang, Dongrui Yang,

Zipeng Han, Todd Schreiner and whose friendship over the years have made this possible. I must also thank Dr. Jiang Zhe, Xiaoliang Zhu and Fan Liu who took time out from his busy schedule to help me proof read my dissertation.

Finally, I would like to thank my parents for their endless love and support at all times.

TABLE OF CONTENTS

Page

LIST OF TABLES

LIST OF FIGURES

CHAPTER I

INTRODUCTION

1.1 Introduction

Quantitative detection of biomarkers, as indicators of biological states, is an important task in disease diagnosis [2] [3], biodefense [4], environmental monitoring [5] and biological research [6] [7] [8] [9]. In medicine, macromolecular and cellular biomarkers are often isolated from serum, urine or other fluids [10] [11] [12]. Quantitative detection of these biomarkers is a powerful tool in the early detection/diagnosis stages of disease, in the monitoring of the effectiveness of treatment and the discovery of new drugs, etc. [13]. On the other hand, due to the complexity of human biology and the heterogeneity of diseases, a single biomarker is insufficient to provide enough information for disease diagnosis [14] [15] [16]. Thus, a device for disease related biomarker detection should meet two basic requirements: quantitative detection with high sensitivity and multiplex capability. A rapid and portable detection with minimum steps is also essential for on-site disease diagnosis.

1.2 Motivation

An immunoassay is the most commonly used technology that enables highly sensitive detection of macromolecular and cellular biomarkers [17] [18]. Compared with conventional immunoassay, recent studies show that immunosensor chips are promising platforms for immunoassays with many advantages including low sample consumption, high sensitivity, rapid, automatic and capable of multiplexed detection [19] [20] [21] [22].

The recent development in label-free and fully integrated immunosensor chips further improves their performance and extends their application to on-site disease diagnosis [23] [24]. A label-free immunosensor chip avoids labeling of detection antibody, which not only reduces the assay steps, but also eliminates the loss of binding affinity due to the labeling process [25] [26]. Microparticles, as micro carriers, are a promising platform for immunoassays due to their large surface to volume ratio, which increases the interaction between the target molecule and capture antibody. Recently, several approaches to label-free immunoassays based on the immunoaggregation of MPs have been developed to quantitatively detect macromolecule concentrations. However, these methods rely on bulky and expensive off-chip instruments including light/fluorescence microscopy, flow cytometry and light scattering [27] [28][29][95], making them impractical for on-site diagnosis. Thus, the first objective of this project is to develop a label-free, compact, low cost immunoaggregation assay based on a micro resistive pulse sensor for quantitative biomarker detection.

Due to the complexity of human biology and the heterogeneity of diseases, single biomarker detection is insufficient to provide enough information for disease diagnosis [14]

[15] [16]. Based on the solid support for capture antibody immobilization, two strategies for multiplexed detection are planer arrays and suspension arrays (immunoassays based on MPs) [30]. The recovery of the antibody activities in a planer array for reuse is difficult [31]. The MP encoding methods can be further categorized into spectrometric, electronic, graphical or physical methods [30]. However, most of these encoding methods are dependent on optical detection [32] [33] [30] [34] [35]. Although electric encoding, such as radio frequency (RF) encoding, only requires an electronic reader [36], the large size of RF chips (~8 mm × 1 mm × 1 mm) limits their application in immunosensor chips. Thus, the second objective of this project is to study the multiplexed methods for micro resistive pulse immunoaggregation sensors based on the physical encoding approach, such as the size and magnetic properties of the MPs.

Cellular biomarkers, such as pathogen cells and cancer cells, represent another important class of biomarkers for many applications such as disease diagnosis, food industry, environmental monitoring, biodefense and biological research. Two major strategies for cellular biomarker detection are polymerase chain reaction (PCR) and immunoassay [37]. Although a PCR-based sensor chip has a high sensitivity, the PCR-based biosensor chip is complicated because of the need for temperature control for thermocycling and on-chip cell lysis [38] [39]. For an immunosensor chip, cellular biomarker detection is based on the specific binding between receptors on the cell surface and antibody immobilized on a solid surface [38] [9]. Thus the surface immobilization of antibody is crucial for the sensitivity of an immunosensor [9]. However maintaining the function of surface immobilization is difficult due to the limited lifetime of the antibody, and it is also a challenge to reproduce the surface antibody coverage for reuse of the sensing

surface [37]. Microparticles are an emerging technique for surface modification of immunosensor chips [31]. The use of functionalized MPs can significantly reduce the difficultly in the surface modification of immunosensor chips. Thus, the third objective of this project is to develop a new two-stage micro resistive pulse sensor with a surface coating of antibody functionalized MPs for pathogen cell detection. A detailed review of immunosensor chips is presented in Chapter II.

1.3 Research objectives

The main research objective of this project is to develop label-free, rapid, portable and multiplexed micro resistive pulse sensors (RPSs) to quantitatively detect macromolecule and cellular biomarkers. Specific objectives are described in detail in the following sections.

Part I Study of the micro resistive pulse sensor (RPS) chip and quantitative immunoaggregation assay

- Design and fabricate the RPS chip using soft lithography micromachining.
- Calibrate the RPS chip to ensure its sizing and counting performance.
- Study the performances of the RPS chip and the immunoaggregation assay using goat anti-rabbit IgG as a model biomarker.
- Study the performances of the RPS chip and the immunoaggregation assay for human ferritin detection in a complex media.

- Demonstrate the tunable detection range of the RPS chip using various MP concentrations.

Part II Study of the multiplexed RPS immunoaggregation chips

- Study the performance of the immunoaggregation assay using 2.00 μm antibody functionalized MPs.
- Design and fabricate the two-stage RPS chips.
- Demonstrate the feasibility of the multiplexed immunoaggregation assay for human ferritin and mouse anti-rabbit IgG measurement.

Part III Study of the two-stage RPS chips for pathogen cell detection

- Design and fabricate the two-stage RPS chips.
- Study the performance of the two-stage RPS in terms of specific capture efficiency and nonspecific capture efficiency.
- Demonstrate the feasibility of pathogen cell detection in a mixed population with control cells.

1.4 Summary

The rest of this dissertation is arranged as follows: in Chapter II, the background and a literature review on recent developments in immunosensor chips are presented. Next, in Chapter III, to prove the concept of the immunoaggregation assay in a micro resistive pulse sensor, a model biomarker detection is studied. In Chapter IV, the micro resistive

pulse sensor and immunoaggregation assay are applied to human ferritin detection in a complex media. Various MP concentrations are also applied to human ferritin detection to achieve a tunable detection range. In Chapter V, a two-stage RPS and immunoaggregation assay using a mixture of MPs for multiplexed detection is presented. In Chapter VI, a two-stage RPS coated with antibody functionalized MPs for cellular biomarker (pathogen cell) detection are presented. Finally, the conclusions and future thoughts are presented in Chapter VII.

CHAPTER II

BACKGROUND AND LITERATURE REVIEW

2.1 Immunosensors for macromolecule detection

Immunoassays are the most widely used tools for macromolecule detection, based on the recognition of specific binding between target molecule and capture antibody [23]. Recent studies on immunosensor chips as promising platforms for immunoassays show that immunosensor chips have many advantages compared with the conventional Enzyme-Linked Immunosorbent Assay (ELISA) including low sample consumption, high sensitivity, fast, automatic and capable of multiplexed detection [40] [22]. On-site diagnostic applications also require the development of label-free, fully integrated, low-cost and multiplexed immunosensors with minimum assay steps [23] [24]. In this chapter, immunosensors for macromolecule detection are reviewed in respect of the following aspects: immunosensor chips for macromolecule detection, multiplexed immunosensor chips and immunosensor chips for cellular biomarker detection.

2.1.1 Enzyme immunoassay/Enzyme-linked immunosorbent assay

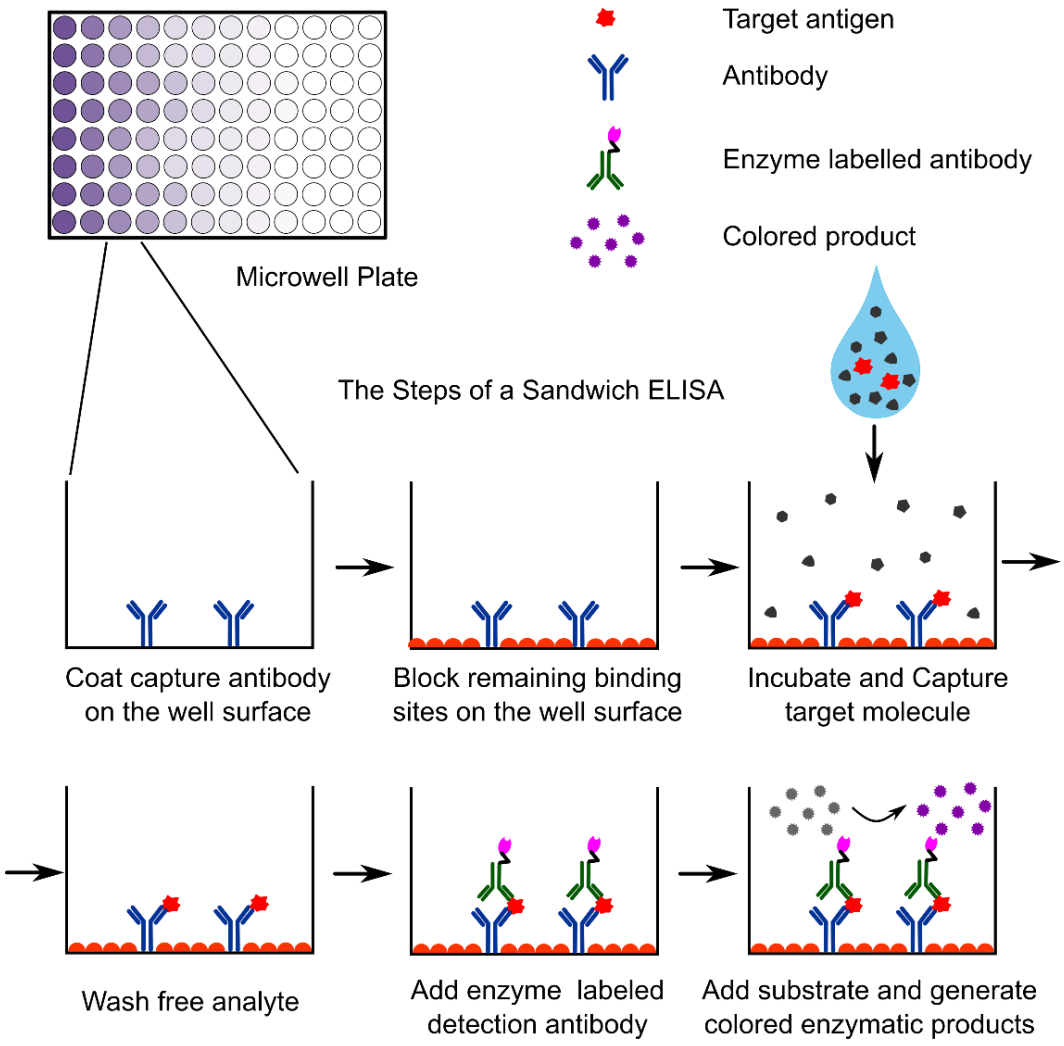

Figure 2.1 A sandwich ELISA typically requires six steps and runs on a microtiter plate

The most commonly used technique to detect macromolecule at present is the Enzyme immunoassay/Enzyme-linked immunosorbent assay (EIA/ELISA) [17] [18]. Performing an ELISA involves labeling the enzyme on target macromolecule and determining the macromolecule concentration by monitoring the generation of colored enzymatic products. Before the invention of ELISA, the immunoassay was conducted

using radioimmunoassay (RIA) [41] [42] [43], which not only introduced safety concerns regarding the use of radioactive labels [44], but also suffered from a poor reproducibility [45]. In ELISA, the enzyme labeled on the target biomolecule is stable and only introduces color change without any health hazard problems [46] [47] and the sensitivity of ELISA is comparable with the RIA [48]. As a nonradioactive immunoassay, ELISA has been wildly used in medicine, various industries and biomedical research [44], and has proven to be both robust and reliable [21]. Currently, there are four types of ELISA: direct ELISA, indirect ELISA, sandwich ELISA and competitive ELISA [23]. Using a sandwich ELISA as an example, the general testing procedures are shown in Figure 2.1.

A conventional ELISA is usually conducted in the microtiter plate, as shown in Figure 2.1. . A sandwich ELISA requires the following steps, 1) coating the capture antibody on the well, 2) blocking remaining binding cites to avoid nonspecific binding, 3) capturing of the target molecule, 4) washing free target molecule, 5) binding the detection antibody with enzyme labels and 6) generation of colored products. At least 100 μL sample is delivered into each micro well [35]. Using a larger volume of micro well has two drawbacks: 1) large consumption of expensive sample, and 2) long diffusion time of regents [49]. In each step, the incubation may take from several hours to one day to complete. Thus, a conventional ELISA is a time-consuming and labor-intensive process, which limits its clinical application [50] [51]. A microtiter plate reader is bulky, expensive and requires skilled personal, which is another drawback of a conventional ELISA [44] [51].

2.1.2 Recent development in immunosensor techniques

Benefiting from a large surface area to volume ratio and miniaturized structure, microfluidics immunosensors have many advantages compared with a conventional ELISA, including low sample consumption, rapid detection, high sensitivity and portable, capabilities for multiplexed and automatic detection [19] [20] [21] [22]. In an immunosensor, target molecule recognition is also achieved through specific binding between target molecule and capture antibody as in the conventional ELISA shown in Figure 2.1. In order to report this binding event, a label-based immunosensor uses fluorescent, luminescent or electrochemical labels to generate a detectable signal. In comparison, a label-free method measures the change of mass, electrical or other properties caused by the presence of target molecule without any labeling process [52]. Thus, immunosensors can be categorized into label-based or label-free methods [53].

Based on the types of detection signal, the label-based immunosensor chips can be further divided into two groups, optical immunosensors and electrochemical immunosensors. Types of optical labels include fluorescence [54][55], luminescence [56], colorimetric [57] [58] and micro/nano particle labels [59] [60]. Fluorescence is the most commonly used label because of its many advantages including high sensitivity and ease of detection [35] [61]. Laser diodes are commonly used as a light source for fluorescence excitation [62] [63]. An alternative for laser diodes are LEDs [64] [65], which are lower in cost but have more divergence. Compared with fluorescent labels, the use of luminescent labels offers a simpler optics setup because luminescent emission is generated through a photochemical reaction and a light source is not required. The use of a luminescent label

also increases the signal to noise ratio (SNR) by the reduction of background interference caused by excitation light. The colorimetric labeling method is easy to use and cost effective, and is well-established in conventional ELISA. However, it also suffers from poor sensitivity compared with other labeling methods. Quantum dots are also used as labels in immunosensor chips to address the problems of fluorescent labels including photo bleaching, broad emission spectrum and limited in color options [66] [67]. However, quantum dots are difficult to synthesize, to functionalize, have limited shelf life and are more expensive than fluorophores [68]. Two major concerns with these optical labeling methods are: 1) difficult to fabricate the on-chip optics including lens [65], filter [69], waveguide [63] [64], light source [27] [70] and detector [71]; and 2) limited in multiplexed assay because fluorescence has a broad emission spectrum and less color options [61].

Another type of label-based immunosensor is the electrochemical immunosensor. Usually, an electrochemical immunosensor has three electrodes which are the working electrode, counter electrode and reference electrode. The working electrode is coated with capture antibody. The use of label-based electrochemical immunosensors involves: 1) labeling with enzyme, or other electroactive molecules or nanoparticles; and 2) measuring the current as a function of applied voltage between the working and reference electrodes [52]. The measured current is proportional to the enzyme activity and represents the target molecule concentration. Besides enzyme labels, nanoparticle labels are also used in electrochemical immunosensors. Nanoparticles have a large surface to volume ratio and high binding efficiency which leads to a high sensitivity in macromolecule detection [72]. The nanoparticle labels used in electrochemical immunosensor chips include metal particles [73] [74], carbon nano tubes [75] [76] and quantum dots [77] [78]. Because the

electrochemical immunosensors only have electronic components they are cost effective and easy to integrate on a sensor chip. However, the disadvantages of electrochemical immunosensors include: 1) difficulties in maintaining the functionality of the surface modification for a long time due to the instability of antibody [79]; 2) a large applied voltage may damage the modification of capture antibody on the electrodes [52]; and 3) the performance of electrochemical immunosensors is affected by nonspecific absorption, pH and ionic concentration [68] [52].

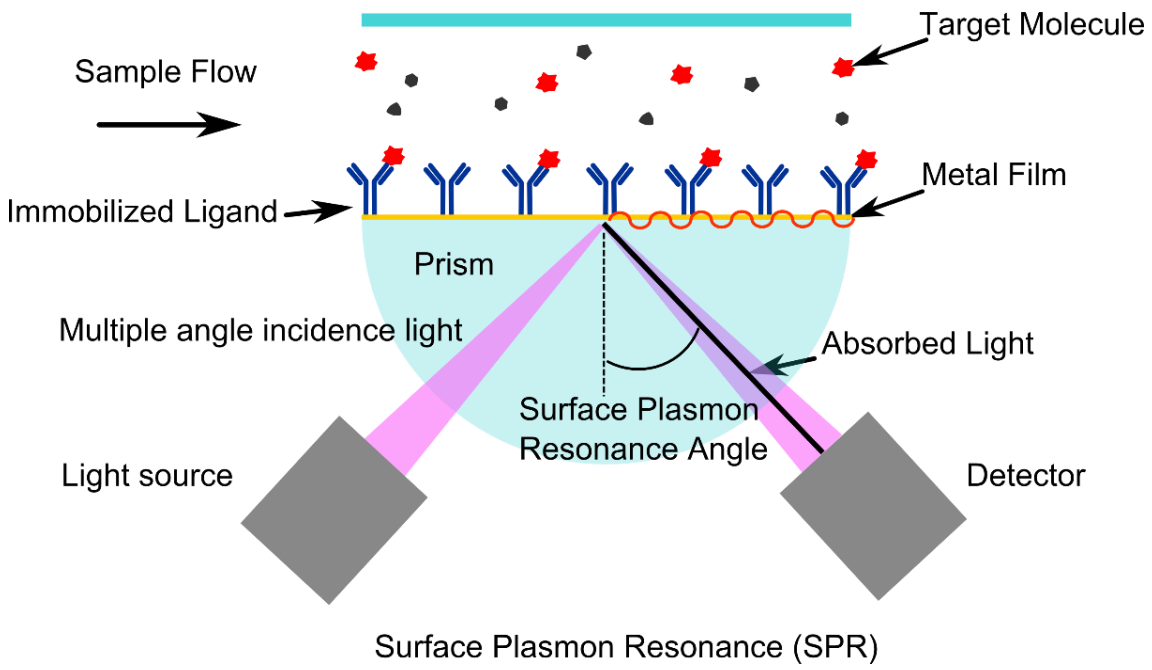

Figure 2.2 Sensing principle of surface plasmon resonance (SPR)

A label-free immunosensor is preferred for macromolecule detection for two major reasons. Firstly, the surface functionalization of a label-free immunosensor is simple and only requires immobilization of capture antibody on the sensor chip surface, compared with a label-based immunosensor chip which has a "capture antibody – target macromolecule – detection antibody" sandwich structure; secondly, labeling of detection

antibody may reduce the binding affinity of the capture antibody [25] [26]. The label-free immunosensors can also be categorized into optical immunosensors, electrochemical immunosensors and mechanical immunosensors [61]. The label-free optical immunosensors include surface plasmon resonance (SPR) spectroscopy [80], surface-enhanced Raman spectroscopy (SERS) [81], capillary electrophoretic immunoassays (CEIA) [82] [83], photonic crystals sensors [84], optical microcavity resonators [85], reflective interferometry [86] and imaging ellipsometry [87]. The sensing principle of an SPR is shown in Figure 2.2. Antibody is immobilized on a metal film. An incident light containing multiple incident angles is reflected on the metal film. Free electrons at the metal surface absorb the incident light at a certain incident angle (SPR angle) and transfer it to a surface plasmon wave. The absorbed light can be observed by a detector. The SPR angle is very sensitive to the surface refractive index. The binding of capture antibody and target molecule causes a change of refractive index of the metal film, which leads to a shift of SPR angle, as shown in Figure 2.2. Thus the target molecule concertation can be detected through the measurements of the SPR angle. Due to the complicated optics setup, the optical detection instruments are very expensive. For example, SPR is a well-established and commercially available instrument. A commercially available SPR instrument (for example, Biacore SPR Systems, GE) costs $120,000–$250,000, and each test may consume one electrode chip, which costs $60-$120 [88]. As discussed above, another common problem shared by all optical sensor chips is the fabrication of on-chip optics and detectors. The details of label-free optical immunosensor chips are reviewed in [40] [61] [68].

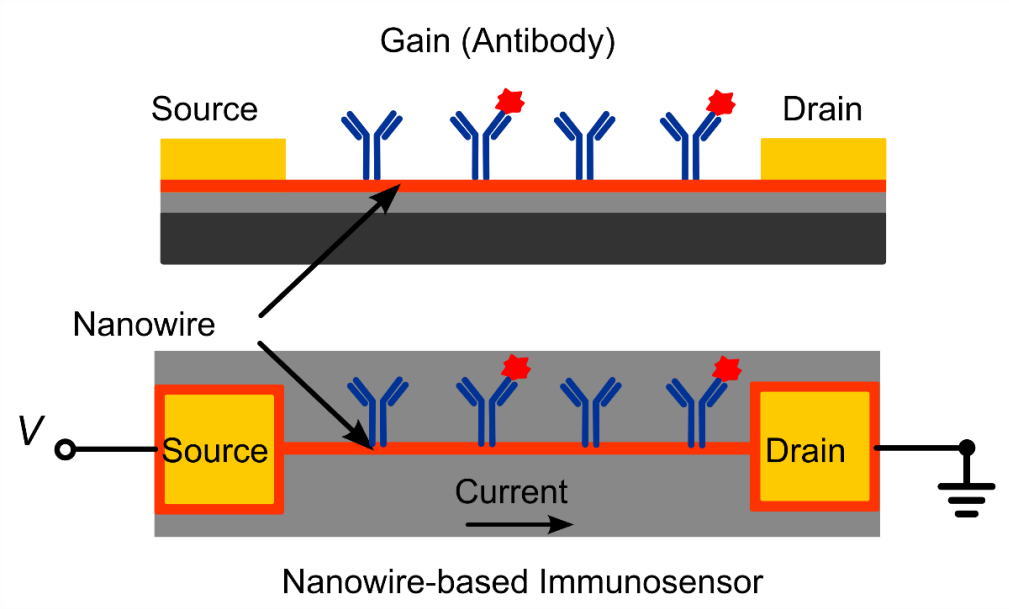

Figure 2.3 Sensing principle of nanowire-based FET immunosensor

In the category of label-free immunosensors, electrochemical and mechanical immunosensors are preferred because most of them only require electrical components, which are easy to integrate on sensor chips. Label-free electrochemical sensors are based on a change in electrical properties (dielectric constant, charge state [52]) caused by the binding between antigen and antibody. For electrochemical impedance spectroscopy (EIS) based sensors, the antibody coated on the working electrode is used to bind the target macromolecule. This binding event will trigger the impedance change and is observed through the EIS [89]. Both multi frequency and signal frequency excitation are applied to EIS to detect the impedance changes [72]. The use of signal frequency measurement reduces the testing time and enables a real-time detection. Another label-free approach is the field effect transistor (FET) sensor, as shown in Figure 2.3. For a nano wire FET, the conductance between source and drain is controlled by the voltage applied at the gate

electrode. The nano wire coated with capture antibody acts as the gate electrode. The target molecule has a net negative or positive charge in aqueous solution. Thus, the binding between target molecule and capture antibody will increase or decrease the surface charge of the nano wire (gate electrode) and change the conductance between the drain and source electrodes. Thus, the binding event and the concentration of target molecule can be monitored by measuring the conductance change. Nano wire FET has an ultrahigh sensitivity which may enable single molecule detection [90]. However, fabrication of nano wire FET and maintaining the activity of capture antibody are difficult.

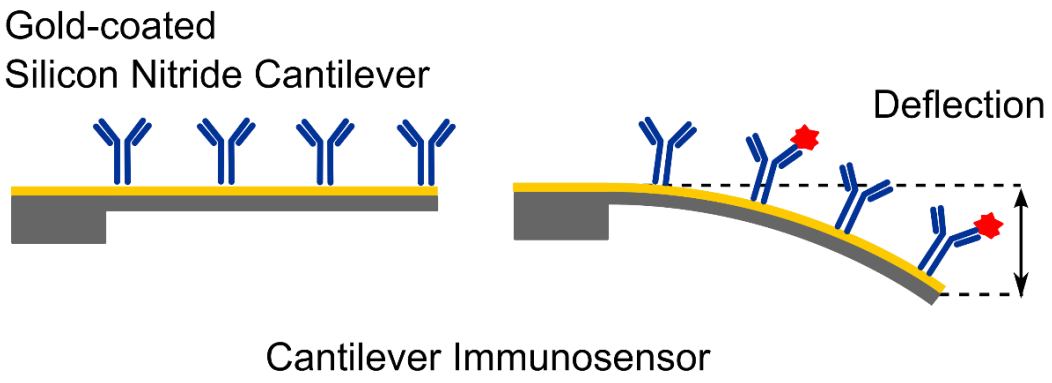

Figure 2.4 Sensing principle of cantilever immunosensor

Mechanical label-free methods are based on the mass change caused by target macromolecule binding. For example with a micro cantilever sensor, as shown in Figure 2.4, the cantilever surface is immobilized with capture antibody and is able to capture the target macromolecule. This binding event leads to an increase of mass of the cantilever beam, and further causes the deformation of the micro cantilever. This deformation can be detected through optical detection [91] or electrical detection [92]. However, the micro

cantilever beam sensor is easily affected by the environment. For example, a small temperature change during a measurement will also cause a deflection of the micro cantilever, causing false positives. A quartz crystal microbalance (QCM) is another well-established immunosensor based on mass change. The binding of target molecule increases the mass on the QCM surface and causes displacement of the crystal oscillation, which leads to a resonant frequency shift. Thus, the measured resonant frequency represents the binding event and target macromolecule concentration. However, QCM is very sensitive to temperature variations, electronic noise and mechanical drift [93].

The above mentioned immunosensor chips are based on immobilization of capture antibody on a planner surface, which is a tedious process and requires skilled personnel. More importantly, the immobilized capture antibody has a short life cycle. Microparticles, as micro carriers, are another option as solid support for antibody immobilization.

2.1.3 Immunosensor based on microparticles

As discussed above, most immunosensor chips use planner surfaces in the microchannel as solid supports for capture antibody. The surface of the MPs is another option as a solid support with many advantages. Firstly, MPs have an extremely large surface to volume ratio, which enables high efficiency interactions between target macromolecule and capture antibody coated on the MPs. Secondly, MPs are easy to manipulate. The use of MPs not only simplifies the process of immobilization of the capture antibody, but also eliminates the difficulties in recovery of biological activity of the capture antibody for reuse of the immunosensors. Thirdly, compared with spatially

dividing a plane surface and coating each sub-plane with different antibody for multiplexing, it is much more convenient to coat MPs with various capture antibody for a multiplexed immunoassay [35]. Microparticle based immunoassays are well developed and commercially available, for example with the xMAP technology. An immunoassay based on MPs with detection by fluorescent flow cytometry is shown in Figure 2.5.

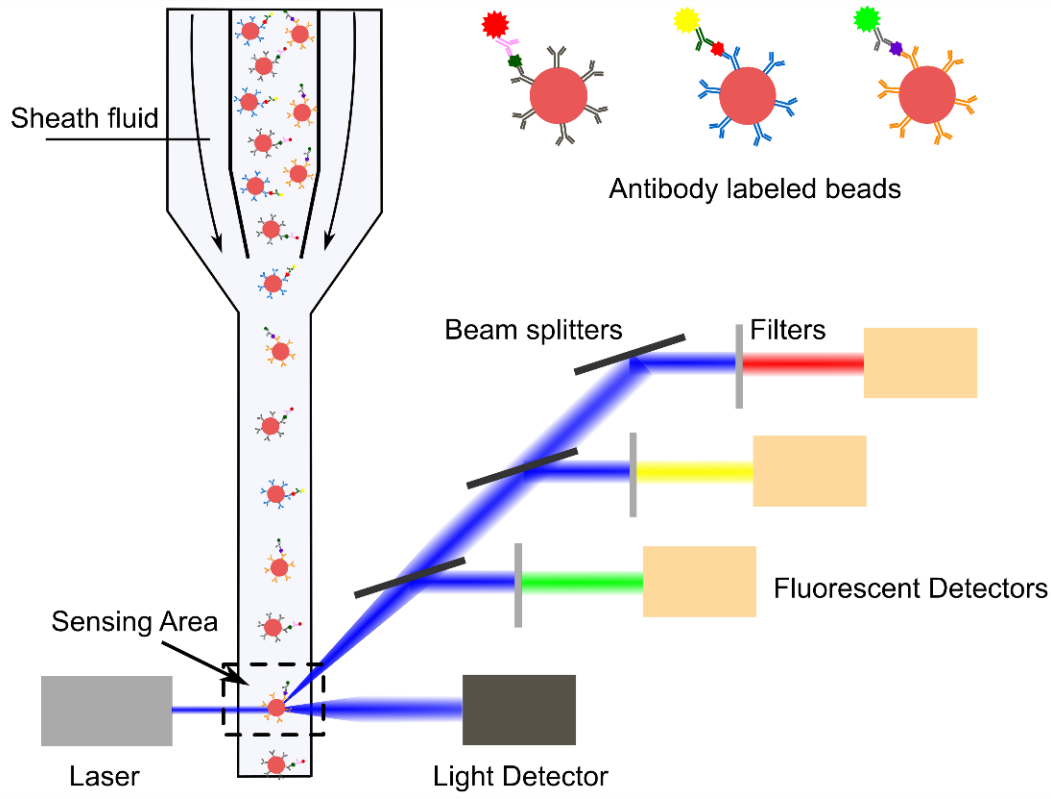

Figure 2.5 Working mechanism of immunoassay based on microparticles and flow cytometry for multiple molecule detection

As shown in Figure 2.5, the capture antibody coated on the MPs target the macromolecule and detection antibody tagged with different color fluorescent dyes are formed in the sandwich ELISA structure. To achieve a multiplexed detection, MPs encoded with different florescent colors flow through the sensing area of a flow cytometry. A laser

beam provides the florescent excitation. The passage of a particle causes forward scatter and side scatter of the laser beam. Beam splitters and filters are used to decode the florescent color and determine the target macromolecule concentration. Although MP based immunosensors have many advantages, most of these chips rely on optical detection [35]. Recent studies show that the immunoaggregation assay is an emerging technique for quantitative biomarker detection [94] [95] [28] . Currently, most immunoaggregation assays rely on optical detection [29] [96] [27]. Because the immunoaggregation assay is based on MP aggregation triggered by target molecule, a resistive pulse sensor, which is highly sensitive to the size change of MPs, is an ideal detector for the immunoaggregation assay.

2.1.4 Immunoaggregation assay

Comparing with ELISA, an immunoaggregation assay has many advantages. Firstly, an immunoaggregation assay does not require labeling steps. Normally, an immunoaggregation assay only has one step, which significantly reduces the assay time and labor intensity. Secondly, microparticles have large binding surface to volume ratio and fast diffusion rate, which promote the reaction between analyte and capture antibody. Thirdly, the surface modification of microparticles is simple. It is also convenient to conduct a multiplexed assay using microparticles coated with various capture antibodies. Fourth, microparticles are easy to manipulate in a microfluidic device. Thus, immunoaggregation assays are suitable for the use in miniaturized systems [95]. Conventional immunoaggregation assays were introduced by Singer and Plotz [97].

Commercially available immunoaggregation assay kits based on conventional immunoaggregation assays are capable of identifying bacterial, fungal and viral diseases and macromolecule including hormones and proteins [94]. There kits are inexpensive, portable and able to make detection of biomarkers by the naked eye. In order to conduct a conventional immunoaggregation assay, unknown sample, negative control (without biomarker) and positive control (with biomarker) are mixed with antibody functionalized microparticles. The presence of target biomarkers causes aggregation of the antibody functionalized microparticles. If the unknown sample contains target biomarkers, the presence of target biomarkers can be identified by comparing test results between the unknown sample and positive control (visible aggregation cluster are formed in both of them). However, conventional immunoaggregation kits are unable to quantitatively measure the biomarker concentration and only able to detect the presence of biomarkers.

Recent studies proved that the immunoaggregation assay is also able to quantitative analysis of macromolecule concentration. Depending on the state of the aggregates [95], the on-chip immunoassays were performed as a doublet assay [29] [96] [27] and a cluster assay [94] [95] [28]. The detection methods for immunoaggregation assays include optical detection (turbidimetry [98], light microscopy [27] [28], fluorescent microscopy [29] and light scattering [29]), magnetophoresis [96], and resistive pulse sensing [1] [99]. High sensitive immunoaggregation assays were also achieved through the alignment of aggregates in sensing channels using hydrodynamic [100], magnetic [27] or ultrasonic [95] focusing. Among these detection methods, the turbidimetry is based on bulk detection which measures the loss of intensity of transmitted light caused by scattering of the aggregates suspension. The turbidimetry is unable to detect individual aggregate, thus it

has a poor detection limit [28]. Light scattering is another optical detection method. Pamme et al reported a microfluidic device for counting and sizing immunoaggregates using laser light scattering [101]. The scattering density is proportional to the volume of aggregates. A commercial immunoaggregation assay kit for C-Reactive protein (CRP) detection was tested in their studies. A detection limit of 100 ng/mL was achieved. However, from their measurement results, light scattering was also unable to differentiate microparticle doublets. Although distinguishing microparticle doublets is extremely difficult, quantitative detection of microparticle doublet is able to increase the detection sensitivity [29] [102]. Light microscopy is simple and easy to obtain, which is suitable for resource-limited area. Recently, Wu et al demonstrated that an immunoaggregation assay based on light microcopy is able to detect human ferritin concentrations as low as 0.1 ng/mL, which is lower than the detection limit of most commercial ELISA kits [103]. This high sensitive detection was achieved through doublet assay. However light microscopy has a manual readout which means it is labor intensive and only has a low throughput. Wiklund et al reported a fluorescence microscopy based image analysis method for classification of singlets and doublets of microparticles [102]. By using this method, microparticle singlets, doublets and triplets can be differentiated in the measurement results. Using fluorescent microscopy to differentiate aggregate doublets not only requires a long assay time due to the use of an image recognition algorithm, but also requires large data storage which make it impractical for real-time detection. Kim et al also demonstrated an immunoaggregation assay based on magnetophoresis [96]. In their study, the presence of mouse IgG caused the aggregation of 1 μm polystyrene microparticles and 50 nm magnetic particles. Both of polystyrene microparticles and magnetic particles were coated with goat anti-mouse IgG.

The aggregates' velocity introduced by the magnetic field was used as an indicator of mouse IgG concentration. The detection limit of 15.6 ng/mL was achieved. They also used fluorescent encoded microparticles to prove this method can be applied to a multiplexed detection. However, image analysis is required to track the movement of aggregates, which increases the assay time and reduces the throughput of this device. The aforementioned methods are all based on optical detection. Recent studies also utilized resistive pulse sensors for immunoaggregation assay. A resistive pulse sensor only involves electrical detection and has a high accuracy in particle sizing, which makes it an ideal detector for immunoaggregation sensing. The use of resistive pulse sensors for immunoassays is reviewed in next section 2.1.5.

As mentioned before, in order to achieve a highly sensitive detection, particle forcing techniques were applied to the immunoaggregation assay including hydrodynamic [100], ultrasonic [95] [104], capillary electrophoresis (CE) [105], and magnetic [27] focusing techniques. Nilsson et al proved that the capillary electrophoresis is able to separate microparticles from their aggregates based on their electrophoretic mobility [105]. The electrophoretic mobility is determined by the electric charge of antibody coated on microparticles. In order to detect the presence of human chorionic gonadotropin (hCG), two kinds of antibody were used in their experiments (antibody B is directed against the α-subunit of hCG and antibody A is directed against the β-subunit of hCG). Only one type of antibody was coated on the each microparticle. The mobility of antibody B coated microparticles is higher than the mobility of antibody A coated microparticles. Thus, the aggregates formed by these two types of microparticles has an intermediate mobility between these two types of single microparticles. CE was then used to separate two types

of single microparticles and their aggregates. However, CE detection only has a low throughput and low sensitivity.

Under an ultrasonic standing ware (USW) field, microparticles are driven to the pressure node of the standing wave. Instead of relying on Brownian motion, the use of USW force increases the probability of microparticle collisions and further enhances the sensitivity of immunoaggregation assay [106]. Thomas et al demonstrated that the use of USW focusing significantly reduces the lower detection limit from 300 ng/mL to 230 pg/mL comparing with a conventional test-card procedure [107]. However, USW relies on radio frequency exaction, which not only requires a complicate setup, but also introduces bubbles into the microfluidics system which will cause a false detection of aggregates. Afshar et al demonstrated a 3D magnetic focusing method to align particles in the microchannel in order to aid the microparticle doublet recognition. The microparticle doublet was detected under a light microscope. This method was used for the detection of the bBSA concentrations in a model immunoaggregation system. A detection limit of approximately 400 pg/mL was achieved. One problem for magnetic focusing is that magnetized microparticles tend to form nonspecific aggregates, which will be counted as immunoaggregates and lead to errors in biomarker concentration measurement.

Although focusing of aggregates is able to aid in the optical detection of aggregate doublets, quantitative detection of microparticle doublets is still a problem in immunoaggregation assays. It is worth mentioning here focusing methods are not limited to these four methods. A detailed review of particle focusing methods for microfluidic devices can be found in [108].

2.1.5 Micro resistive pulse immunosensors

Resistive pulse sensing/Coulter counter principle has been applied in particle sizing and counting since the 1940s [109]. A resistive pulse sensor consists of three components including a sensing channel, a pair of inlet/outlet reservoirs and a pair of electrodes. The transit of a particle through the sensing channel causes a resistive pulse between the electrodes. The amplitude of the resistive pulse represents the size of the particle, and the counts of resistive pulses is used to calculate the particle concentration. The conventional resistive pulse sensor is well-established instrument and commercial available. The detection range of a commercial device is from 0.4 to 1600 μm in diameter (e.g. Multisizer 4 COULTER COUNTER, Beckman Coulter).

Recent studies show that micro resistive pulse sensors are promising tools for macromolecule detection. There are two major resistive pulse sensing strategies for macromolecule detection: 1) direct detection using nanopores, and 2) using microparticles as biomarker carriers to amplify the resistive pulse signal. Because the sensitivity of a resistive pulse sensor is inversely proportional to the volume of the sensing channel [109], a resistive pulse sensor with a nano scale sensing channel (10 to 100 nm [47]–[55]) has an extremely high sensitivity but a low limit of detection, which is able to directly detect nano bio-objects, such as DNA [110], [111], RNA [112], virus [113], [114] and protein [115]–[117]. Three types of nanopores for macromolecule detection have been utilized: biological pores [118], artificial pores [119] [120] and hybrid nanopores [121]. Comparing with biological pores, such as α-hemolysin pores, artificial pores have many advantages including tunable pore size, stability over a wide range of voltages, temperatures, and pH

[119]. In addition, three parameters of the resistive pulses can be used for macromolecule characterization: amplitude of the pulse (indicative of object size), pulse width (indicative of object mobility) and blockage (indicative of specific binding) [121].

Another strategy for macromolecule detection is to use microparticles to amplify the resistive pulse signal. Carbonaro et al reported an immunoassay based on resistive pulse sensing and antibody functionalized microparticles to detect the presence of biomarkers [115]. In this methods, 470 nm microparticles were coated with capture antibody, after antigen and detection antibody were captured on the microparticles, the microparticles' diameter increased from 470 nm to 490 nm. This diameter change was detected by the RPS as an indicator of the presence of target biomarkers. They also demonstrated that the use of various antibody functionalized microparticles is able to achieve a multiplexed detection. However, there are two limitations of this device: 1) the resistive pulse change due to the small change of diameter (because of the nano size of the biomarkers) is difficult to measure, and 2) this method is unable to evaluate the concentration of target biomarkers.

2.2 Multiplexed immunosensors

The multiplexed detection of disease related biomarkers is important for two major reasons: firstly, due to the complexity of human biology and the heterogeneity of diseases, single biomarker detection is insufficient to provide enough information for disease diagnosis [14] [15] [16]. Secondly, the multiplexed detection of biomarkers associated with different stages or classification of diseases is able to increase the accuracy in disease diagnosis [122] [123] [124] [125]. Based on the solid support for capture antibody

immobilization, the multiplexed approaches are divided into two categories [30] [126]: planar arrays and suspension arrays (immunoassays based on micro particles). In term of planar arrays, the surface encoding method involves spatially coating support surface in an array with multiple types of capture antibody [127]; while the suspension arrays use microparticles as capture antibody carriers.

2.2.1 Planar arrays

Label-based multiplexed immunosensors. A planar array immunosensor is well-established as high-throughput devices with high sensitivity less sample consumption [128]. Base on the labeling method, planar arrays immunosensors can be categorized as optical immunosensors (fluorescence [15] [129], luminescence [130], [131], [132], colorimetric [133], [134]) and electrochemical immunosensors [135]. The solid support for a planar array includes glass slide, nitrocellulose membranes, microparticles, or microtiter plates. However, the most challenge for a planar array is the surface modification of a planar array. Currently, the fabrication methods of a planar array include contact printing, non-contact printing, microfluidics-based printing, microstamping, lithography, cell-free protein expression microarray [136]. The drawback for these methods includes antibody compatiabltity, low signal to noise ratio [128]. The lack of specific capture molecule is another problem that limits the broader use of planar microarray technology[128].

Label-free multiplexed immunosensors. Label-free multiplexed immunosensors include optical (SPRi [137], [138], SERS [139]), electrochemical (nanowire [140]), and mechanical (QCM [141] and micro cantilever [142], [143]) immunosensors. Surface

plasmon resonance imaging (SPRi) Although planner array immunosensors are well-developed, and some of them are commercially available [144], as discussed previously, the use of optical immunosensor chips are time consuming in setting up, difficult to integrate onto a sensor chip, and require expensive readers and skilled personnel. In comparison, microparticles encoding methods have many advantages including large multiplexed capacity, large surface area to volume ratio and easy-to-use.

2.2.2 Suspension arrays

Compared with planar arrays, suspension arrays based on microparticles have many advantages including easier surface modification, faster reaction kinetics, and better reproducibility [145] [146]. The microparticles encoding methods are classified as spectrometric, electronic, graphical, or physical methods [30]. A spectrometric encoding is based on the specific wave length of light or radiation. The fluorescent encoding is discussed in section 2.1.3 (see Figure 2.5). Other spectrometric encoding methods include colorimetric [147] [148], Raman tags [149][150], and Quantum dot encoding [151]. The disadvantages of spectrometric encoding include 1) limited multiplexed capacity; 2) low signal to noise ratio due to the interference between exaction signal and emission signal, and 3) bulky and expensive detection setups. As shown in Figure 2.5, a beam splitter and a detector are required for decoding each fluorescence color, which increase the complexity and cost of the flow cytometer. Among the electronic encoding methods, the radiofrequency (RF) tag encoding is able to provide $>10^{12}$ types of labels, which represents a nearly unlimited multiplexing capability [36] [152]. This method is based on a radio-

frequency identification technique. However, due to the large size of the RF chips (~8 mm × 1 mm × 1 mm), it is impossible to encode each microparticles with RF tags [126]. Graphical multiplexing approaches rely on patterning of various structures on the micro carriers, for example, striped rods [32], dot-pattern particles[33] or barcode micro/nano probes [30] [153], However, fabrication of these micro carriers is difficult, and detection of these graphical labels normally requires optical setups with high resolution and accurate alignment [126]. Physical encoding rely on encoding micro carriers with physical properties, such as size [155] [156], density, refractive index [156], shape [157], and composition [22]. However, most of these methods also rely on optical detection. The needs of bulky and expensive optics with high resolution and accurate alignments makes these methods impractical for on-site disease diagnosis, especially in a resource limited area.

2.2.3 Multiplexed resistive pulse sensors

There are two major strategies for multiplexed macromolecule detection. The first strategy is based on multichannel (multi-nano pores) approach. The second strategy is based on microparticle multiplexing. Both artificial and biological pores were used in the multiplexed detection studies [158][159][160]. For example, Osaki et al demonstrated a r-Hemolysin nanopore array (8 channels) for molecular and DNA detection [159]. Bell et al demonstrated a multiple glass pores (16 channels) for DNA detection [160]. However, these approaches require a measurement setup for each channel, which limits their multiplexed capacity. Alternative electronic encoding methods were also achieved through

the uses of multi frequency excitation [161] and modification of micro channel structures [162]. However, for the multi frequency excitation method, a limited number of sensing channels can be added to the multichannel devices because of the narrow frequency range in which the resistive pulse sensors display a resistive behavior [163]. For the micro channel structure modification method, this method normally requires the use of a long sensing channel. However, a sensing channel with increased length has a low sensitivity, because the sensitivity is inversely proportional to the channel length. A decoding algorithm is also required, making this method time-consuming.

Recently, Platt et al utilized a resistive pulse sensor to detect platelet-derived growth factor via DNA aptamer−nano rod aggregation [99]. In this method, different types of biomarker caused different shapes of aggregates (which are called “end-on-end” or “side-on” aggregates). The shape of the aggregates was distinguished based on the changes in resistive pulse height and width (transit time of particles). However, this method was unable to detect small changes in biomarker concentration because of the large deviations in resistive pulse signals at each biomarker concentration caused by the high aspect ratio of nano rods and aggregates formed with different shapes and orientations. Billinge et al reported a label free detection of biomarker using aptamers and tunable resistive pulse sensor [164] [165]. In their approach, the particle rate, defined as the counts of particles passing through a tunable pore per minute, was used as an indicator of target protein concentration. The particle rate decreased with an increase of protein concentration. However, the detection range of this method is affected by the particle concentration.

2.3 Micro resistive pulse immunosensors for cellular biomarkers detection

Polymerase chain reaction (PCR) and immunoassay are two major methods for cellular biomarker detection [37]. Although a PCR-based sensor chip has a high sensitivity, it requires a long reaction time or a multi-step sample preparation procedures including cell lysis and enrichment steps [39]. The PCR-based biosensor chip is also complicated because of the on-chip temperature control for thermocycling and on-chip cell lysis [38] [39]. For an immunosensor, cellular biomarker detection is based on the specific binding between receptors on the surface of the cells and antibody immobilized on a solid surface. This binding event is then transduced to a detectable electrical or optical signal [9] [38], and detected through either labeling methods (fluorescence [166], luminescence [167], colorimetric [168] or magnetic particle [169]) or label-free methods (SPR [170], QCM [170]).

Recent studies have also utilized resistive pulse immunosensors for cellular biomarker detection based on two strategies [171], [172]. The first strategy is to use an antibody functionalized sensing channel. The transit-time increase is used as an indicator of a target cell: when a target cell passes the sensing channel, the transit-time was larger than that of a non-target cell due to the specific interaction between surface markers on a target cell and capture antibody coated on the sensing channel. The second strategy is to use an antibody functionalized capture chamber. Resistive pulse sensors were used to monitor the count of target cells captured in this chamber in order to measure the concentration of the target cells. Carbonaro et al demonstrated device based on transit-time differentiation for CD34 surface marker detection [171]. The sensing channel of this device

was immobilized with CD34 antibody. They proved that a target cell with CD34 surface marker has a larger transit-time than for the non-target cells (without the CD34 surface marker). However, the transit-time is dependent on the flow velocity, the sensing channel structure and off-axis effect [173]. Their results showed that the transit-time of target cells had a large variation and overlapped with the transit-time distribution of non-target cells. Thus, a transit-time modeling algorithm is required to further differentiate target cells from non-target cells. To further expand the performance of a transit-time differentiation based device and achieve a multiplexed detection, Karthik et al demonstrated a node-pore resistive pulse sensor which was able to simultaneously detect a single cell with up to five surface markers [174]. The sensing channel of this device was divided into five segments. Each segment was functionalized with one type of antibody. As a cell transits through the sensing channel (five segments in series), it will generate a resistive pulse consisting of five sub-pulses. The width of each sub-pulse represents the transit-time of a cell through one segment. By using this five-segment sensing channel, five surface biomarkers can be identified in a single test. However, there are two issues limiting the performance of this device. First, the increased length of the sensing channel not only increases the flow resistance, but also reduces the throughput of this device. Secondly, a long sensing channel has a low sensitivity, because the sensitivity is inversely proportional to the length of the sensing channel.

In addition to transit-time based strategy, Douglas et al demonstrated a resistive pulse sensor for detection and identification of bacterial based on the capture chamber modification. In order to capture *E.coli*, the capture chamber of this device was functionalized with anti- *E.coli* antibody. The captured *E.coli* increased the resistance of

the capture chamber, which was used as an indicator of *E.coli* concentration. However, there are two drawbacks of this device. Firstly, the detection of *E.coli* was achieved through the bulk measurement of the chamber resistance. This device is unable to count each individual *E.coli*, and is also unable to provide the accurate concentration of the *E.coli*. Secondly, the large capture chamber with large resistance reduces the sensitivity of the resistive pulse sensor. Because a detectable resistance change requires a large amount of *E.coli* captured in the chamber. Thus, each test took a long time to complete. In order to provide the accurate count of target cells, one alternative option is to use two pair of resistive pulse sensors to measure and count cells entering and exiting the capture chamber. Nicholas et al demonstrated a differential counter for CD4 T lymphocyte detection [172]. The capture chamber of this device was functionalized with CD4 antibody. Two resistive pulse sensors were located at the entrance and the exit of the capture chamber in order to count the CD4 cells captured in the chamber. The resistive pulse sensors detected target cells based on the surface modification of sensing channels or capture chambers. However, maintaining the function of surface modification for a long period of time or reproducing the surface antibody coverage to reuse the sensor are difficult [37] [175]. In particular, regenerating the surface modification (surface antibody coverage) in a microchannel is a significant challenge [37] [175]. It is worth mentioning that microparticles coating inside of a microchannel via an external magnetic field can significantly reduce the difficulties in surface modification of immunosensor chips [31]. For example, Kralj et al demonstrated a simple packed bed device for circulating tumor cells (CTCs) capture [176]. Avidin-functionalized microparticles were constrained in the microfluidic device by a weir structure and used to capture human breast cancer cells labeled with Biotinylated anti-

EpCAM. Their results shows this device had a capture efficiency up to 70%. There are several disadvantages of this device, firstly, this device requires the labeling of target cells, which increases the assay steps. Secondly, the optical detection is time-consuming and requires bulk and complicate setups.

It is worth mentioning that a resistive pulse sensor is also able to identify cells according to other properties including size [177][178][179], dielectric properties [180] [181] [182][183], and mechanical properties [184]–[186]. For example, circulating tumor cells (CTCs) normally have larger size than other blood cells [177], a micro resistive pulse sensor was used to differentiate model CTCs according their size [177]. Another example is the complete blood count (CBC) test. CBC test is used to detect a wide range of blood disorders, including anemia, infection and blood cancers. The analysis time is critical in CBC test [187]. Compared with traditional electronic particle counter, a micro resistive pulse sensor is able to rapid analysis blood sample with less sample consumption [187]. The mechanical property, especially the deformability, is associated with a range of diseases. For example, the deformability of red blood cells (RBCs) is related to severity of malaria [188]. Recent studies utilized micro resistive pulse sensor to evaluate the deformability of RBCs and monitor treatment of the of the malaria [189] [190]. Despite the promises, simply using the resistive pulses to detect cells has low specificity, i.e., it is very likely the two type of cells have size and deformability overlapping in a real sample with unknown contents.

2.4 Summery

Immunosensors for macromolecule and cellular biomarker detection have been reviewed in this chapter in three aspects: label-free immunosensors, multiplexed immunosensors and resistive pulse sensor chips for cellular biomarker detection. A label-free immunosensor chip is preferred for macromolecule detection for two major reasons. Firstly, a label-free immunosensor has a minimum number of assay steps without labeling of the detection antibody; secondly, the chemical labeling process may reduce the binding affinity of the capture antibody [25] [26]. Based on the types of detection signals, all-electronic detection is preferred because the electronic components are easy to integrate on a sensor chip, and easy to use. Immunoaggregation assay is a label-free technique which is able to quantitatively detect macromolecule concentration. However, most of the current studies of immunoaggregation assays rely on optical detection. A resistive pulse sensor chip is highly sensitive to size change. Thus, the combination of immunoaggregation assay and resistive pulse sensing is a promising approach for macromolecule biomarker detection.

Another important function of immunosensors is multiplexed detection capability. Compared with planar arrays, microparticles with a large surface area to volume ratio enable a high efficiency of interaction between target macromolecule and the capture antibody immobilized on the microparticles' surface. However, most microparticles based encoding methods rely on optical detection. It is worth mentioning that it is feasible to use micro resistive pulse sensors for multiplexed detection. The microparticles can be encoded with physical properties such as size and the transit time through the resistive pulse sensor.

The size encoding method is more reliable because the transit time is also affected by the flow rate and microchannel geometry.

The restive pulse sensor chip is also able to detect cellular biomarkers based on the interactions between receptors on the cell surface and the capture antibody coated on the microchannel. For immunosensor chips, maintaining the function of surface immobilization and regenerating the surface activities to reuse the sensor are difficult. The use of microparticles can significant reduce the difficulty in surface modification of immunosensor chips.

CHAPTER III

DEMONSTRATION OF MICRO RESISTIVE PULSE IMMUNOAGGREGATION SENSOR

3.1 Design concept and sensing principle

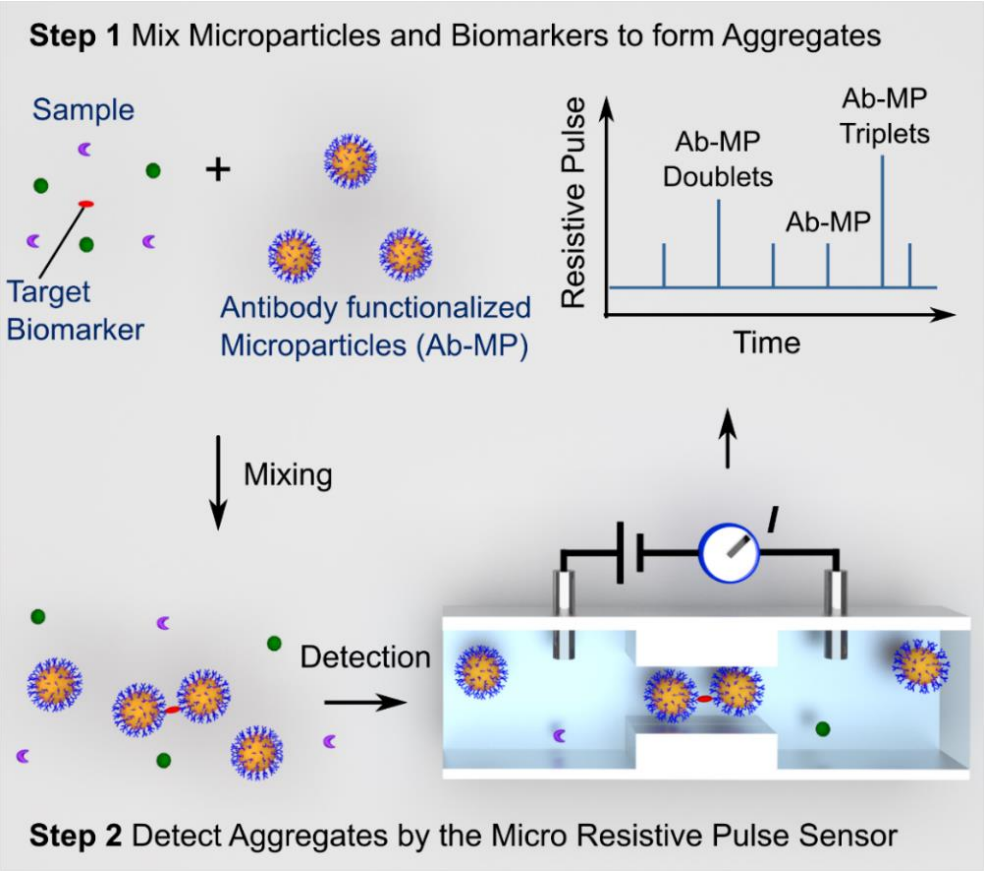

Figure 3.1 Schematic of the immunoaggregation assay mechanism. Target biomarkers and antibody functionalized microparticles (Ab-MP) are mixed to form aggregates, which are detected by a micro resistive pulse sensor (reproduced with permission from Yu Han et al [1]. Copyright 2014 American Chemical Society)

In this chapter, I will present a single channel micro resistive pulse immunoaggregation sensor for biomarker detection. Figure 3.1 illustrates the immunoaggregation assay mechanism. The immunoaggregation assay consists of two major steps: firstly, biotinylated polyclonal antibody (Ab) conjugate with streptavidin coated microparticles (MPs) through streptavidin-biotin interaction to form the antibody functionalized microparticles (Ab-MPs). Then, Ab-MPs are mixed with a sample containing the target biomarkers. The specific binding between target biomarker and the polyclonal Ab on Ab-MPs triggers the aggregation of Ab-MPs; secondly, formed Ab-MP aggregates are detected by a micro resistive pulse sensor. When each particle passes through the sensing channel, it generates a resistive pulse between the pair of electrodes. The amplitude of the resistive pulse is proportional to the volume of the particle [145] [146]. The volume fraction of Ab-MP aggregates to all detected particles represents the level of the biomarker concentration.

The advantages of this approach are multiple. Firstly, the immunoaggregation does not require the labeling of fluorescence or enzyme labels, and reduces the assay steps. Secondly, instead of direct detection of nano sized macromolecule, the detection of micro sized aggregates significantly amplifies the resistive pulse signal and eliminates the difficulties in fabrication of nano size sensing channels; thirdly, the use of micro sized sensing channel also increases the throughput of the immunoassay.

3.2 Fabrication and calibration of the micro resistive pulse sensor

The micro resistive pulse sensor was fabricated using standard photolithography and calibrated with standard microparticles.

3.2.1 Device fabrication

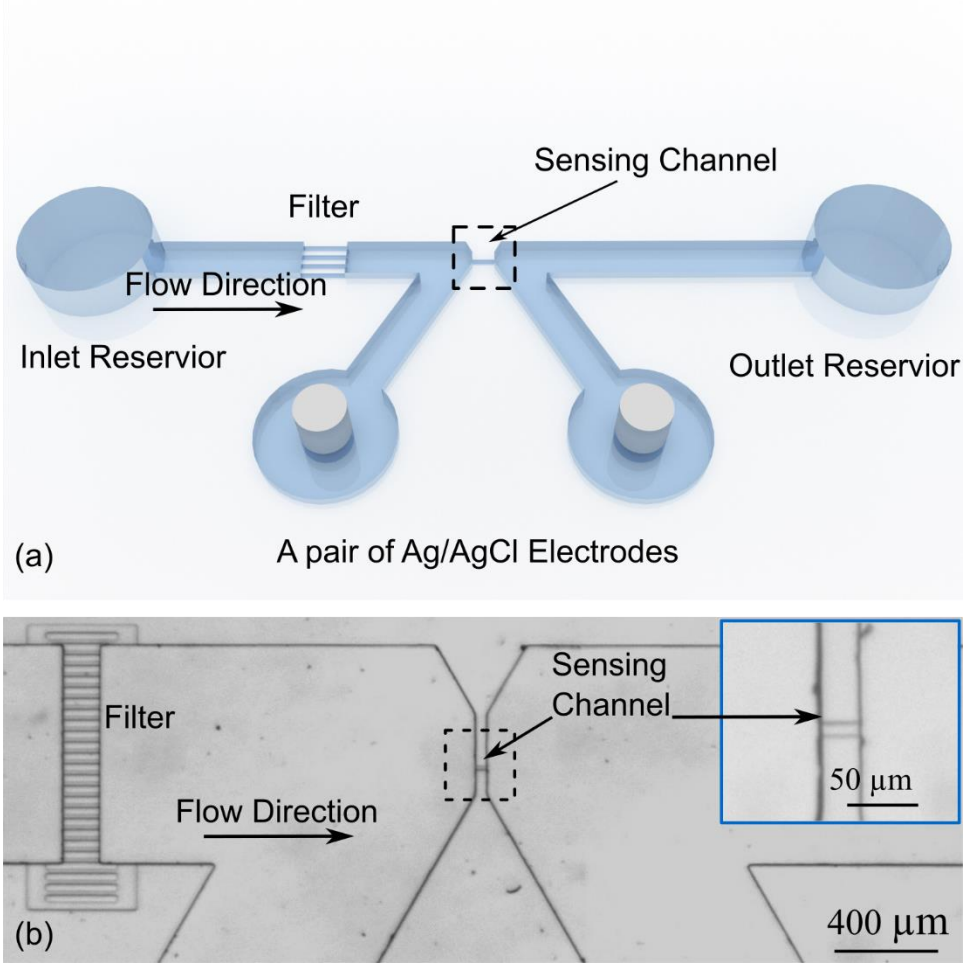

Figure 3.2 (a) Schematic of the micro resistive pulse sensor; (b) microscopy image of sensing channel, and on-chip filter. (reproduced in part with permission from Yu Han et al [1]. Copyright 2014 American Chemical Society)

As shown in Figure 3.2, the micro resistive pulse sensor consists of four parts: 1) a sensing channel with a width of 10 µm and a length of 30 µm to detect aggregates; 2) an on-chip filter with a pore width of 10 µm; 3) a pair of Ag/AgCl electrodes to measure the resistive pulses; and 4) inlet and outlet reservoirs (see Figure 3.2 (a)). It is worth mentioning here that if Ab-MPs are on a micro scale (a few microns), most aggregates are Ab-MP

doublets, which has also be shown in [27]. Thus most aggregates can pass through the 10 × 10 μm filter. The micro resistive pulse sensor was fabricated using two-step photolithography. As shown in Figure 3.3.

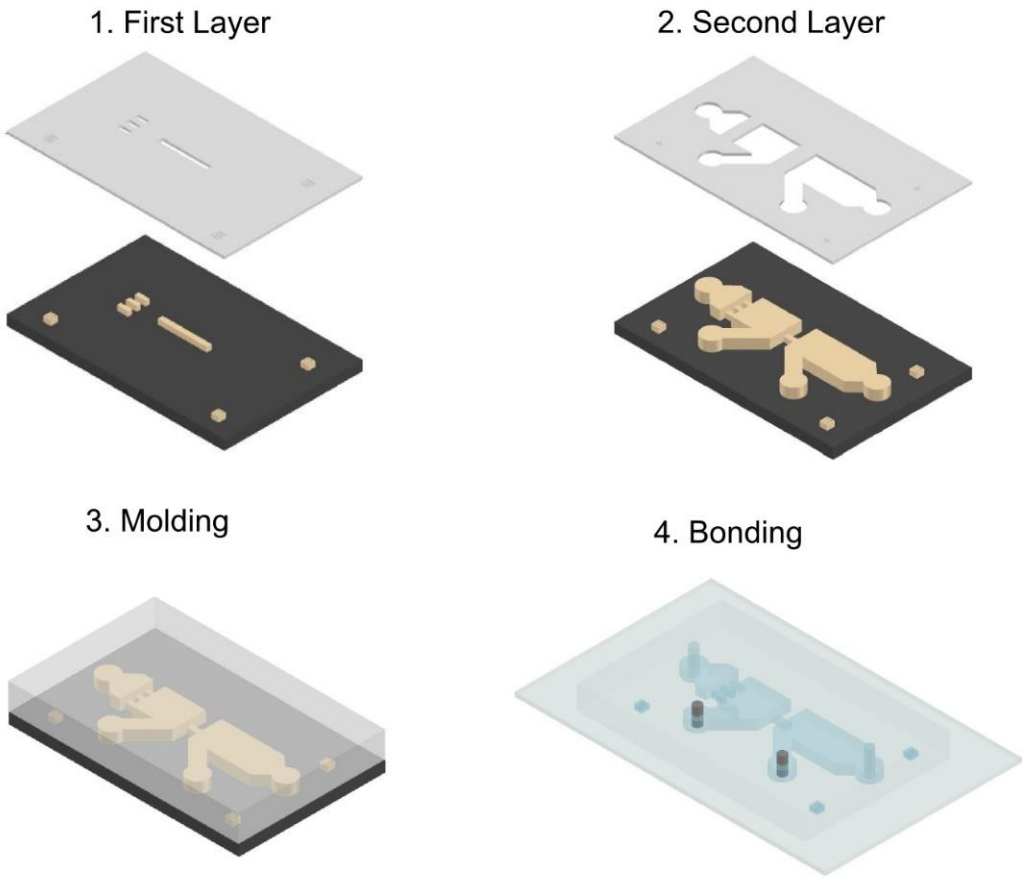

Figure 3.3 Fabrication process of the two-layer SU8 mold and the micro resistive pulse sensor

The fabrication process of the two-layer SU8 mold and the micro resistive pulse sensor are shown in Figure 3.3. Firstly, a 10 μm thick SU8-5 layer was spin coated on a silicon wafer followed by a photolithograph step to define the pattern of the sensing channel and the filter; then the second layer of SU8-2025 (40 μm thick) was spin coated on top of the first layer to fabricate the reservoirs. Next, polydimethylsiloxane (PDMS)

was poured onto the two-layer SU8 mold, degassed and cured to form the microchannel. Inlet and outlet holes were punched to load and unload the sample. Two holes located on each side of the sensing channels were punched on the PDMS slab for insertion of the inlet/outlet tubing and a pair of Ag/AgCl electrodes. Finally, the PDMS channel was bonded to a glass slide via plasma treatment, and a pair of Ag/AgCl electrodes were inserted in the punched electrode holes to make the final device.

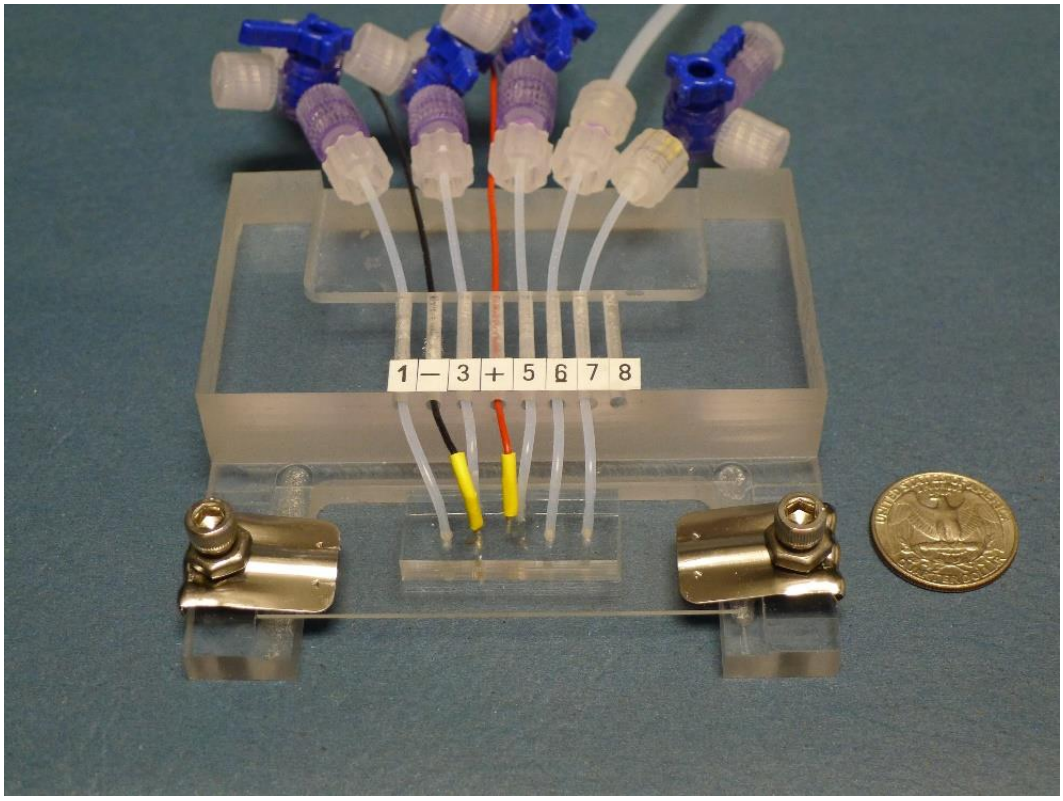

Figure 3.4 Picture of the micro resistive pulse sensor with fluidic connections and a pair of Ag/AgCl electrodes (black and red wires in the picture)

The fluidic connections are shown in Figure 3.4. The black and red wires were connected with Ag/AgCl electrodes, as shown in Figure 3.2 (a). The #1 and #6 tubing were

connected to the outlet reservoir and inlet reservoir, respectively. The other tubing were only used for cleaning purpose after each test.

3.2.2 Calibration

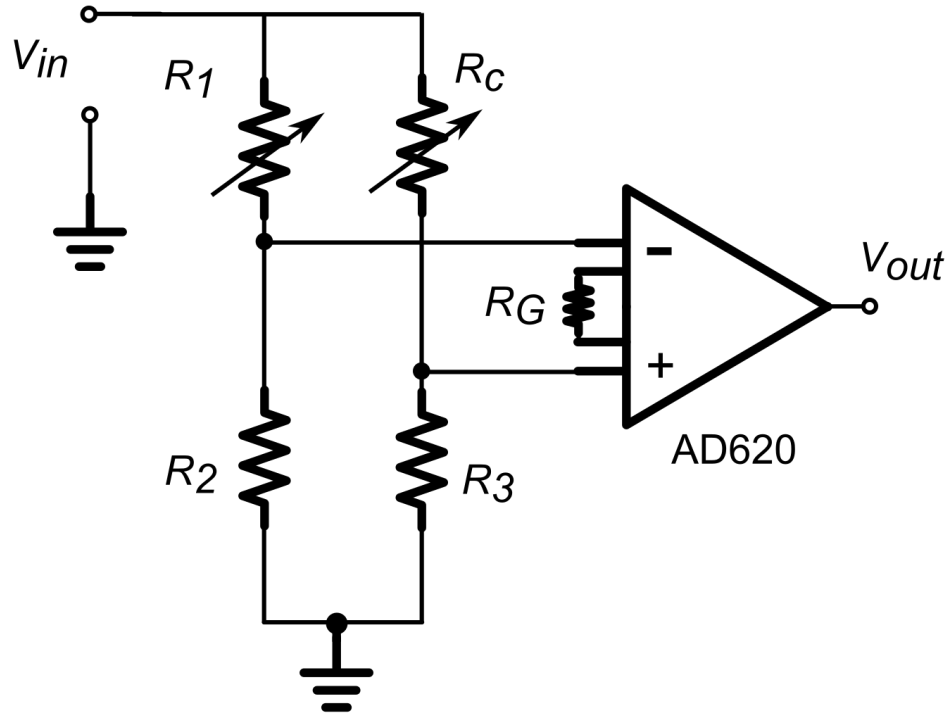

Figure 3.5 Measurement circuit for the micro resistive pulse sensor

The measurement circuit for the resistive pulse sensor chip is shown in Figure 3.5. The micro resistive pulse sensor is modeled as a variable resistor *Rc*; Resistors $R_2 = R_3 =$ 500 kΩ. A variable resistor R_1 ranging from 500 kΩ to 1 MΩ was set to match *Rc*. The gain of the differential amplifier, AD620, was programmed to be 50 using an external gain resistor $R_G = 1$ kΩ. The input DC voltage, $V_{in} = 2.4$ V, was provided by a function generator (33220A, Agilent). The output signal was recorded by a data acquisition card (NI USB-

6251, National Instruments) at a sampling rate of 1 MHz. Finally, a custom peak detection algorithm (Matlab, MathWorks) was used to count the resistive pulses and back calculate the particle size.

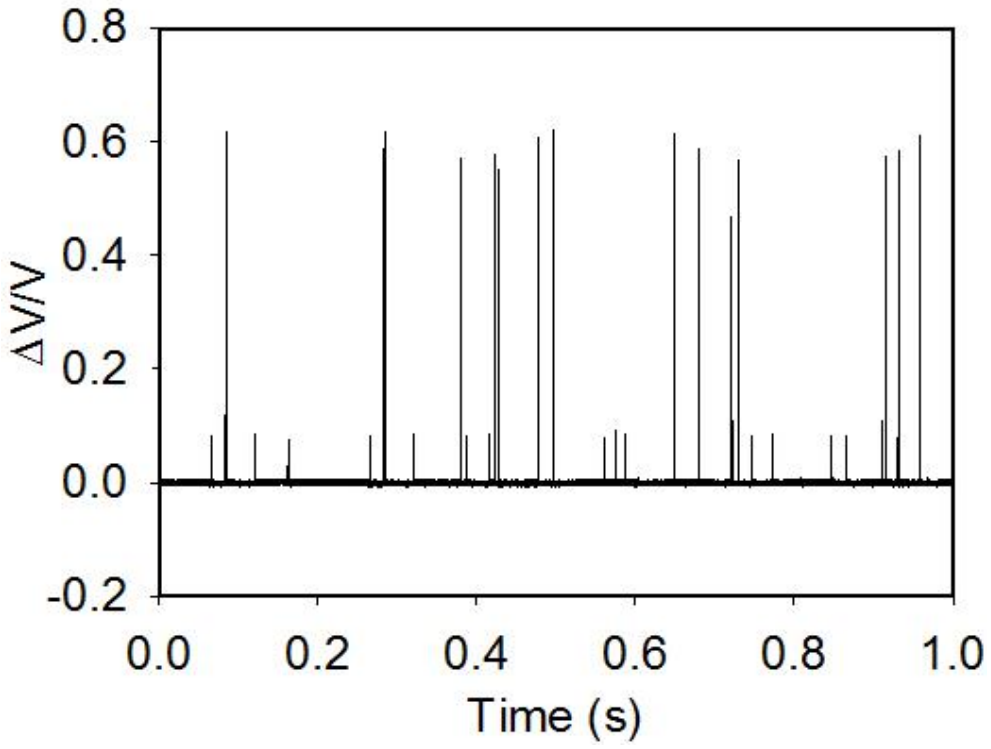

Figure 3.6 Typical resistive pulses caused by particle passages. Each pulse represents one particle passing through the sensing channel. Small and large pulses represent 2.80 μm and 5.00 μm MPs

Figure 3.6 shows the typical relative pulse caused by the passage of MPs. Each pulse represents one particle passing through the sensing channel. The amplitude of each pulse is proportional to the volume of the particle. Small and large pulses represent 2.80 μm and 5.00 μm MPs, respectively. The particle sizes were back calculated using equation 3.1 [191] [109]:

$$\delta R/R = \left(d^3/LD^2\right)\cdot\left[\left(D^2/2L^2\right)+1\Big/\sqrt{1+\left(D/L\right)^2}\right]\cdot F\left(d^3/D^3\right) \qquad (3.1)$$

where R is the resistance of the sensing channel, d is the diameter of the particle, D and L are the characteristic diameter and the length of the rectangular sensing channel and F is the correction factor. In our design, D was calculated to be 11.29 μm using $D = (4 \cdot A/\pi)^{1/2}$, where A is the cross-sectional area of the sensing channel. F was taken to be 1.0 [109].

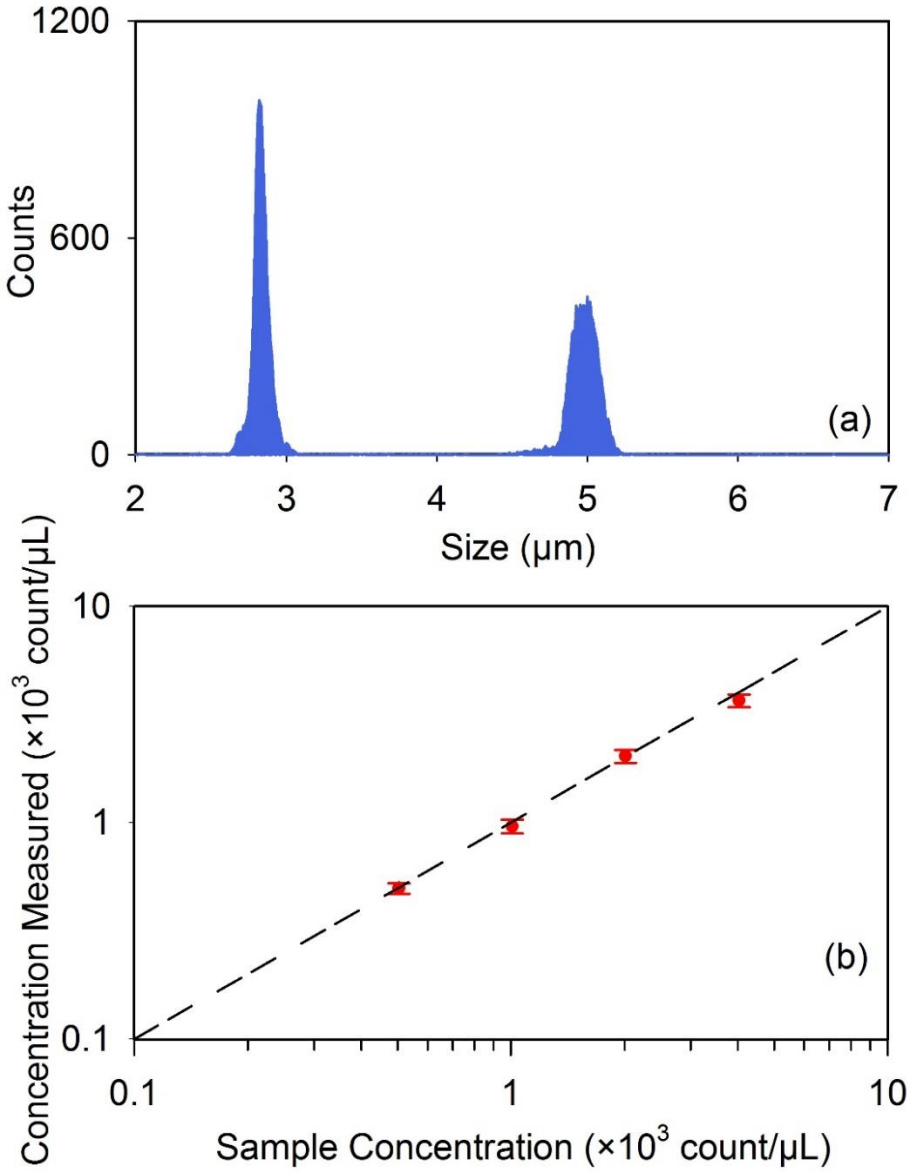

Figure 3.7 Calibration of sizing and counting performance of the resistive pulse sensor. (a) 2.80 μm and 5.00 μm MPs were used for the sizing calibration; (b) 2.80 μm MP with four concentrations were used for the counting calibration

Two kinds of MP were used to calibrate the counting and sizing performances of the resistive pulse sensor. The diameters of MPs are 2.80 μm (Dynabeads M-280, Life Technologies, USA) and 5.00 μm (79633 FLUKA, Sigma Aldrich). The measured sizes, which were back calculated from the resistive pulses using equation (3.1), were 2.80 ± 0.16 μm and 4.91 ± 0.37 μm, as shown in Figure 3.7 (a). The sizing error of the micro resistive pulse sensor was less than 2%. For the concentration calibration, 2.80 μm MPs with four concentrations of 500 count/μL, 1000 count/μL, 2000 count/μL and 4000 count/μL were tested separately. The concentration was calculated by dividing the number of particles (resistive pulses) by the volume of the flow within the same time duration. As shown in Figure 3.7(b), the measured concentrations were 497 ± 28 count/μL, 960 ± 70 count/μL, 2025 ± 138 count/μL and 3657 ± 240 count/μL, which are in good agreement with the actual MP concentrations (the counting error was less than 9%.).

3.3 Study of a model biomarker immunoaggregation assay

To prove that the presence of a target biomarker is able to trigger the aggregation of antibody functionalized MPs, goat anti-rabbit IgG, as a model biomarker, was employed in this section. The concentration of goat anti-rabbit IgG ranged from 16.0 to 320.0 ng/mL. To prepare antibody functionalized MPs (Ab-MPs), the biotinylated rabbit anti-goat IgG antibody (Ab) were conjugated to 2.80 μm MPs (MP, Dynabeads M280, Life Technologies, USA). The details of sample preparation were reported in our previous paper [1]. The Ab-MPs concentration was 1.74×10^3 count/μL. At each test, 100.0 μL of goat anti-rabbit IgG was mixed with 100.0 μL of Ab1-MP1s for 30 mins to form the aggregates. The aggregates

were then driven through the micro resistive pulse sensor with a syringe pump (KDS Legato 270, KD Scientific) at flow rate of 100.0 µL/hr. It is worth mentioning here at current flow rate, the typical particle transit time was about 0.1 ms, and about 100 data points were acquired to ensure the detection of a particle passage.

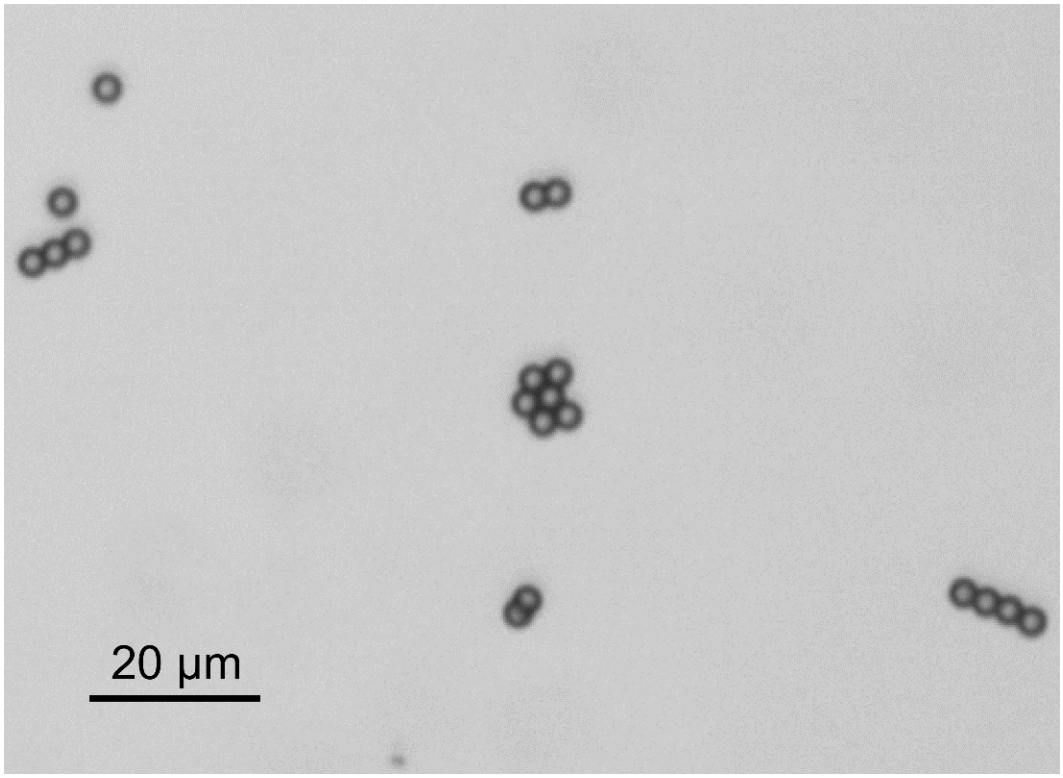

Figure 3.8 The optical image of singlet Ab-MPs and Ab-MP aggregates at Ab-MPs concentration of 1.74×10^3 count/µL and the goat anti-rabbit IgG concentration of 160 ng/mL

Figure 3.8 shows the optical image of an Ab-MPs singlet and formed Ab-MP aggregates. The microscopy image proved the formation of immunoaggregates. As discussed earlier, the volume fraction of immunoaggregates, defined as the volume ratio of aggregates to all detected MPs, represents the levels of goat anti-rabbit IgG concentration. Next, the micro resistive pulse sensor was used to detect a large population of

immunoaggregates in order to accurately calculate the volume fraction. It is worth mentioning here that in a resource limited area, examination of aggregates under a light microscope is an alternative solution for immunoaggregation assays with drawbacks such as labor intensive and low accuracy. To prove the micro resistive pulse sensor is able to differentiate singlet Ab-MPs, doublet Ab-MPs and triplet Ab-MPs. The measured resistive pulses are shown in Figure 3.9.

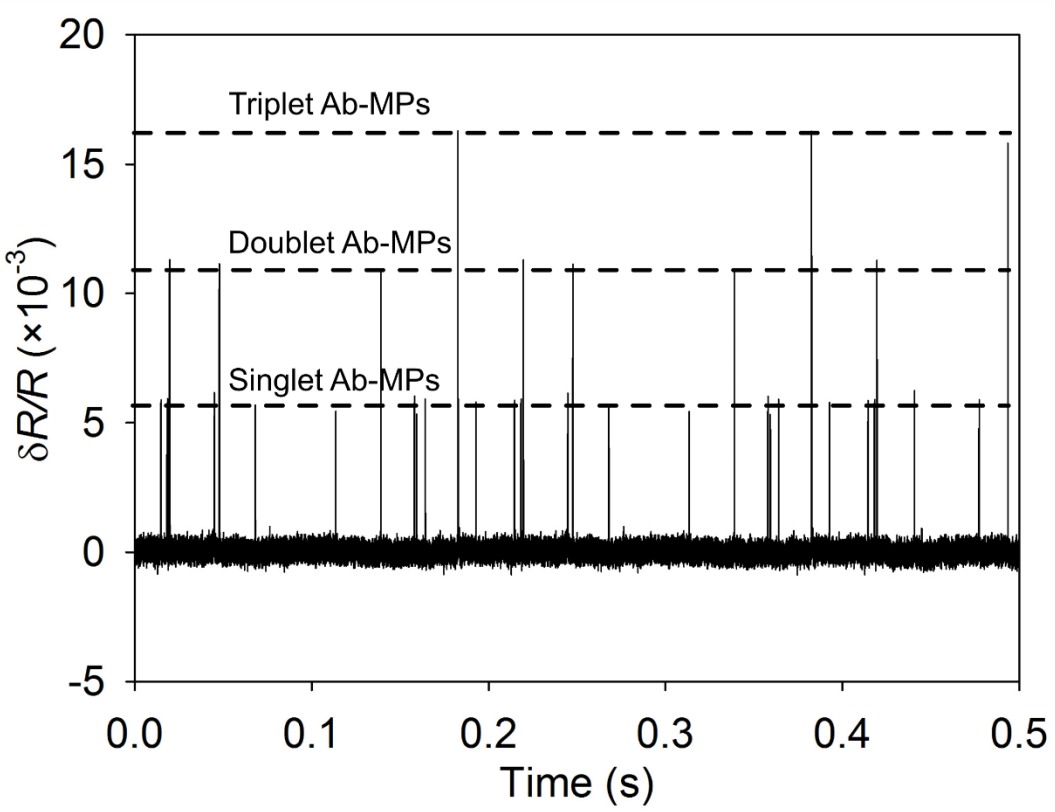

Figure 3.9 Relative resistive pulses caused by Ab-MP singlets, Ab-MP doublets and Ab-MP triplets at Ab-MPs concentration of 1.74×10^3 count/μL, and the goat anti-rabbit IgG concentration of 160 ng/mL

As discussed previously, accurate measurement of Ab-MP doublets can improve the sensitivity of immunoaggregation assays [102]. Figure 3.9 shows the clear difference

between Ab-MP singlets and two types of Ab-MP aggregates, this proves that the micro resistive pulse sensor chip is very sensitive to the size change compared with other optical sizing methods [51], [101]. Although we observed aggregates formed by more than three Ab-MPs under the light microscope, the small amount of aggregate was unable to represent the real volume fraction of aggregates. This also proves that a micro resistive pulse sensor, which is able to detect a large number of particles in a short time, has a higher accuracy than optical detection.

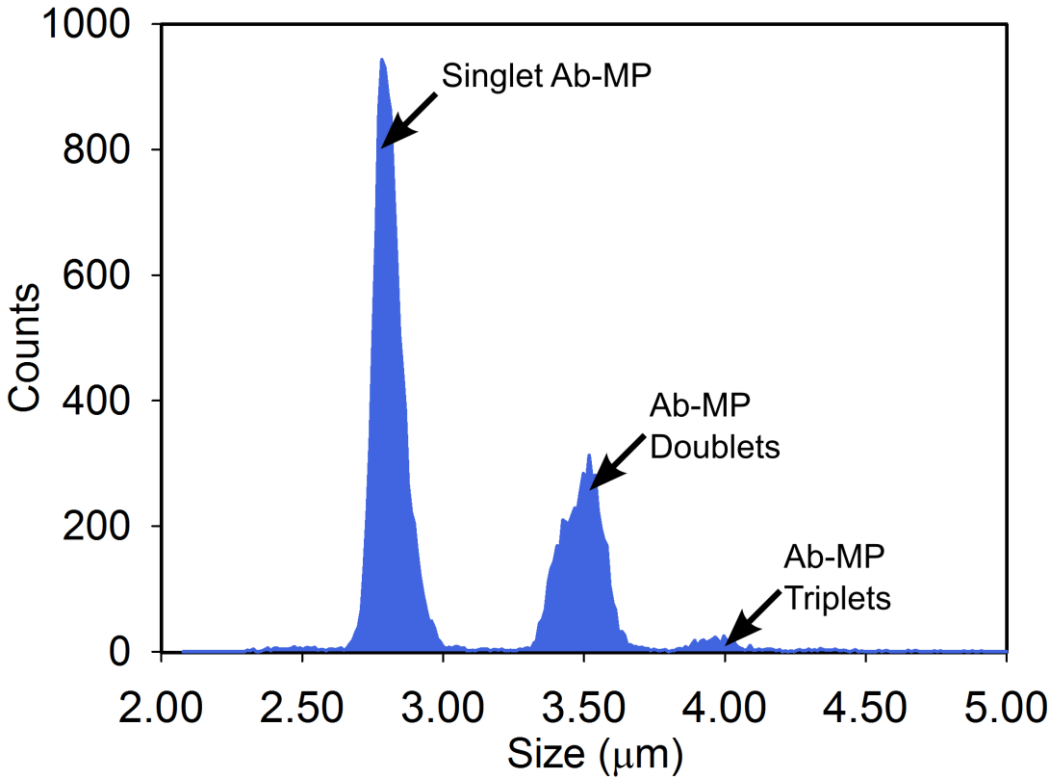

Figure 3.10 Size and count distribution of Ab-MP at goat anti-rabbit IgG concentration of 160 ng/mL. The volume fractions of aggregates was 40.3%

Figure 3.10 shows the aggregate size distribution at a biomarker concentration of 160 ng/mL. From Figure 3.10, the number of aggregates with more than three Ab-MPs was

very small. This proves that 1) the filter has a minor effect in blocking Ab-MP aggregates; and 2) the sensing channel with 10 × 10 μm cross section is suitable for 2.80 μm Ab-MP aggregate detection. In the above tests, a total of 16.2×10^3 particles were detected in less than 15 mins. To prove the volume fraction of aggregates represents the level of biomarker concentration, similar experiments were conducted with goat anti-rabbit IgG concentrations ranging from 16.0 to 320 ng/mL, while the Ab-MPs concentration (1.74×10^3 count/μL) was kept constant. Each goat anti-rabbit IgG concentration was repeated five times to ensure accuracy. A control experiment was also conducted to evaluate nonspecific aggregation. Without adding goat anti-rabbit IgG to the Ab-MPs solution, the volume fraction of nonspecific aggregation was 11.0 ± 2.6 %.

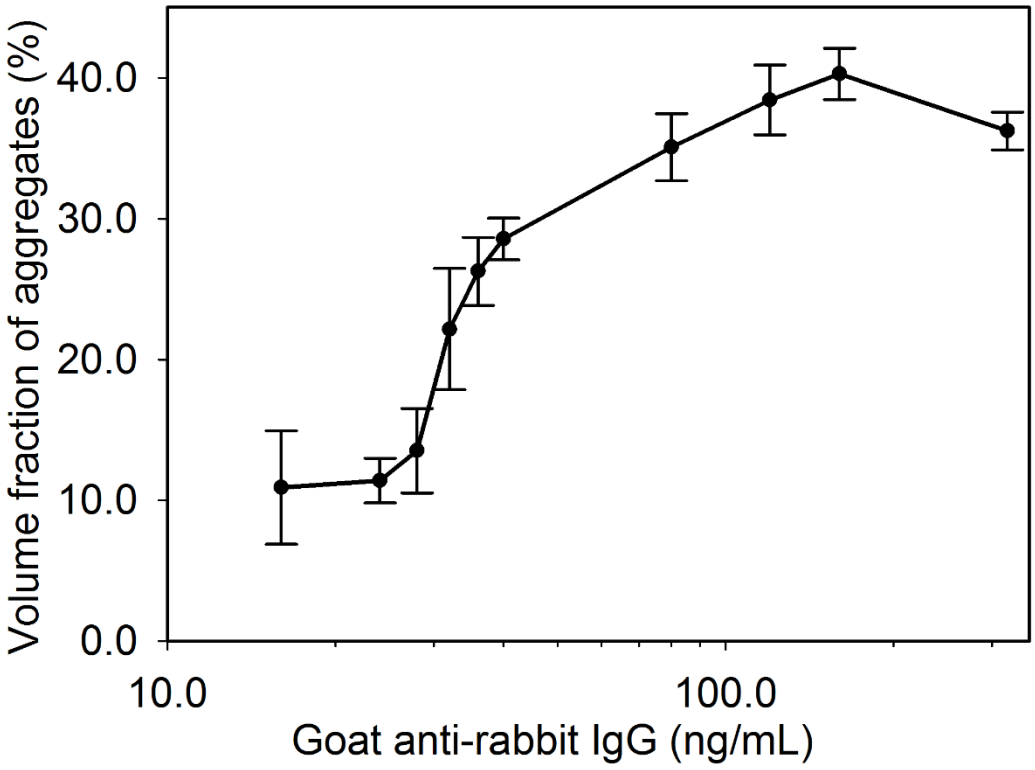

Figure 3.11 Volume fraction of Ab-MP aggregates as a function of goat anti-rabbit IgG concentrations ranging from 16.0 to 320 ng/mL

As shown in Figure 3.11, as the goat anti-rabbit IgG concentration increased from 16.0 to 320 ng/mL, the aggregation ratio was increased from 10.9 to 40.3%. Note that at a high biomarker concentration > 320 ng/mL, the biomarkers occupied all the binding sites of the antibody for forming the aggregates; hence the volume fraction started to drop. The above test results demonstrated the feasibility of the immunoaggregation assay based on the micro resistive pulse sensor for sensitive biomarker detection.

3.4 Summery

The design concept and sensing principle of the immunoaggregation assay and micro resistive pulse sensor has been demonstrated in this Chapter. The goat anti-rabbit IgG, as a model biomarker, successfully caused the immunoaggregation of rabbit anti-goat IgG antibody factionalized MPs. A detection range from 16.0 to 160 ng/mL was achieved. The volume fraction of immunoaggregation increases with an increase in biomarker concentration. However, at high biomarker concentrations, the saturation of the binding sites prevents the formation of immunoaggregates. The above tests showed that the immunoaggregation assay performed with a micro resistive pulse sensor is able to quantitatively detect biomarker concentrations.

CHAPTER IV

HUMAN FERRITIN IMMUNOAGGREGATION ASSAY

4.1 Study of human ferritin immunoaggregation assay

In Chapter III, the design concept and sensing principle of the micro resistive pulse immunoaggregation sensor were proved using goat anti-rabbit IgG as a model biomarker. In this chapter, the micro resistive immunoaggregation sensor was applied to human ferritin detection. Ferritins are a class of iron storage proteins and they are widely distributed in vertebrates, invertebrates, plants, fungi and bacteria. For humans, an increase in iron levels can promote the growth of a wide variety of tumors and infectious microorganisms [1]. Ferritin measurement is considered the most reliable method for the evaluation of iron stores in serum [193].

To prepare anti human ferritin antibody functionalized MPs (Ab-MPs), streptavidin-functionalized magnetic MP were conjugated with biotinylated anti ferritin antibody (Ab, US 152 Biological, USA) through streptavidin-biotin binding. Three Ab-MP concentrations were prepared which were 0.880×10^3, 3.50×10^3 and 14.0×10^3 count/μL. Human ferritin (US Biological, 164 USA) concentrations ranged from 0.104 to 416 ng/mL At each test, 333.4 μL of Ab-MP solution was mixed with 166.7 μL of human ferritin solution at different concentrations for 30 min in a thermal mixer at a speed of 650 rpm at

room temperature. Then, the sample solutions were loaded into the micro resistive pulse immunoaggregation sensor using a syringe pump (KDS Legato 270, KD Scientific) at flow rate of 80 μL/hr. The measurement setup shown in Figure 3.5 was used in this test.

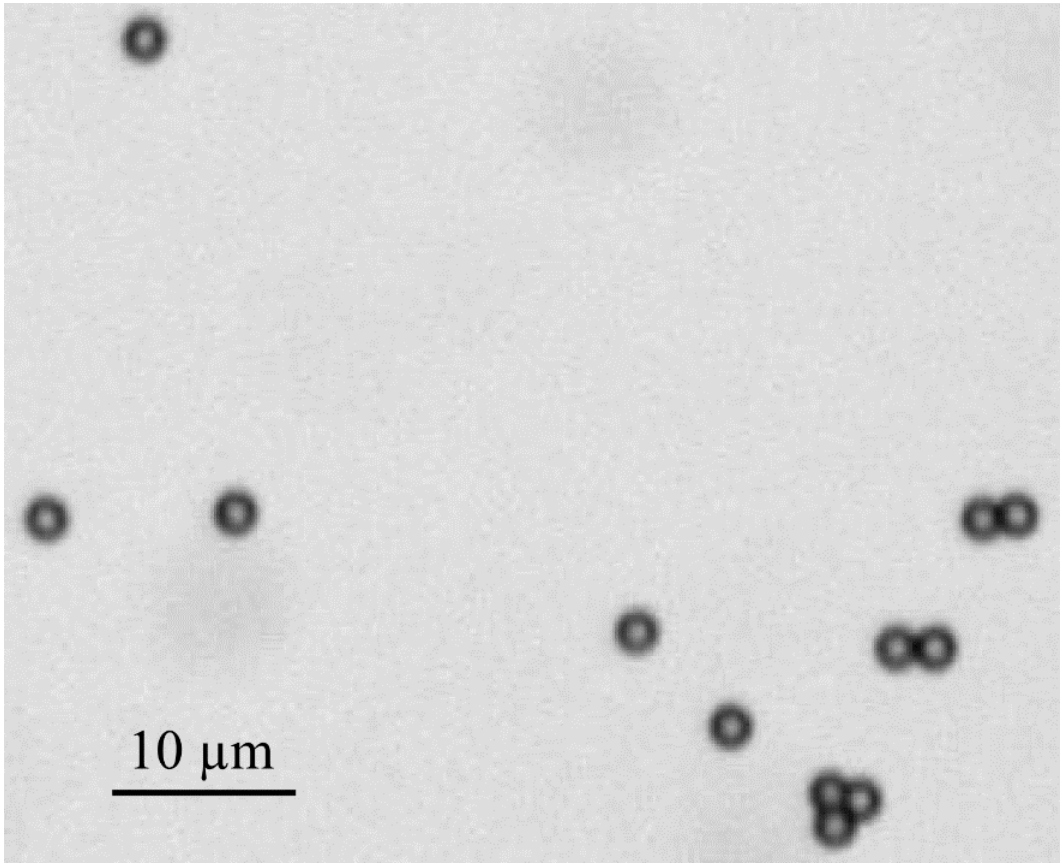

Figure 4.1 The microscopy image of Ab-MP aggregates formed at human ferritin concentration of 41.6 ng/mL and Ab-MP concentrations of 3.50×10^3 count/μL

The formation of immunoaggregates were confirmed under the light microscope. Figure 4.1 shows the immunoaggregates formed by Ab-MPs at human ferritin concentration of 41.6 ng/mL and Ab-MP concentration of 3.50×10^3 count/μL. The counts and size distributions of Ab-MP aggregates were measured by the micro resistive pulse sensor and plotted in Figure 4.2.

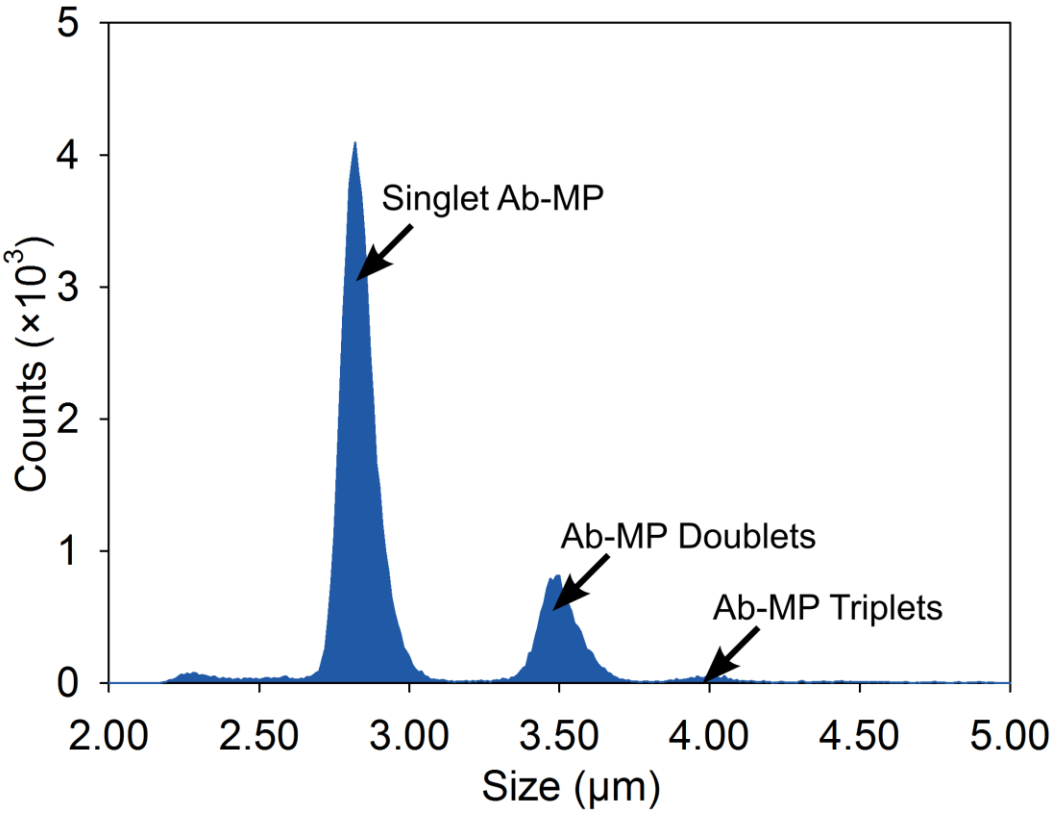

Figure 4.2 Counts and size distribution of Ab-MP singlets and aggregates at human ferritin concentration of 41.6 ng/mL and Ab-MP concentrations of 3.50×10^3 count/μL

Figure 4.2 shows the counts and size distributions of Ab-MP aggregates at a ferritin concentration of 41.6 ng/mL. From left to right, three peaks centered at 2.80 ± 0.21 μm, 3.50 ± 0.19 μm and 3.98 ± 0.12 μm represent the Ab-MP singlets, Ab-MP doublets and Ab-MP triplets, as marked in Figure 4.2. The calculated equivalent spherical diameter (ESD) of Ab-MP doublets and triplets are 3.53 μm and 4.04 μm, respectively, which matched well with the measured results. It is worth mentioning here that the volume fraction of aggregates formed by more than three Ab-MPs compared to all aggregates/particles was less than 1%, which can barely be seen in Figure 4.2. The narrow size distribution of aggregates may provide a higher multiplexing capability when the

particle size is used as an encoding property. Because the detection limit of the immunoaggregation method is mainly controlled by nonspecific aggregation, Ab-MP solution without any human ferritin was used to evaluate nonspecific aggregation, as shown in Figure 4.3.

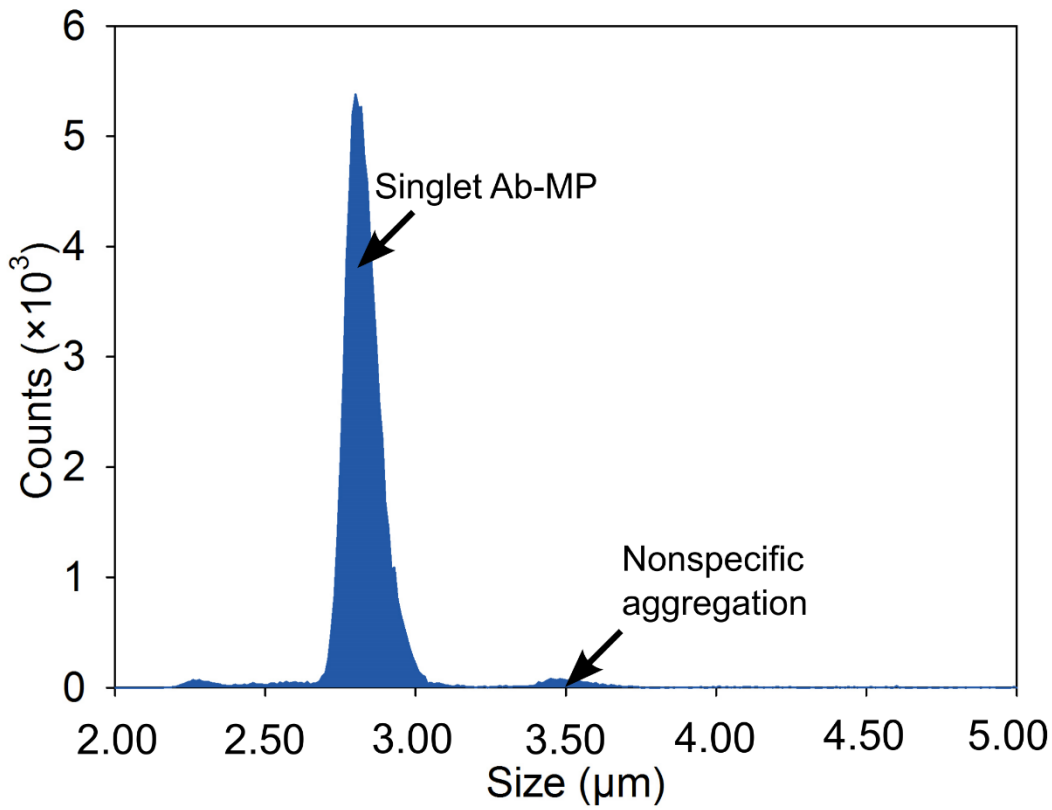

Figure 4.3 Counts and size distribution of Ab-MP nonspecific aggregation at Ab-MP concentration of 3.50×10^3 count/μL

Figure 4.3 shows counts and size distribution of Ab-MP nonspecific aggregation. When the Ab-MP concentration is 3.50×10^3 count/μL, the volume fraction of nonspecific Ab-MP aggregates is 0.051 ± 0.006. Next, similar tests were conducted at various human ferritin concentrations ranging from 1.04 ng/mL to 208 ng/mL. The Ab-MP were kept at a constant concentration of 3.50×10^3 count/μL. The counts of singlet Ab-MP and Ab-MP

aggregates were obtained using the same procedure. After the nonspecific aggregates were subtracted from the measured immunoaggregates, the volume fractions of Ab-MP aggregates at different ferritin concentrations were plotted in Figure 4.4, as a function of the ferritin concentration. To ensure repeatability, at each ferritin concentration, 10 immunoaggregation samples were prepared and measured.

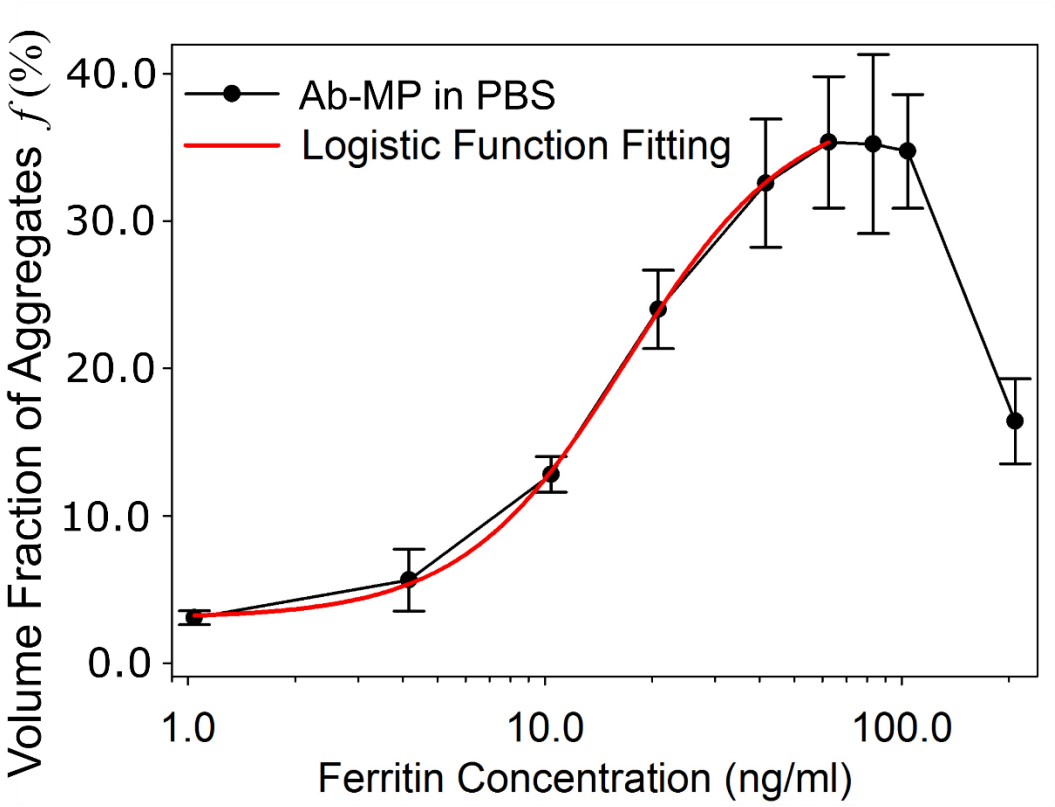

Figure 4.4 The volume fraction of Ab-MP aggregates at various human ferritin concentrations ranging from 1.04 to 208.0 ng/mL. The Ab-MP concentration was 3.50×10^3 count/μL

As shown in Figure 4.4, the measurement curve in the range from 1.0 ng/mL to 62.4 ng/mL can be fitted with a logistic function:

$$f_1(x) = 0.034 + \frac{0.358}{1 + (x/15.935)^{-2.126}} \tag{4.1}$$

where the coefficient of determination (R^2) of the fitted curve is 0.998. As shown in Figure 4.4, the volume fraction of aggregates, f_1, increased with the increase of ferritin concentration, x, in the range from 1.04 ng/mL to 62.4 ng/mL. The maximum volume fraction (35.4%) occurred at 62.4 ng/mL. Above 62.4 ng/mL, f_1 reduced with the increase in the ferritin concentration. This is because higher ferritins concentrations saturated the binding sites on the Ab-MPs and prevented the formation of Ab-MP aggregates.

Disease related biomarkers are often isolated from a complexing media such as blood, urine, etc. [193]. One long-standing challenge for biomarker detection in a complex media is the nonspecific binding between non-target molecules to capture probes. In order to prove that nonspecific binding has a negligible effect on the human ferritin immunoaggregation assay, 10% fetal bovine serum (FBS, Sigma-Aldrich, USA) was used as a complex media to mimic a real disease diagnosis condition. First, in order to evaluate the nonspecific aggregation, samples containing 10% FBS without any human ferritin were mixed with 3.50×10^3 count/μL of Ab-MPs solution, then tested by the micro resistive pulse sensor. To ensure accuracy, five samples were prepared and tested. The volume fraction of nonspecific aggregates was 0.054 ± 0.011. As discussed previously, without adding 10% FBS, the volume fraction of nonspecific aggregates was 0.051 ± 0.006. Thus, the 10% FBS has a negligible effect on nonspecific aggregates. To prove the micro resistive pulse sensor is able to quantitatively detect human ferritin in a complex media, samples containing 10% FBS and human ferritin ranging from 0.104 ng/mL to 104 ng/mL was mixed with 3.50×10^3 count/μL of Ab-MP solution, then tested by the micro resistive pulse sensor. To ensure accuracy, at each human ferritin concentration, 10 samples were prepared

and tested. The relationships between human ferritin concentration and volume fraction of aggregates is shown in Figure 4.5.

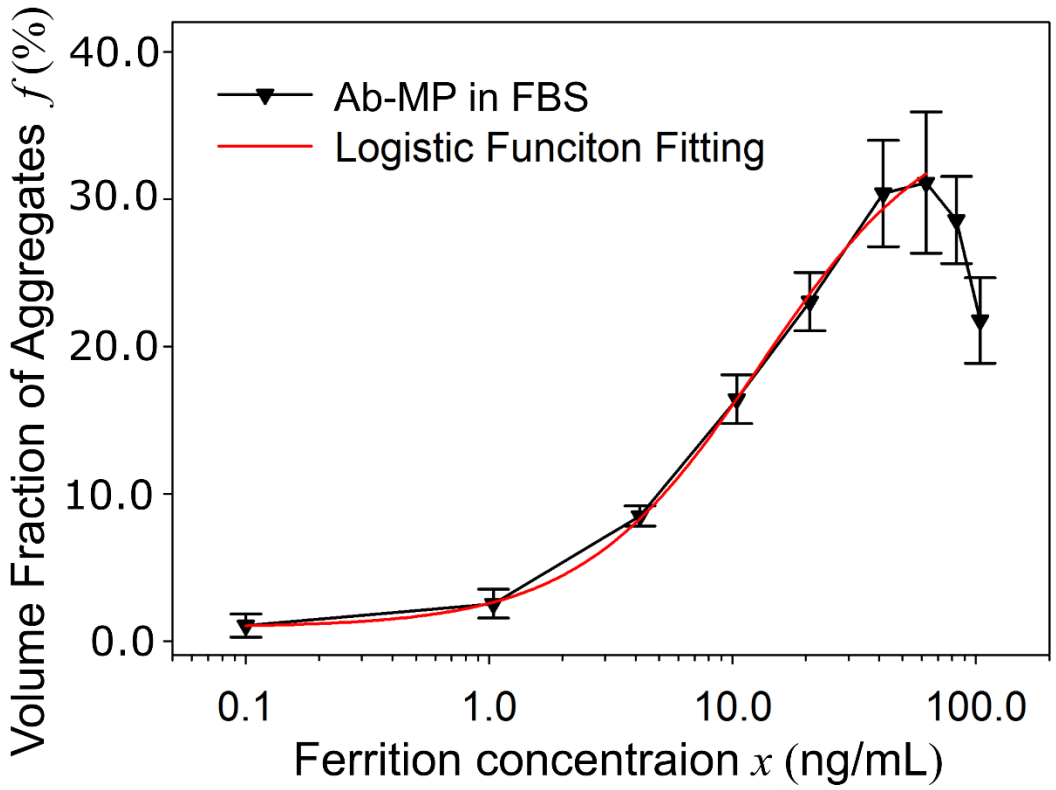

Figure 4.5 The volume fraction of Ab-MP aggregates as a function of human ferritin concentrations ranging from 0.104 to 104 ng/mL. The Ab-MPs concentration was 3.50×10^3 count/μL

The measurement curve in the range from 0.104 ng/mL to 62.4 ng/mL in Figure 4.5 can be fitted with a logistic function:

$$f_2(x) = 0.009 + \frac{0.356}{1 + (x/12.964)^{-1.183}} \tag{4.2}$$

The coefficient of determination (R^2) of the fitted curve is 0.999. As shown in Figure 3.14, the volume fraction of aggregates, f_2, increased with an increase of ferritin concentration, x, in the range of 0.104 ng/mL to 62.4 ng/mL; the maximum volume fraction (31.1%)

occurred at 62.4 ng/mL. Without adding 10% FBS to the Ab-MP solution, the maximum volume fraction (35.4%) also occurred at 62.4 ng/mL, as shown in Figure 4.4. This indicates that the detection range is not affected by FBS. Hence the micro resistive pulse immunoaggregation sensor can be used for biomarker detection in complexed media. The limit of detection (LOD) is the smallest biomarker concentration that has a volume fraction of specific aggregation significantly larger than the volume fraction of nonspecific aggregation. The volume fraction of aggregates at the limit of detection (f_{LOD}) is given by:

$$f_{LOD} = f_0 + 3 \times \sigma_0 \tag{4.3}$$

where f_0 is the volume fraction of nonspecific aggregates. σ_0 is the standard deviation of the nonspecific aggregation. For the experiment shown in Figure 4.4, f_0 = 5.1%, σ_0 = 0.6%. Thus, f_{LOD} = 6.9%. By using equation 4.2, the detection limit of human ferritin is 0.6 ng/mL. Note that the volume fraction of nonspecific aggregates, 5.1%, was subtracted from f_{LOD} before using equation 4.2.

4.2 Tunable detection range with multiple microparticle concentrations

It is hypothesized that the Ab-MPs concentration may affect the detection range because: 1) a higher Ab-MP concentration provides a larger total surface area and larger number of binding sites and hence is able to capture more biomarkers, which may result in a larger upper detection limit; 2) a lower concentration of Ab-MPs with limited binding sites is easily saturated, and hence may have a better detection resolution for detection of low concentration biomarkers. To prove this hypothesis, three Ab-MP concentrations (0.880×10^3, 3.50×10^3 and 14.0×10^3 count/μL.) were evaluated using human ferritin

with concertation ranging from 0.104 ng/mL to 416 ng/mL in 10% FBS. To ensure accuracy, at each human ferritin concentration, 10 samples were prepared and tested. The results are shown in Figure 3.15. It is worth mentioning here that, before this test, 10% FBS without human ferritin was mixed with three concentrations of Ab-MPs as negative controls to evaluate the nonspecific aggregation. At each Ab-MP concentration, the five negative controls were prepared and tested. Volume fractions of nonspecific aggregates for the negative controls were 0.045 ± 0.008, 0.054 ± 0.011 and 0.049 ± 0.002 for Ab-MP concentrations of 0.880×10^3, 3.50×10^3 and 14.0×10^3 count/μL, respectively, which were close to that in PBS at the concentration of 3.50×10^3 count/μL. The results proved that 1) Ab-MPs are stable in the complex medium, and 2) the change of Ab-MP concentrations has a negligible effect on nonspecific aggregation.

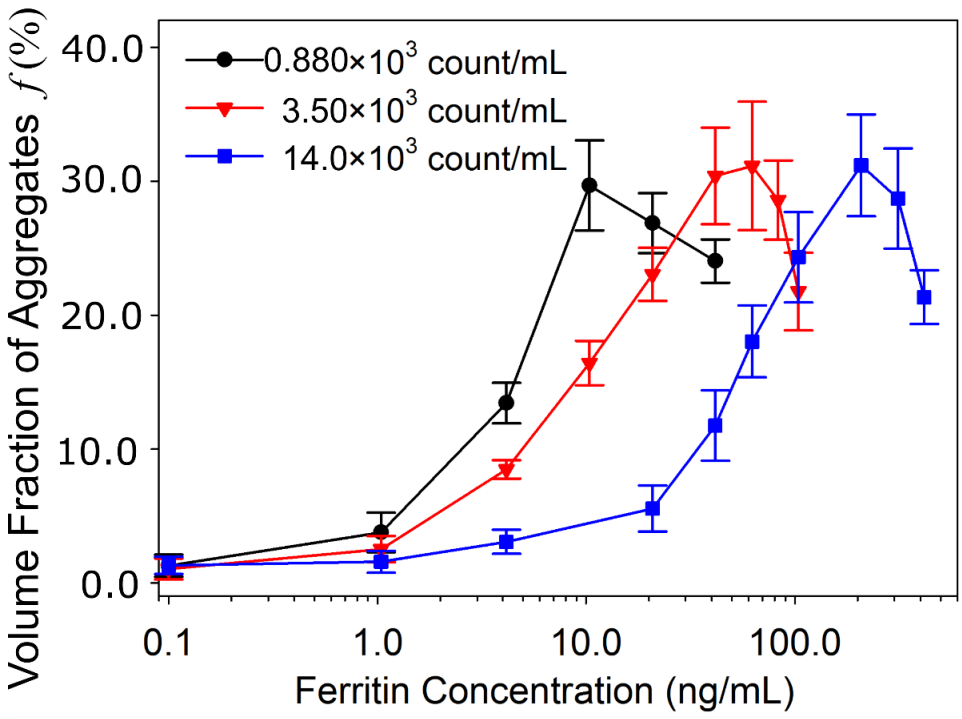

Figure 4.6 The volume fraction of Ab-MP aggregates as functions of human ferritin concentrations ranging from 0.104 to 416 ng/mL

The three curves shown in Figure 4.6 were also fitted with logistic functions from 0.104 ng/mL to the peak position. The R^2 was greater than 0.998. For the three Ab-MP concentrations, 0.880×10^3 (black line), 3.50×10^3 (red line) and 14.0×10^3 count/μL (blue line), the detection ranges were 0.104 to 10.4 ng/mL, 0.104 to 62.4 ng/mL and 0.104 to 208 ng/mL, respectively. This proves that the use of a higher Ab-MP concentration is able to increase the upper detection limit for detection of high concentration biomarkers. In comparison, the detection range shifted to lower concentrations when a low Ab-MP concentration was used, because low concentration Ab-MPs only have limited binding sites and are easily saturated. The maximum volume fractions of aggregates were 29.7%, 31.1% and 31.2% for Ab-MP concentrations of 0.880×10^3, 3.50×10^3 and 14.0×10^3 count/μL. The maximum volume fractions of aggregates of these three Ab-MP concentrations were close to each other. Thus, with a reduced detection range, a lower Ab-MP concentration was more sensitive to a lower biomarker concentration, as shown in Figure 4.6. For example, for a ferritin concentration ranging from 0.104 ng/mL to 10.0 ng/mL, the use of a low Ab-MP concentration (black curves) was able to differentiate the difference in ferritin concentration, while the use of high Ab-MP (red and blue curves) concentrations was unable to. Thus, the sensitivity and detection range of the immunoaggregation assay are tunable by adjusting Ab-MP concentrations. Another alternative method to detect the higher biomarker concentration is to serial dilute the sample and detect using lower microparticle concentration. It is worth mentioning here, the dilution process has a negligible effect on the immunoaggregation.

Compared with currently available ELISA kits, as listed in Table 3.1, the micro resistive pulse immunoaggregation sensor has a low limit of detection, at 0.60 ng/mL. To

further decrease the lower detectable biomarker concentration, one possible solution is to use aptamer functionalized micro particles with higher binding affinity to the given biomarker, which is expected to improve the volume fraction at lower biomarker concentration. The lower and upper detection limits can be extended by decreasing and increasing the concentrations of Ab-MPs. Without any labeling process, the immunoaggregation assay has less assay steps, and takes less than 1 hour. In comparison, the conventional ELISA method takes several hours to a day to complete. The estimated cost of an immunoaggregation assay (~$10), is comparable with the cost of a commercial ELISA test. However, the microplate photometer for ELISA costs a few thousand dollars, while a resistive pulse sensor chip only requires a portable and cost-effective electronic data acquisition device, which costs less than $100.

Table 3.1 Commercial available human ferritin ELSA kits

Products	Detection limit (ng/ml)	Vendors
ab108837	1.6	Abcam
25 FERHU E01	5.0	ALPCO
FER31-K01	6.0	Eagle Biosciences
RCAN-F-4280R	7.5	BioVendor

4.3 Summery

In this Chapter, the micro resistive pulse sensor was used to detect human ferritin concentrations in a complex media. A detection range from 0.104 to 208 ng/mL was achieved. The lower limit of detection, 0.1 ng/mL, is lower than that of commercial ELISA

kits. The test results also indicated that antibody functionalized MPs were stable in 10% fetal bovine serum (FBS) and adding 10% FBS had a negligible effect of nonspecific aggregation. In addition, the detection range can be shifted to lower and higher biomarker concentrations by decreasing and increasing MP concentrations.

CHAPTER V

MULTIPLEXED IMMUNOAGGREGATION ASSAY

5.1 The design concept of the multiplexed immunoaggregation assay

The studies shown in Chapters III and IV have shown that the micro resistive pulse immunoaggregation sensor is able to quantitatively detect biomarker with high sensitivity. Two types of macromolecule, goat anti-rabbit IgG and human ferritin, were detected separately. To detect multiple biomarkers simultaneously, a multiplexed immunoaggregation assay is studied in this Chapter, based on size and the magnetic properties of MPs.

5.1.1 The design concept and sensing principle

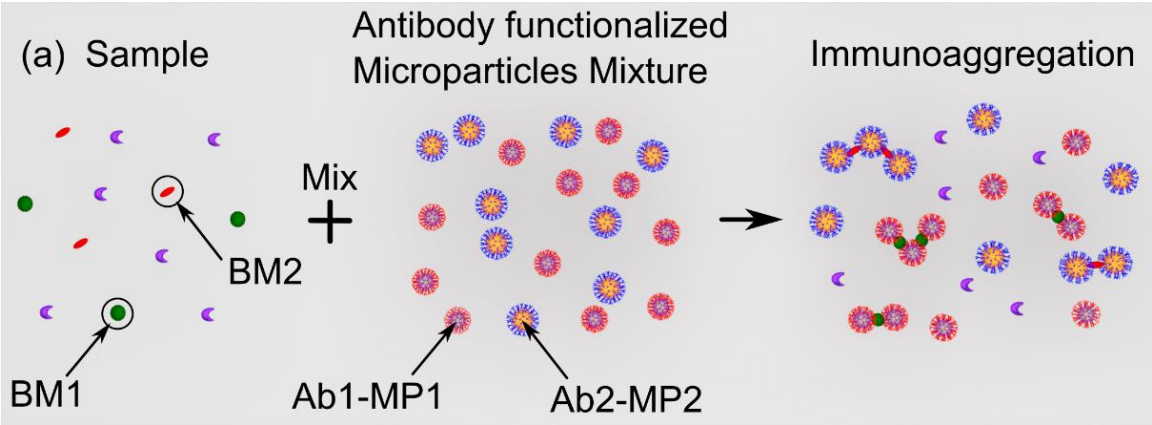

Figure 5.1 Schematic of the multiplexed immunoaggregation assay mechanism

Figure 5.1 shows the multiplexed immunoaggregation assay mechanism. Two types of Ab-MPs are used to detect two types of biomarker (BMs). Firstly, the sample solution containing two target biomarkers, BM1 and BM2, is mixed with the mixture of antibody functionalized MPs, Ab1-MP1 and Ab2-MP2. Ab1, immobilized on Ab1-MP1s is specific to the biomarker BM1. Thus, the presence of BM1 triggers the aggregation of Ab1-MP1s. The volume fraction of Ab1-MP1 aggregates to all detected Ab1-MP1s represents the concentration of BM1. Similarly, BM2 causes the aggregation of Ab2-MP2 due to the specific binding between BM2 and Ab2, and the volume fraction of Ab2-MP2 aggregation is indicative of BM2 concentration. The two-stage resistive pulse sensor (two-stage RPS) is used to differentiate Ab1-MP1, Ab2-MP2 and their aggregates, as shown in Figure 5.2.

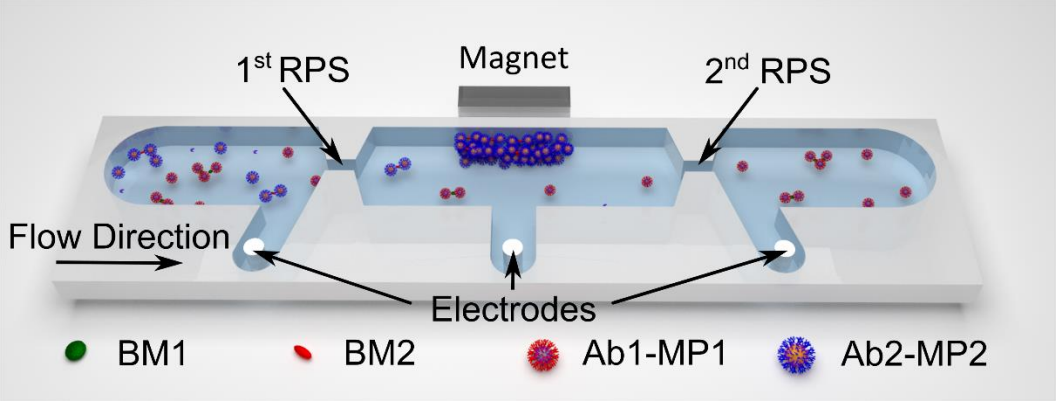

Figure 5.2 Design concept of the two-stage resistive pulse sensor (two-stage RPS) for multiplexed immunoaggregation assay

As shown in Figure 5.2, biomarker sample and Ab-MP mixture are mixed on the sensor chip in the inlet reservoir. The formed aggregates are driven through the two stage resistive pulse sensors (RPS) in series. The 1st RPS are used to detect the size and count of Ab1-MP1, Ab2-MP2 and their aggregates. The volume fraction of Ab-MP doublets is

indicative of biomarker concentration. For example, the volume fraction of Ab1-MP1 doublets, which is defined as the ratio between the volume of formed Ab1-MP1 doublets and total volume of Ab1-MP1 singlets and doublets, is indicative of BM1 concentration. The volume fraction of Ab2-MP2 doublet is defined in the same way and is indicative of BM2 concentration. The diameter of Ab1-MP1 is appropriately selected to ensure that the Ab1-MP1 doublet is smaller than the Ab2-MP2 singlet. Thus, the 1st RPS is able to differentiate Ab1-MP1, Ab2-MP2 and their doublets according to their size, to further calculate the BM1 and BM2 concentrations.

To further extend the multiplexed capability, Ab1-MP1, Ab2-MP2 and their doublets are differentiated according to their magnetic properties. Ab1-MP1 conjugated with Ab1 are non-magnetic particles while MP2 conjugated with Ab2 are magnetic particles. Ab2-MP2s and their aggregates can be captured in the capture chamber where an external magnetic field is applied. Hence only non-magnetic particles (Ab1-MP1s) and their aggregates are detected by the 2nd RPS, while the 1st RPS detects all particles and aggregates. The difference of aggregates measured by the 1st RPS and the 2nd RPS represents the magnetic particle aggregates, which are indicative of the concentration of BM2. Hence with the two stage resistive pulse sensing device, multiple biomarkers can be detected in terms of size and magnetic properties of the formed aggregates.

5.1.2 Fabrication, measurement setup and test procedure

Figure 5.3 shows the sensing channels and capture chamber of the two-stage RPS. The two-stage RPS consists of four parts.

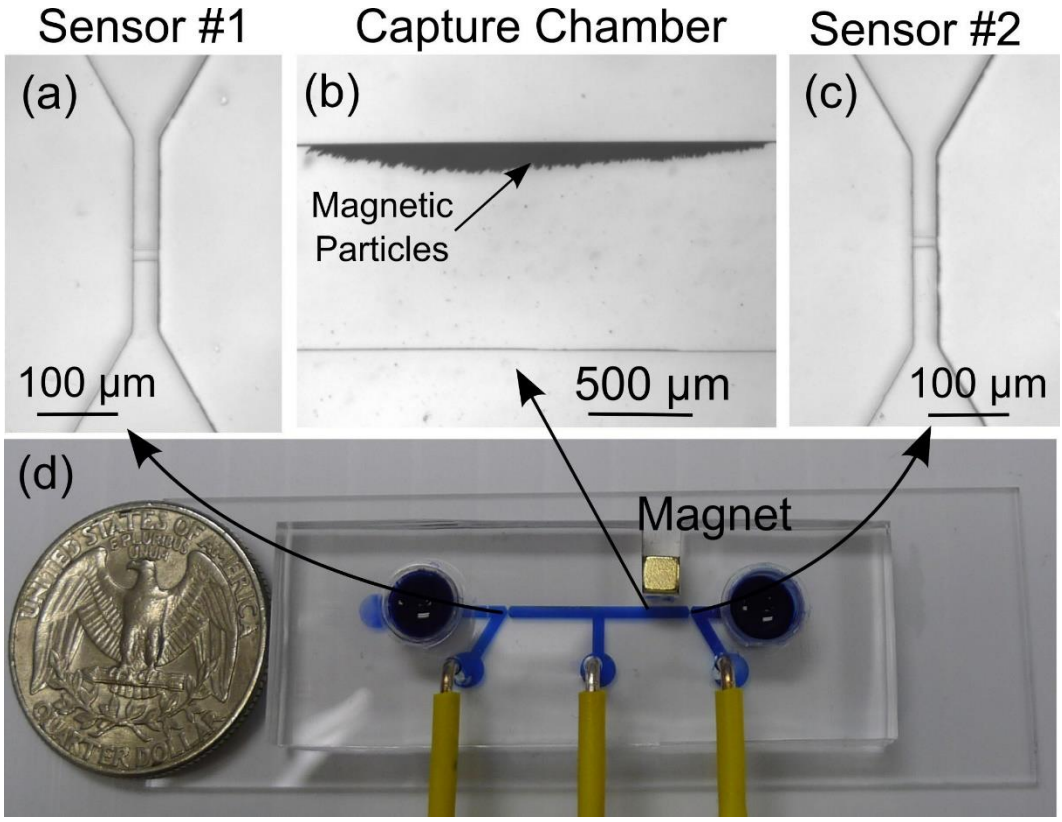

Figure 5.3 Microscopic image of two-stage RPS. (a) 1st RPS; (b) capture chamber; (c) 2nd RPS; (d) image of the two-stage RPS with three Ag/AgCl electrodes and an external magnet

Figure 5.3 (a-c) shows the sensing channels and capture chamber of the two-stage RPS. The two-stage RPS consists of: 1) two sensing channels with a width of 10 µm and a length of 30 µm to detect aggregates, 2) a capture chamber with width of 1 mm and a length of 15 mm to capture magnetic Ab2-MP2 aggregates, 3) inlet and outlet reservoirs, and 4) three Ag/AgCl electrodes to measure the resistive pulses (as shown in Figure 5.3(d)). A two-layer SU8 mold, consisting of patterns for the sensing channel (with a thickness of 10 µm), capture chamber and reservoirs (with a thickness of 40 µm), was created by two-step photolithography. Two-step photolithography is discussed in section 3.1.1 (Figure 3.3). Two sizes of Ab-MPs were chosen for the multiplexed detection. They are rabbit anti-mouse IgG antibody (Ab1) functionalized MPs (Ab1-MP1, average diameter of 2.00 µm,

non-magnetic MP, Polysciences, Inc., USA), and anti-human ferritin antibody (Ab2) functionalized MPs (Ab2-MP2, average diameter of 2.80 μm, magnetic MP,). The Ab-MPs were prepared using the same procedures as discussed in section 3.3. For each test, 166.7 μL of biomarker sample and 333.4 μL of Ab-MP mixture were mixed on a thermal mixer for 30 mins, then 50.0 μL of the mixed sample was driven through the two-stage RPS at a flow rate of 20 μL/hr by a syringe pump (KDS Legato 270, KD Scientific). An external magnet (Grade N42, 3.2 mm × 3.2 mm × 3.2 mm, K&J Magnetics, Inc.) was used to capture the magnetic Ab2-MP2s in the capture chamber. The external magnet was placed 10 mm away from the 1st stage RPS, as shown in Figure 5.3. Using such a large distance reduces the possibility of magnetizing the magnetic MPs before they enter the 1st RPS. Magnetized MPs tend to form nonspecific aggregates, which will be counted as immunoaggregates and lead to errors in biomarker concentration measurement.

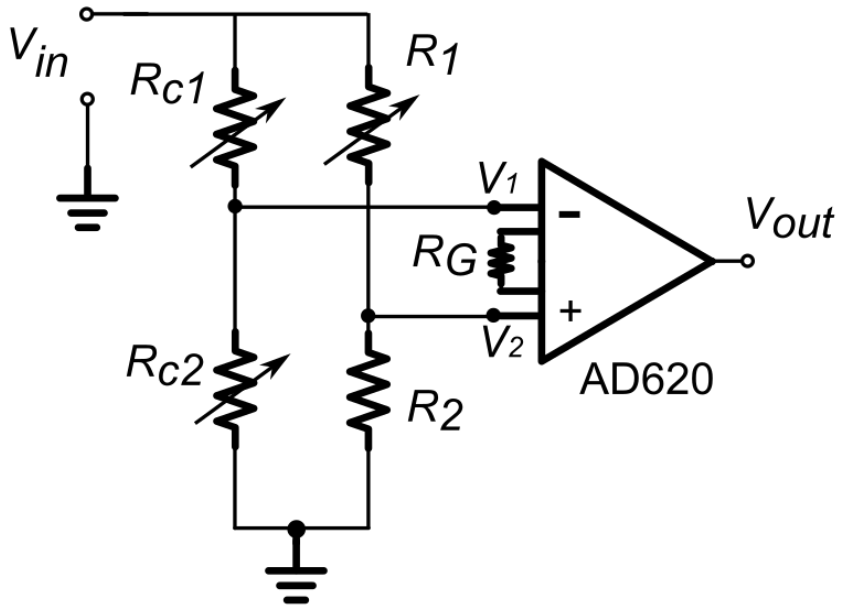

Figure 5.4 Measurement setup and equivalent circuit of the two-stage RPS

The two-stage RPS are modeled as R_{C1} and R_{C2} in the circuit. Variable resistor R_1, ranging from 500 kΩ to 1 MΩ, was used to adjust the difference between the two input voltages (V_1 and V_2) of the differential amplifier to zero at the beginning of each test. R_2 was set to 500 kΩ. The gain of the differential amplifier, AD620, was programmed to be 50 using an external gain resistor R_G = 1 kΩ. The output signal, V_{out}, was recorded at a sampling rate of 500 kHz. A typical output signal generated by the two-stage RPS is shown in Figure 5.5.

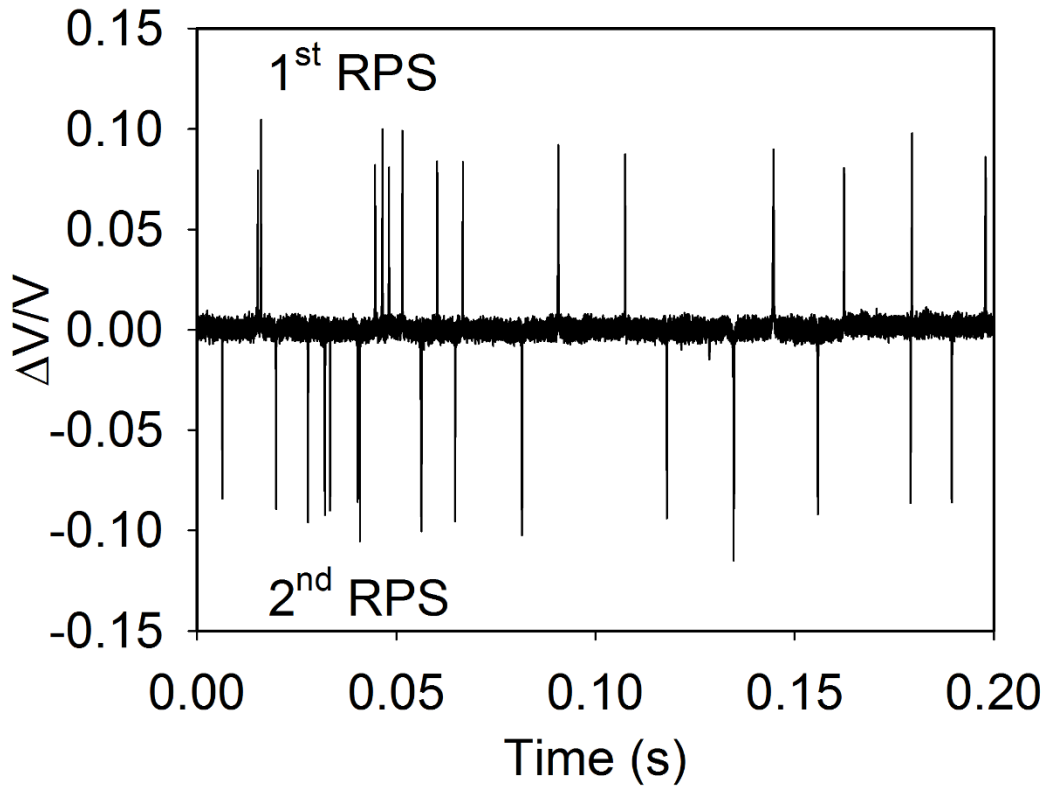

Figure 5.5 Typical resistive pulses measured by the two-stage RPS. The positive and negative pulses represent the passages of Ab2-MP2s through the 1st RPS and 2nd RPS, respectively

The typical resistive pulses caused by the passages of Ab2-MP2s (2.80 μm in diameter) are shown in Figure 5.5. When a particle transits through the 1st RPS, it increases R_{C1} and leads to a positive pulse in the output signal, V_{out}. While the passage of a particle through the 2nd RPS generates a negative pulse in the output signal, V_{out}. From the output signal, the particle sizes were back calculated using equation 3.1. It is possible that particles pass through the two resistive pulse sensors at same time, which will lead to an incorrect count and incorrect concentration measurement. This issue can be overcome by taking two independent measurements of the two RPSs, using two pairs of electrodes.

5.2 The relationship between volume fraction of Ab1-MP1 doublets and BM1 concentrations

The studies presented in this section have two purposes. The first purpose is to prove that the use of Ab1-MP1 is able to quantitatively detect BM1 concentration. Note that the relationship between Ab2-MP2 aggregates and BM2 concentration was studied in section 4.1. The second purpose is to study the concentration of Ab1-MP1 triplets. The calculated equivalent diameter of the Ab1-MP1 triplet is 2.88 μm, which overlaps with the Ab2-MP2 singlet. Thus, Ab1-MP1 triplet concentration should be small and have a negligible effect on the detection of Ab2-MP2 concentration.

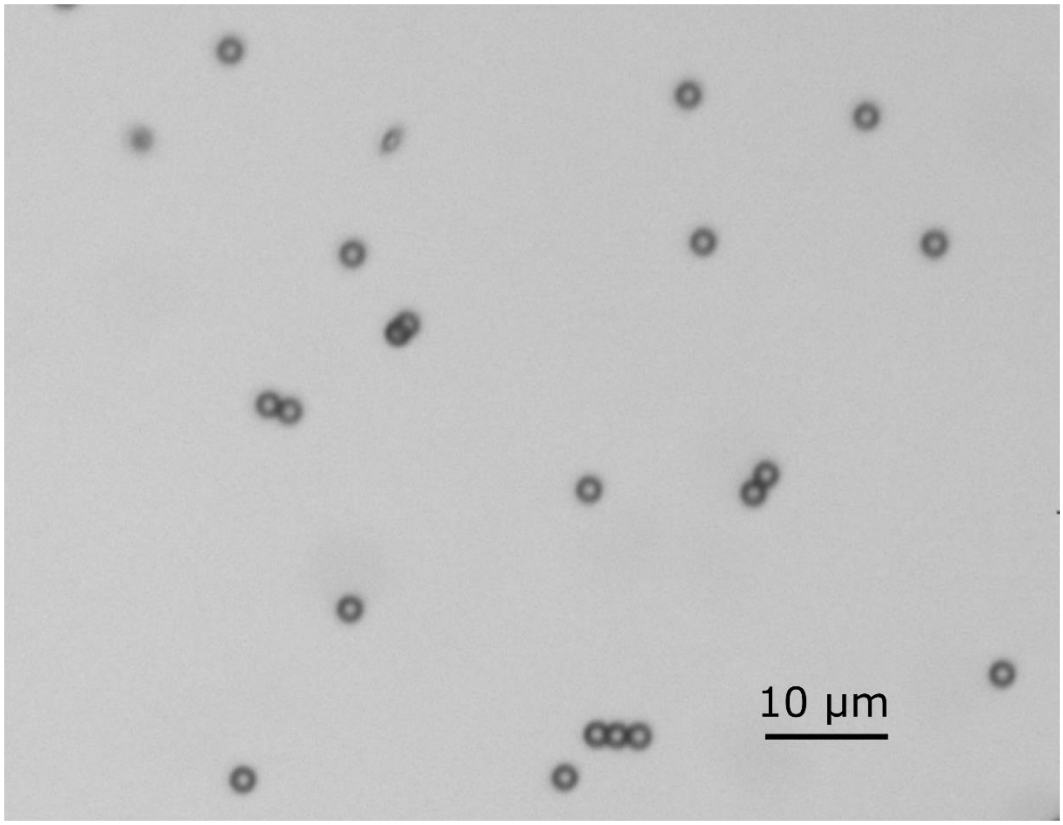

Figure 5.6 Microscope image of formed Ab1-MP1 aggregation. The Ab1-MP1 concentration is 5.80×10^3 counts/mL and BM1 concentration is 24.0 ng/mL

Figure 5.6 shows the microscope image of the formed Ab1-MP1 aggregates. In this test, 166.7 µL of 24.0 ng/mL BM1 was mixed with 166.7 µL Ab1-MP1 solution for 30 mins in the thermal mixer to from the aggregates. The concentration of Ab1-MP1 was 5.80×10^3 counts/mL. Then the formed Ab1-MP1 aggregates were detected by a single channel RPS. The count and size distribution of Ab1-MP1 aggregates are shown in Figure 5.7.

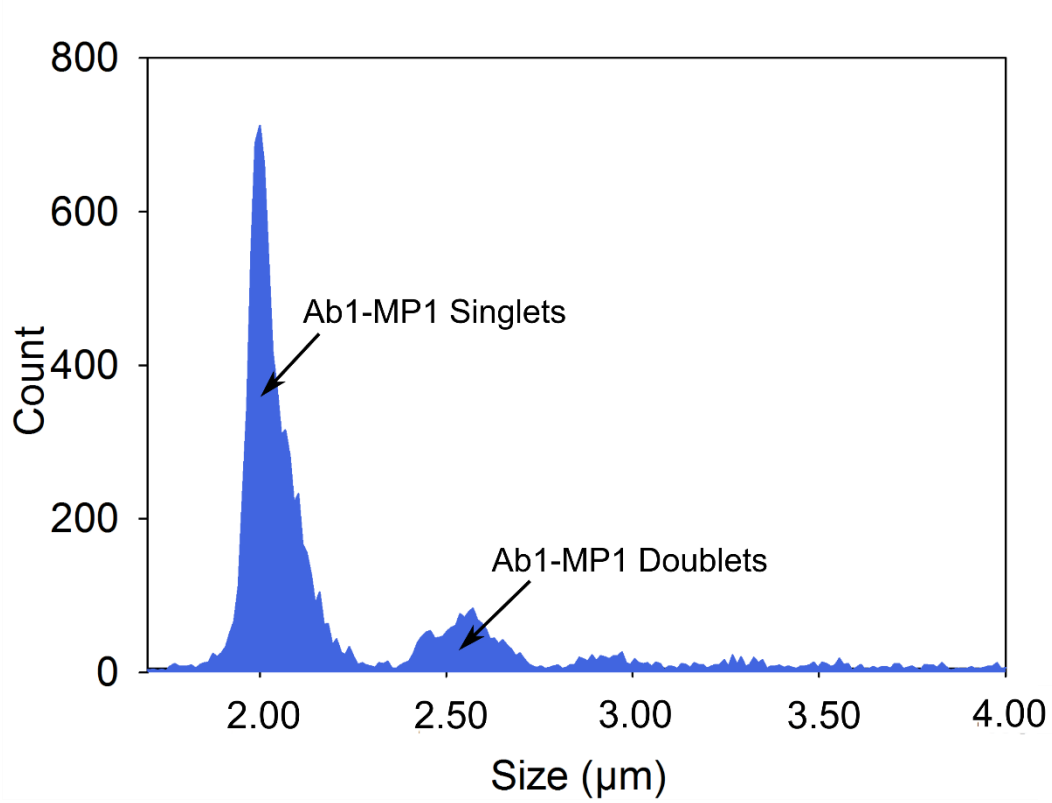

Figure 5.7 Counts and size distribution of the formed Ab1-MP1 aggregation. The Ab1-MP1 concentration is 5.80×10^3 counts/mL and BM1 concentration is 24.0 ng/mL

Figure 5.7 shows the counts and size distribution of Ab1-MP1 aggregates. From left to right, two peaks centered at 2.04 ± 0.07 μm and 2.55 ± 0.09 μm represent singlet Ab1-MP1 and Ab1-MP1 doublets. The calculated equivalent spherical diameter (ESD) of Ab1-MP1 doublets is 2.52 μm, which agrees well with the measured result. The calculated volume fraction of Ab1-MP1 doublets is 27.2%. In order to evaluate the nonspecific aggregation of Ab1-MP1, five Ab1-MP1 solutions without added BM1 were prepared and tested. The volume fraction of Ab1-MP1 doublets caused by nonspecific aggregation was 17.9 ± 0.4%. Next, similar tests were conducted at various BM1 concentrations ranging from 10.4 to 51.2×10^3 ng/mL, the Ab1-MP1s were kept constant at 5.80×10^3 counts/mL.

To ensure the repeatability, at each BM1 concentration, five samples were prepared and measured.

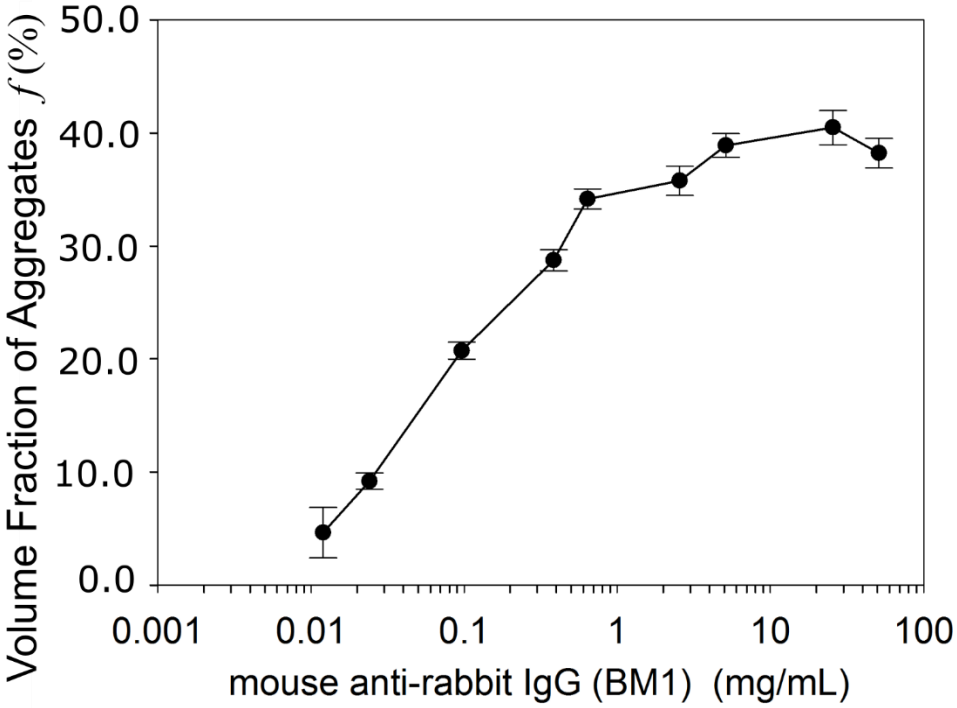

Figure 5.8 The relationship between the volume fraction of Ab1-MP1 doublets and BM1 concentrations. BM1 concentration ranged from 10.4 to 51.2 × 10^3 ng/mL, the Ab1-MP1s concentration was kept at 5.80 × 10^3 counts/mL

As shown in Figure 5.8, the volume fraction of Ab1-MP1 doublets increases with the increased Ab1 concentration. A detection range from 10.4 to 51.2 × 10^3 ng/mL was achieved. This test proved that the use of Ab2-MP2 is able to quantitatively detect BM1s concentrations. The equivalent spherical diameter of the Ab2-MP2 triplet was 2.88 μm, which overlapped with the size of the Ab1-MP1 singlet (2.80 μm). This will cause false counts of Ab2-MP2 singlets. The counts of Ab1-MP1 triplets ranged from 154 to 500 count/μL. In the next study (multiplexed detection with a mixture of Ab1-MP1 and Ab2-MP2), the Ab2-MP2 concentration was chosen to be much higher than the Ab1-MP1

concentration (2.4 times) to ensure that the volume of Ab1-MP1 triplets is negligible compared with the total volume of Ab2-MP2s.

5.3 Multiplexed detection of human ferritin and mouse anti-rabbit IgG

A mixture consisting of Ab1-MP1 and Ab2-MP2 was used to detect BM1 (mouse anti-rabbit IgG) and BM2 (human ferritin) concentrations. Firstly, to confirm the formation of two types of aggregates, Ab-MP mixture containing 5.80×10^3 count/mL of Ab1-MP1 and 1.40×10^3 count/mL of Ab2-MP2 were mixed in a sample containing 24.0 ng/mL of BM1 and 208 ng/mL of BM2. The formed aggregates are shown in Figure 5.9.

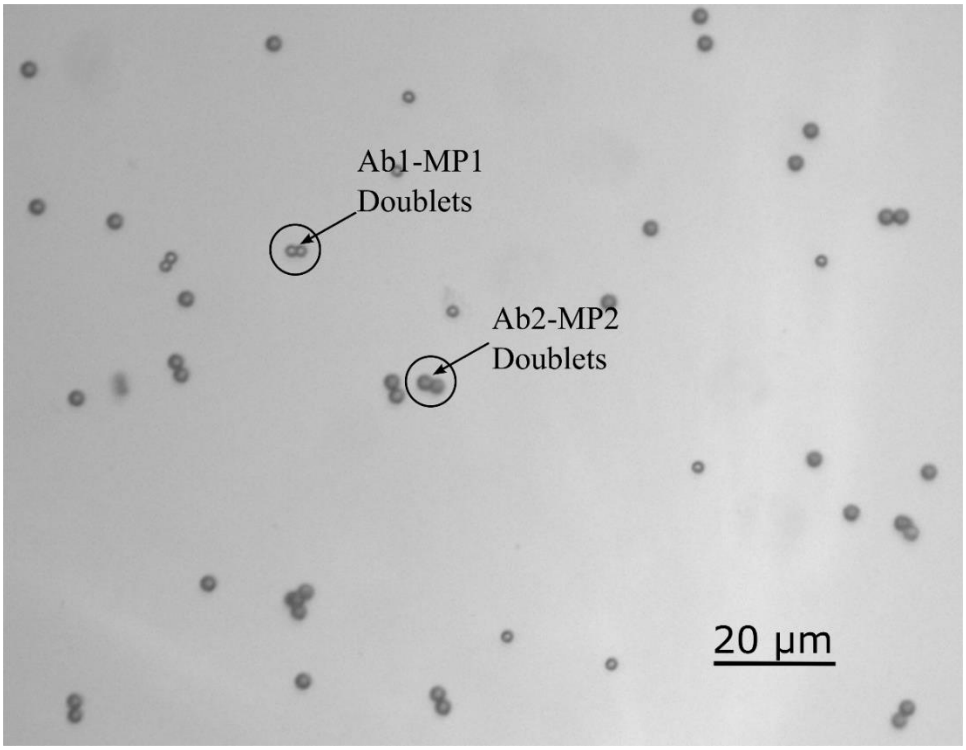

Figure 5.9 Microscope image of formed Ab1-MP1 and Ab2-MP2 aggregates

Figure 5.9 confirmed the formation of Ab1-MP1 and Ab2-MP2 doublets. Next, the formed aggregates were detected by the two-stage RPS. As discussed previously, the 1st RPS was used to differentiate Ab1-MP1, Ab2-MP2 and their doublets according to their size, as shown in Figure 5.10.

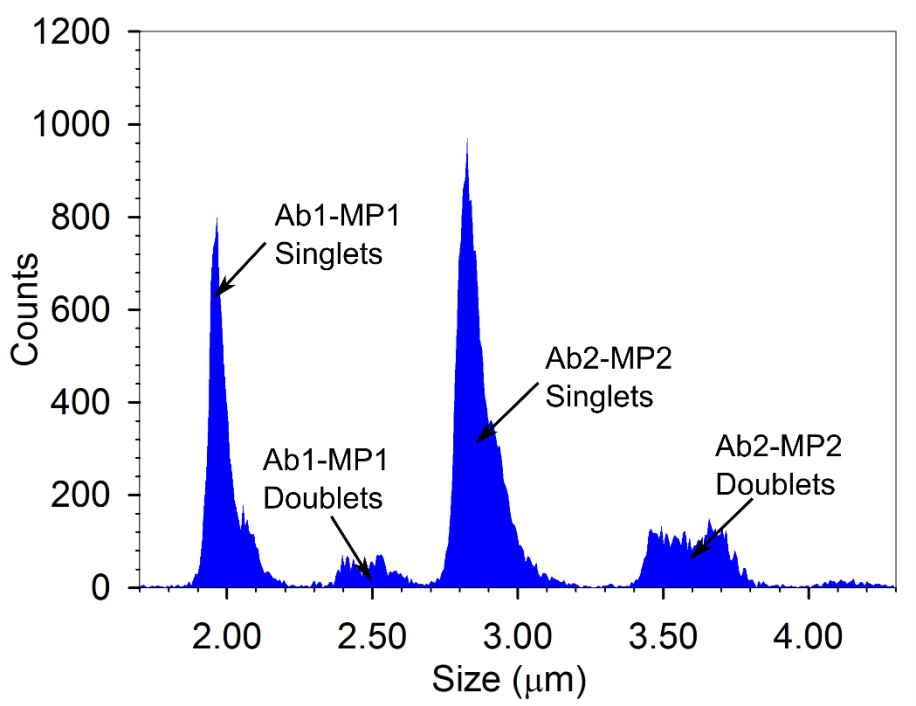

Figure 5.10 Count and size distribution of formed Ab1-MP1 and Ab2-MP2 aggregates

Figure 5.10 shows the counts and size distributions of Ab1-MP1 and Ab2-MP2 aggregates. From left to right, the first two peaks centered at 1.99 ± 0.06 μm and 2.50 ± 0.09 μm represent the distribution of singlets and doublets of Ab1-MP1s. The measured diameters matched well with the calculated equivalent diameter of the Ab1-MP1 doublets, which is 2.52 μm. The third and fourth peaks centered at 2.87 ± 0.07 μm and 3.60 ± 0.11 μm represent the singlets and doublets of Ab2-MP2s. The calculated equivalent diameter of Ab2-MP2s doublets is 3.53 μm, which also matches well with the measured result. The

results shown in Figure 5.10 demonstrated that the 1st-stage RPS is able to differentiate Ab1-MP1s and Ab2-MP2s probes and their doublets according to their size distribution. Next, to prove the volume fraction of Ab1-MP1s doublet, f_1, can be correlated to the concentrations of BM1, similar tests were conducted at various BM1 concentrations ranging from 3.10 to 51.2 × 10^3 ng/mL, while BM2 concentration was kept a constant of 41.6 ng/mL. For each BM1 concentration, five samples were prepared and tested. It worth mentioning that the nonspecific aggregation of Ab1-MP1s and Ab2-MP2s were evaluated before the test. The volume fraction of nonspecific doublets were 17.9 ± 0.4% and 5.3 ± 0.5% for Ab1-MP1s and Ab2-MP2s, respectively. After subtracting the volume fraction of nonspecific doublets, volume fractions of Ab1-MP1s doublets as a function of the BM1 concentrations were plotted in Figure. 5.11.

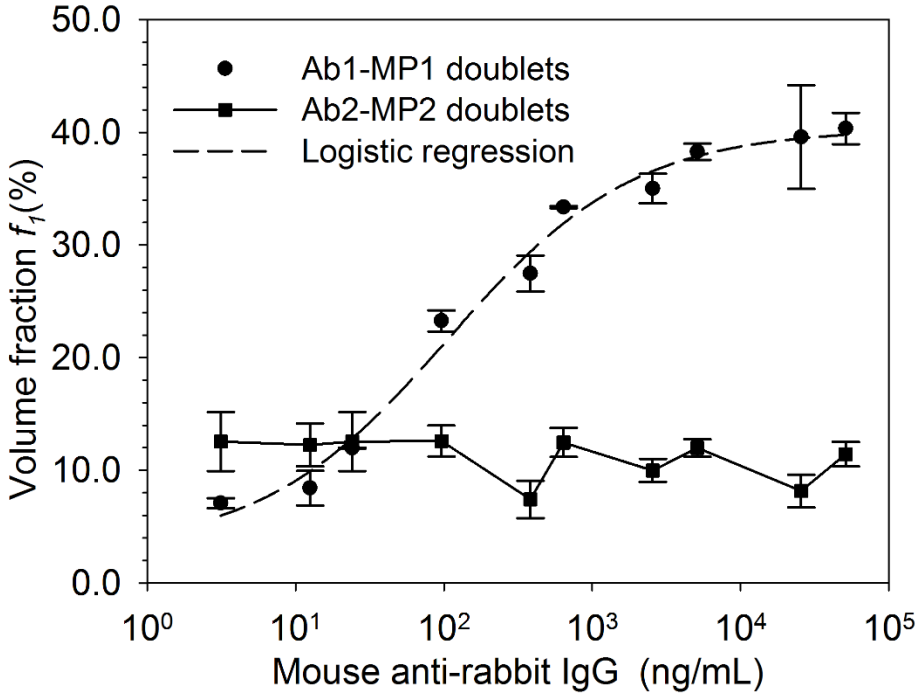

Figure 5.11 Measured relationship between the concentrations of BM1 ranging from 3.10 to 51.2 × 10^3 ng/mL and volume fraction of Ab1- MP1 doublet (f_1)

The relationship between volume fraction of Ab1-MP1s doublets and BM1 ranging from 3.10 to 51.2 × 10^3 are shown in Figure 5.11 (black dots), which can be fitted with a 4-parameter logistic function (dash curve):

$$f_1(x) = 0.030 + \frac{0.370}{1 + (x/106.25)^{-0.690}} \tag{5.1}$$

The coefficient of determination (R^2) of the fitted curve is 0.9883. From 3.10 to 51.2 × 10^3 ng/mL, the volume fraction of Ab1-MP1s doublets, f_1, increased with the increase of BM1 concentration in the range of 3.10 ng/mL to 51.2 × 10^3 ng/mL. The maximum value, f_1 = 40.3%, was achieved at a BM1 concentration of 51.2 × 10^3 ng/mL. The solid line in Figure 5.11 shows the volume fraction of Ab2-MP2 doublets. The average volume fraction of Ab2-MP2 doublets is 11.1 ± 2.0%. As shown in section 5.2, for an Ab1- MP1s concentration of 5.80×10^3 count/μL, the Ab1-MP1 triplets' concentration ranged from 154 to 500 count/μL. Hence if BM2 and Ab2-MP2 are added to the solution with a concentration of 1.40×10^4 count/μL to from aggregates, the volume fraction of AB1-MP1 triplets to total volume of Ab2-MP2s and aggregates is estimated to range from 1.5% to 3.8% at all BM1 concentrations. The value was 1.5% at a BM1 concentration of 24.0 ng/mL. Hence the error caused by the size overlapping of Ab1-MP1s triplets and Ab2-MP2 can be neglected.

Next, we prove that the volume fraction of Ab2-MP2s doublets, f_2, is correlated to the concentration of BM2. In this experiment, the concentration of BM2 was varied from 5.20 ng/mL to 208 ng/mL; while BM1 concentration was kept constant at 24.0 ng/mL, as shown in Figure 5.12. The volume fraction of nonspecific Ab2- MP2 doublets was 5.3 ± 0.5%.

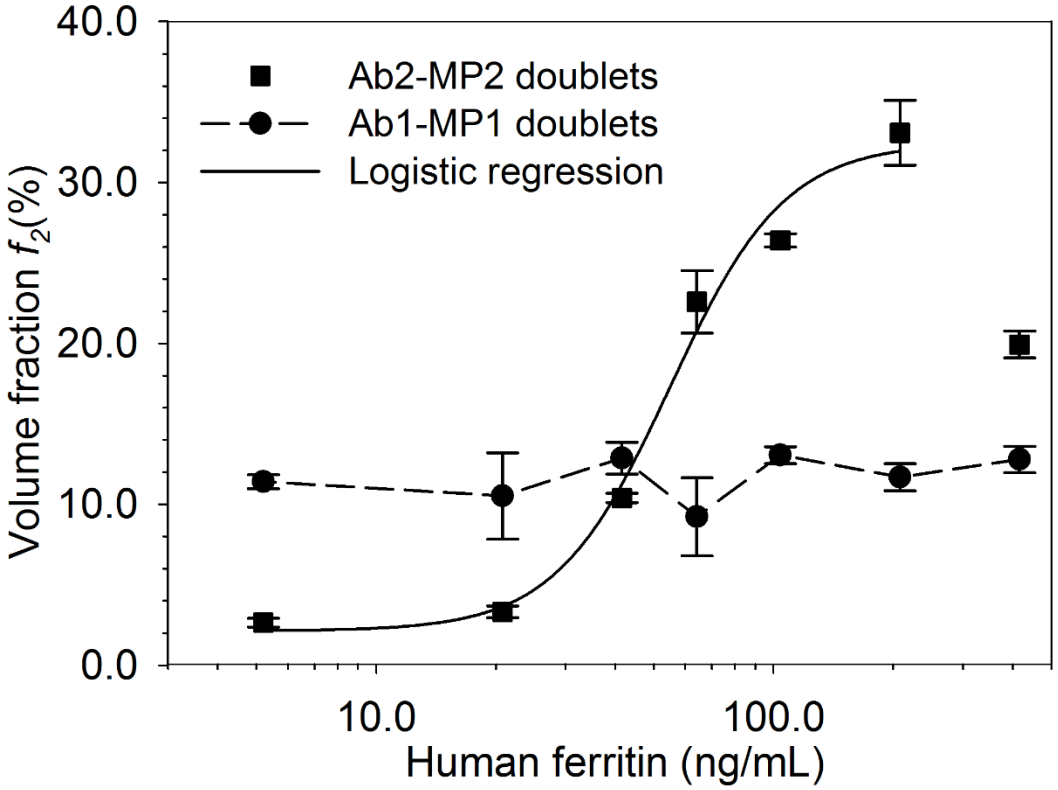

Fig. 5.12 Measured relationship between the concentrations of BM2 ranging from 5.20 to 208 ng/mL and volume fraction of Ab2- MP2 doublets (f_2)

The correlation between the volume fraction of Ab2-MP2 doublets and BM2 ranging from 5.20 to 208 ng/mL was also fitted with a 4-parameter logistic curve (solid curve).

$$f_2(x) = 0.020 + \frac{0.300}{1 + (x/55.00)^{-3.02}} \tag{5.2}$$

The coefficient of determination (R^2) of the fitted curve is 0.9870. The volume fraction of Ab2-MP2s aggregates increased from 2.7 % to 33.1 % with an increase of BM2 concentration in the range of 5.20 ng/mL to 208 ng/mL. With a fixed BM1 concentration of 24.0 ng/mL, the volume fraction error caused by the Ab1- MP1 triplets is estimated to be approximately 1.5%. Hence using the multiplexed immunoaggregation assay we can

confidently measure BM2 concentrations as low as 5.20 ng/mL. The maximum volume fraction (33.1%) occurred at 208 ng/mL. Above 208 ng/mL, the volume fraction f_2 was reduced with an increase of BM2 concentration. This is because the high concentration of BM2 would saturate Ab2 on the surfaces of the Ab2-MP2s; hence the number of unreacted Ab2 on Ab2-MP2s is too low to cause aggregation. The measured average volume fraction of Ab1-MP1s doublets is 11.6 ± 1.4% for the constant BM1 concentration of 24.0 ng/mL. Using equation 5.1 and a BM1 concentration of 24.0 ng/mL, the calculated volume fraction of Ab1-MP1s doublets is 12.8%, which matched well with the measured value (11.6 ± 1.4%). Using equation 2 and a BM2 concentration of 41.6 ng/mL, the calculated volume fraction of Ab2-MP2s is 11.3%, which also matched well with the measurement results in Fig. 5.11 (11.1 ± 2.0%). The results shown in Fig. 5.11 and 5.12 clearly demonstrate: 1) the volume fractions of Ab1-MP1s and Ab2-MP2s, are correlated to the concentrations of BM1 and BM2 in a mixture; 2) the 1st-stage RPS is capable of differentiating Ab1-MP1s and Ab2-MP2s singlets and their doublets according to their size difference.

Next, experiments were conducted to prove that the two biomarkers (BM1 and BM2) can also be detected in terms of the magnetic properties of the aggregates. The magnetic Ab2-MP2 aggregates are correlated to the BM2, and the non-magnetic Ab1-MP1 aggregates are correlated to the BM1. An external magnet was used to capture magnetic particles in the capture chamber while the non-magnetic particles were counted by the 2nd-stage RPS.

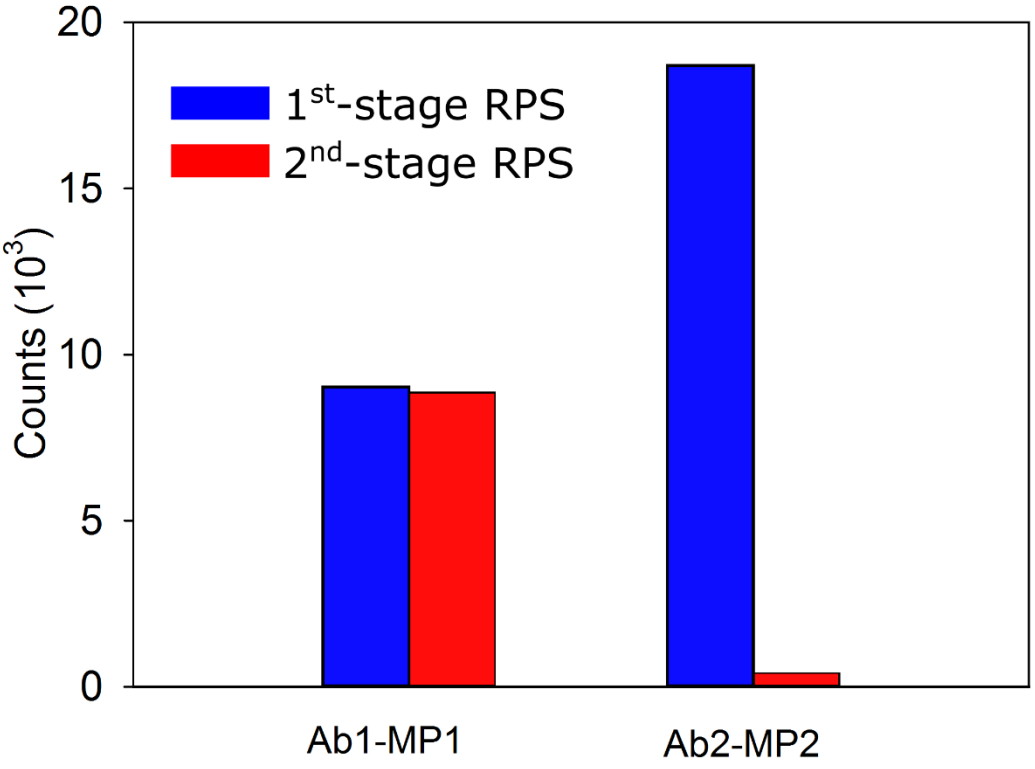

Figure. 5.13 Counts of two types Ab1-MP1s and Ab2-MP2s and their aggregates measured by the two-stage RPS

In order to prove that the external magnet is able to capture magnetic Ab2-MP2s and their aggregates with high efficiency, we compared the count and size distribution measured by the 1st and 2nd RPSs with the following experimental conditions: 1) the biomarker sample contained 208 ng/mL of BM2 without BM1; and 2) the mixture of Ab1-MP1s and Ab2-MP2 was used at the same concentration as the previous experiments. The counts of different-sized particles are shown in Figure 5.13. The capture efficiency is calculated as a ratio of the difference in magnetic particle (magnetic Ab2-MP2 and its aggregates) counts between the 1st RPS and the 2nd RPS over all magnetic particle counts measured by the 1st RPS. From the measurements shown in Figure 5.13, the capture

efficiency was calculated to be great than 98.0%, which is high enough to ensure accurate counts of magnetic particles.

Next, to prove that the 2nd RPS can accurately count and size the nonmagnetic Ab1-MP1, the nonmagnetic Ab1-MP1 doublets measured by the 1st and 2nd RPS were compared with BM1 concentrations ranging from 3.10 to 51.2 × 10^3 ng/mL as shown in Figure 5.14.

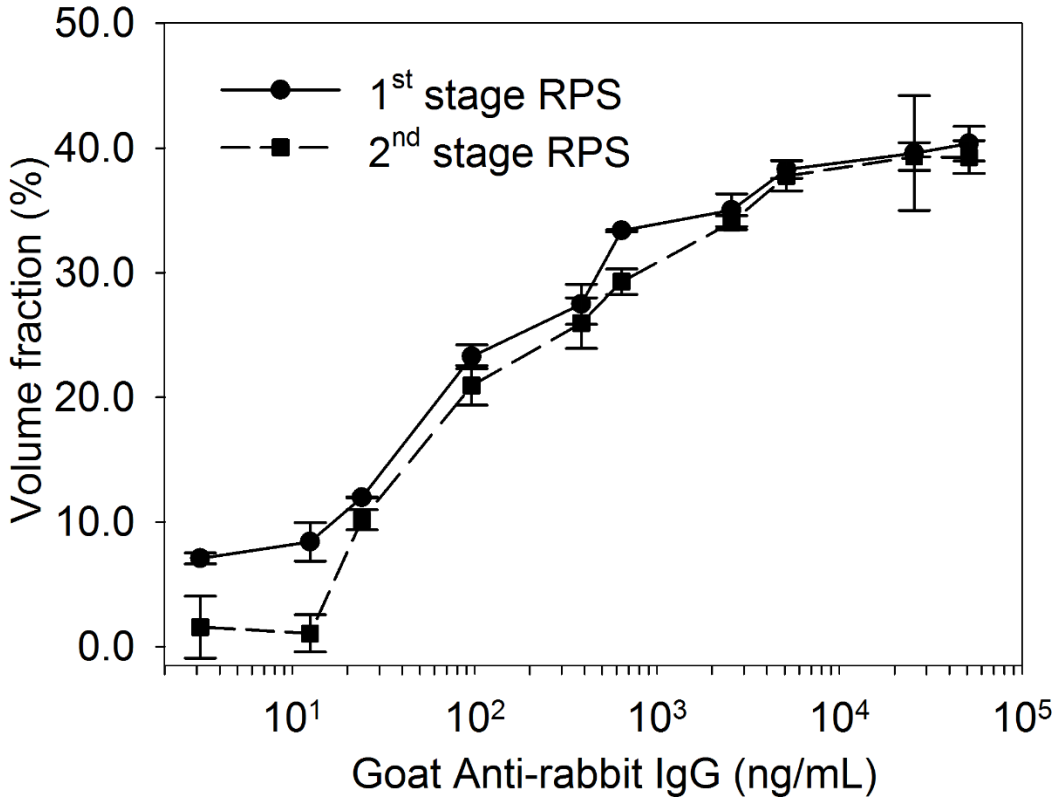

Figure 5.14 Comparison of the volume fraction of the nonmagnetic Ab1-MP1 doublets measured by the 1st and 2nd RPS, respectively. BM1 concentrations ranged from 3.10 to 51.2 × 10^3 ng/mL

The Figure 5.14 shows the volume fraction of nonmagnetic doublets measured by the 1st and 2nd RPS with a BM1 concentration ranging from 3.10 to 51.2 × 10^3 ng/mL. The volume fraction ratio measured by the 1st RPS and 2nd RPS match reasonably well in this

concentration range. For the BM1 concentrations ranging from 24.0 to 51.2 × 10^3 ng/mL, the measurement error ranges from 0.2% to 4.1%. One possible cause for this error is the nonspecific attachment of nonmagnetic Ab1-MP1s and their aggregates. This nonspecific attachment may also lead to larger errors (5.5 % to 7.3 %) at lower BM1 concentrations (3.10 ng/mL and 12.0 ng/mL).

The lower detection limit of the multiplexed immunoaggregation assay is 3.10 ng/mL and 5.20 ng/mL for BM1 and BM2, which are comparable to those of commercial ELISA kits (~6.0 ng/mL for BM1, and ~5.0 ng/mL for BM2).). Three possible solutions to further expand the lower detection limit are: 1) use antibody with higher binding affinity, which will increase the volume fraction of aggregates at lower biomarker concentration, 2) use antifouling materials to avoid nonspecific aggregation, and 3) use various MP concentrations to adjust the detection range, as demonstrated in section 4.2. With the demonstration of the multiplexed immunoaggregation biomarker assay in terms of size and magnetic properties of Ab-MPs, if four types of Ab-MPs are used (2 different-sized magnetic Ab-MPs, and 2 different-sized non-magnetic Ab-MPs), four biomarkers can be detected using the two-stage RPS sensor: the 2nd stage RPS measures the concentration of the two biomarkers that trigger the aggregation of nonmagnetic particles, while the 1st RPS measures all four aggregates. By deducting the nonmagnetic aggregate counts from the 2nd RPS, an additional two biomarker concentrations can be measured in terms of the magnetic aggregate counts. If multiple two-stage RPS are integrated into a device, a large number of biomarkers can be detected via parallel detection.

5.4 Summary

A multiplexed immunoaggregation assay was studied in this Chapter based on size and the magnetic properties of the MPs. Detection ranges from 5.20 to 208 ng/mL and 3.10 to 51.2×10^3 ng/mL were achieved for human ferritin and rabbit anti-mouse IgG detection, respectively. The lower detection limits of the multiplexed immunoaggregation assay are 3.10 ng/mL and 5.20 ng/mL for human ferritin and rabbit anti-mouse IgG, which are comparable to those of commercial ELISA kits (~6.0 ng/mL for human ferritin, and ~5.0 ng/mL for rabbit anti-mouse IgG).

CHAPTER VI

CELLULAR BIOMARKER DETECTION USING A TWO-STAGE MICRO RESISTIVE PULSE SENSOR

6.1 Design concept and sensing principle

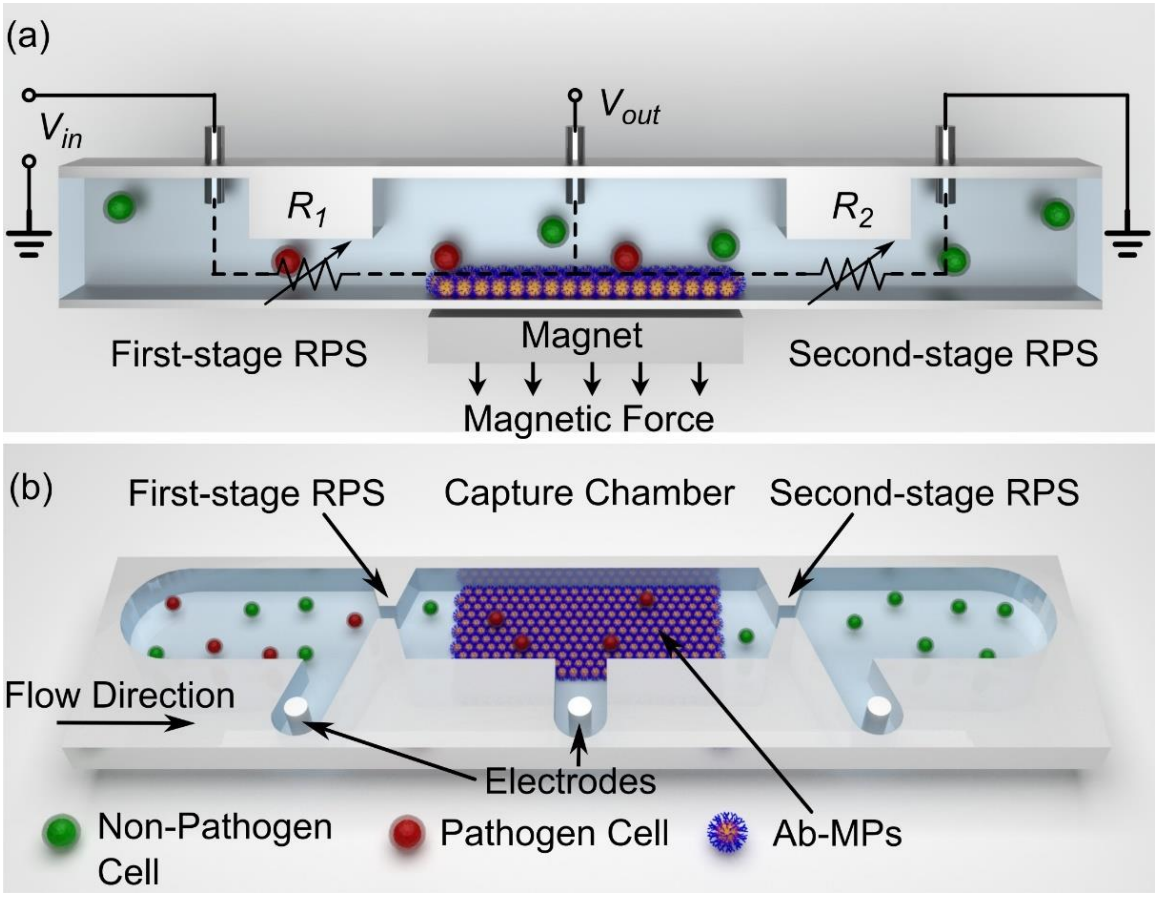

Figure 6.1 Schematic of the two-stage resistive pulse sensor (two-stage RPS) for pathogen detection

Pathogen cells as a type of cellular biomarker are studied in this chapter. Pathogen detection represents an important task for many applications such as disease diagnosis, food industry, environmental monitoring, biodefense and biological research [7] [8] [9]. Rapid analysis is essential in pathogen detection, especially for diagnosis of pathogen infection and controlling the spread of disease [9]. In this chapter, I will present a two-stage resistive pulse sensor for pathogen cell detection based on a simple surface functionalization method by attaching antibody functionalized MPs (Ab-MPs) to the sensing surface via an applied magnetic field, requiring no chemical modification of the surface. Figure 6.1 shows the design concept of the two stage resistive pulse sensor (two-stage RPS) for pathogen cell detection. Firstly, antibodies (Abs), which are specific to the receptors on surface of the target cells are immobilized on the MPs to form Ab-MP. Then, the Ab-MPs are captured in the capture chamber by an external magnet in order to functionalize the capture chamber with Ab-MPs. For each test, a sample solution containing target cells is loaded into the inlet reservoir of the two-stage RPS, then driven through the two-stage RPS. The total number of cells entering the capture chamber is counted by the 1st RPS. While target cells are captured in the capture chamber, non-target cells pass through the capture chamber and are counted by the 2nd RPS. The difference between the counts measured by 1st and 2nd RPS represents the count of target cells.

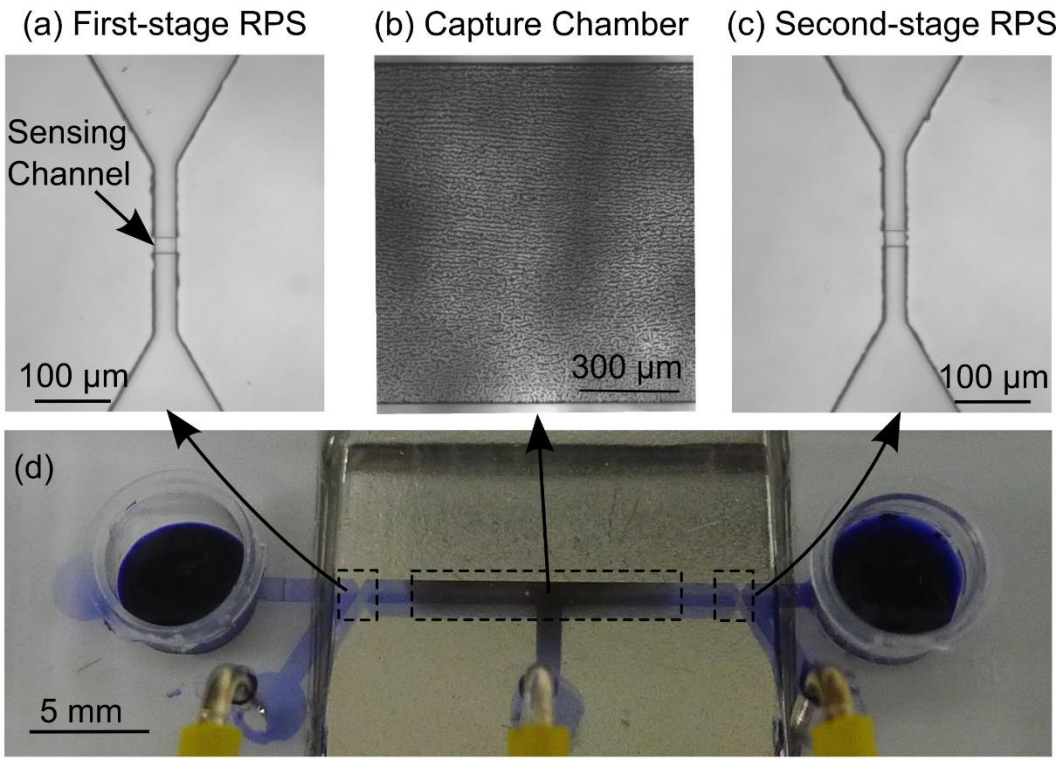

Figure 6.2 Images of the two-stage RPS including sensing channels, a capture chamber and three Ag/AgCl electrodes

The device consists of: 1) two sensing channels with a width of 20 µm, height of 20 µm and length of 30 µm to detect cell transits; 2) a capture chamber with a width of 1 mm, height of 40 µm and a length of 15 mm; and 3) three Ag/AgCl electrodes to detect the resistive pulses. The two -stage PS was fabricated using standard soft lithography, as discussed section 3.11.

6.2 Testing procedure and experiment setup

To functionalize the capture chamber with antibody, at the beginning of each test, 100 µL Ab-MPs were loaded in the inlet reservoir and driven through the capture chamber by the pressure difference between the inlet and outlet reservoirs, at a flow rate of

approximately 200 µL/hr. Two types of Ab-MPs were used in this study. They were the *Saccharomyces cerevisiae* antibody (Ab1, 1 mg/mL, Bio-Rad, USA) functionalized MPs (Ab1-MPs) and rabbit anti-mouse antibody (Ab2) functionalized MPs (Ab2-MPs). Ab-MPs were prepared using the same procedure as discussed in section 3.3. Both Ab1-MPs and Ab2-MPs had a concentration of 7.2×10^4 count/µL. An external magnet (19 mm × 19mm × 19mm, NdFeB, Grade N52, K&J Magnetics, Inc.) was used to capture the Ab-MPs. After 50 µL of MPs were captured in the chamber, the remaining MPs were removed from inlet reservoir, and the inlet reservoir was washed by PBS buffer. Approximately 3.6×10^6 Ab-MPs were loaded to the capture chamber, and were estimated to form ~2 layers of MPs (the estimated thickness of the Ab-MP coating is 5.3 µm).

Two types of cells were tested in this study. Baker's yeast (saccharomyces cerevisiae, Lalvin, Canada) was used as a target cell and algae (*Chlorella*, CAROLINA Biological, USA) was used as a non-target cell. Yeasts are a group of important model microorganisms for many biological studies [194]. Some species of yeast, for example *Candida albicans*, can cause infections in humans [195]. *S. cerevisiae* is well-known in the bakery and brewing industries. However, it is also reported as an unusual cause of life-threatening infection in humans [150] [151]. In our study, *S. cerevisiae* is used as a model cell to prove the concept of the pathogen detection mechanism shown in Figure 6.1. *Chlorella* was used as the control cell, whose size is very close to that of *S. cerevisiae* to prove the device's capability to differentiate target cells from similar sized reference cells. In our study, the concertation of *S. cerevisiae* was varied from 500 to 2000 cells/µL, while the *Chlorella* concentration was kept constant at 1000 cells/µL. The cell concentrations were measured using an Accusizer 780 particle sizer (Particle Sizing Systems, Port Richey,

FL, USA) before each test. We also measured the sizes of both cells using microscopes. The size ranges of *S. Cerevisiae* and *Chlorella* are from 3.2 to 7.4 μm and from 3.4 to 8.4 μm, respectively. To prove that the use of Ab1-MPs is able to capture *S. cerevisiae*, 50 μL of *S. cerevisiae* was mixed with 50 μL of Ab1-MPs. The concentration of *S. cerevisiae* and Ab1-MPs were 1000 counts/μL and 7.2×10^4 count/μL, respectively. Then the sample was observed under a light microscope, as shown in Figure 6.3.

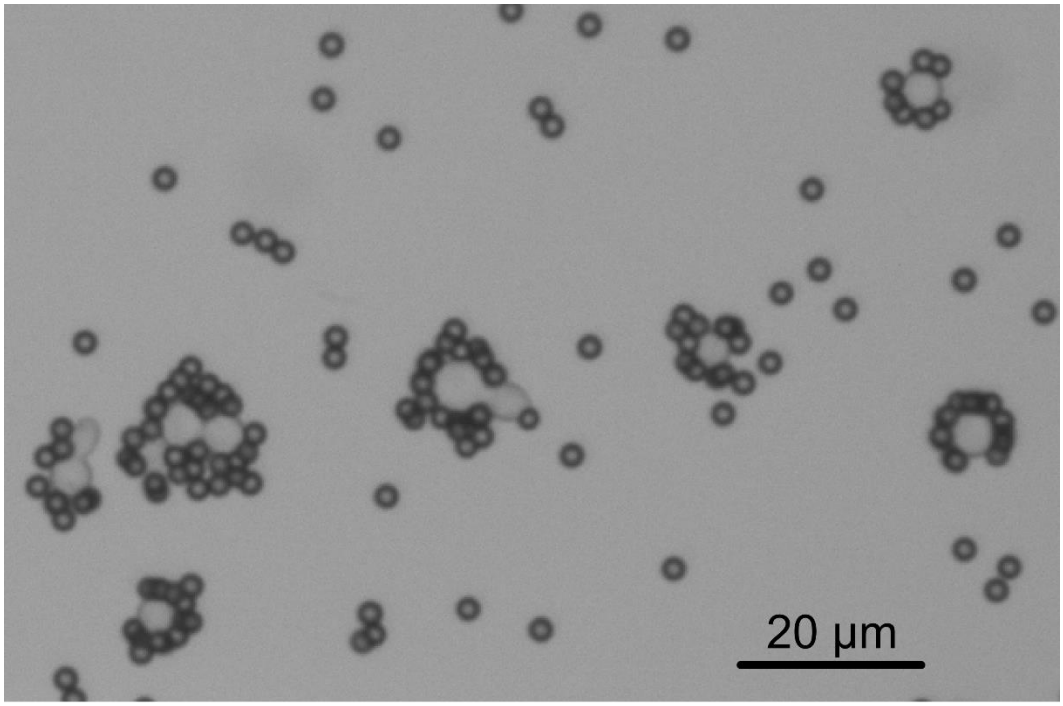

Figure 6.3 *S. cerevisiae* captured by Ab1-MPs. The concentrations of *S. cerevisiae* and Ab1-MPs were 1000 count/μL and 7.20×10^4 count/μL, respectively

Figure 6.3 shows that the Ab1-MPs are able to capture the *S. cerevisiae*. Next, the mixture of *S. cerevisiae* and *Chlorella* was tested by the two-stage RPS. At each test, 100 μL of sample was loaded into the inlet reservoir at a flow rate approximately 20 μL/hr. To provide the pressure difference between inlet and outlet reservoir, the device was placed

vertically and cell samples were driven through the device by gravity. Thus, a bulky springe pump was not necessary. The flow rate was calculated using the volume difference before and after each test and the duration of each test. Resistive pulse responses were record at a sampling rate of 500 kHz.

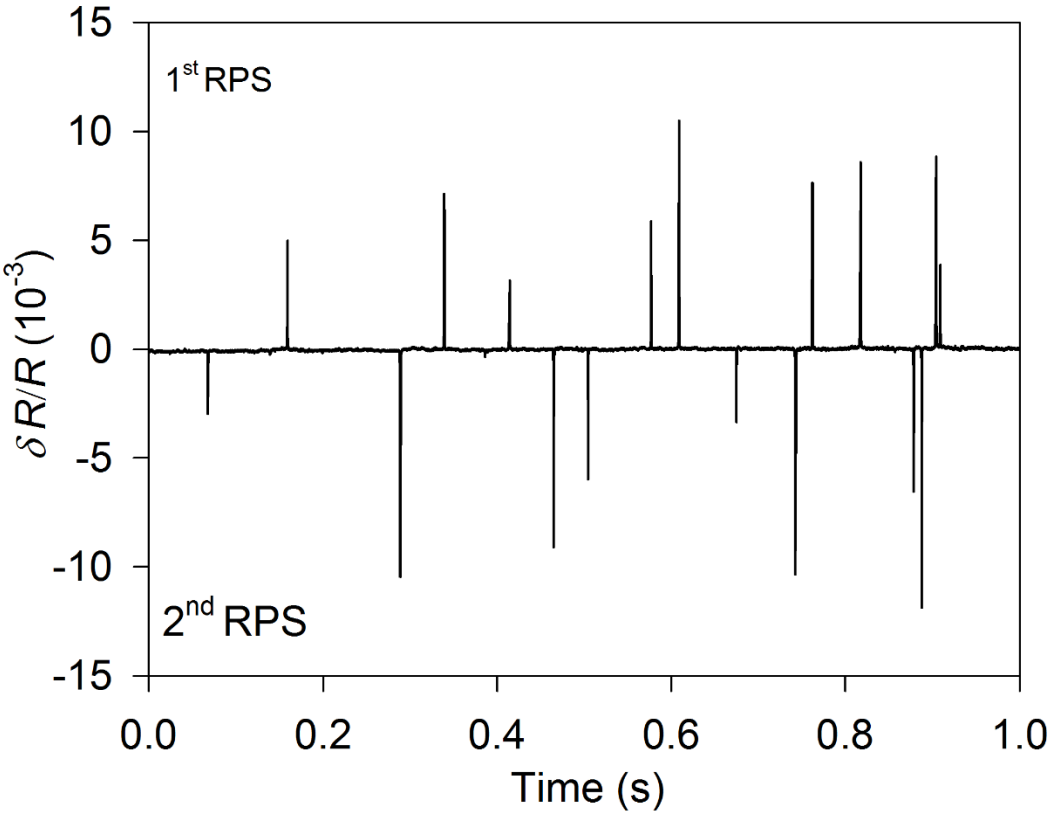

Figure 6.4 Typical resistive pulses generated by the two-stage RPS. The positive and negative pulses represent the passages of cells through the 1st RPS and 2nd RPS respectively

Figure 6.4 shows typical resistive pulses generated by the two-stage RPS. A 7 µL mixture of *S. cerevisiae* and *Chlorella* was tested. Both *S. cerevisiae* and *Chlorella* had a concentration of 1000 count/µL. The equivalent circuit of two-stage RPS was discussed in 5.1.2 (as shown in Figure 5.4). The positive and negative pulses represent the passage of

cells through the 1st and 2nd RPS, respectively. The cell size was back calculated using equation 3.1, and plotted in Figure 6.5. In this design, both width and height of the sensing channel are 20 μm. Thus the characteristic diameter, *D*, was calculated to be 22.57 μm by $D = (4 \cdot A/\pi)^{1/2}$. The correction factor, *F*, was taken to be 1.0 [109].

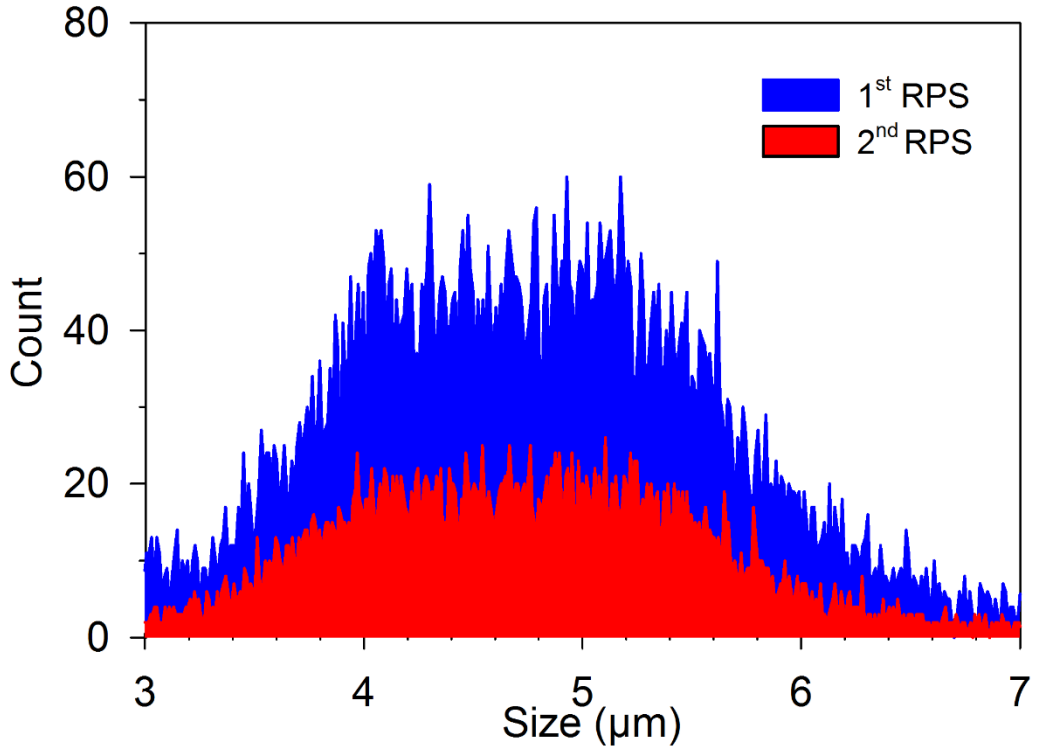

Figure 6.5 Counts and size distribution measured from 1st RPS and 2nd RPS

As shown in Figure 6.5, a total of 13.74×10^4 cells passed through the 1st RPS and entered the capture chamber, while 7.37×10^3 count *Chlorella* cells exited the chamber, implying 6.73×10^3 count *S. cerevisiae* were captured by the capture chamber. The total counts for *S. cerevisiae* and *Chlorella* are in good agreement with the actual numbers calculated from their concentrations (*S. cerevisiae*: 7×10^3counts, *Chlorella*: 7×10^3 counts and total counts: 14×10^3counts).

6.3 Capture efficiency of target and non-target cells

The target cell detection of the two-stage RPS is based on an assumption that all target cells are captured by the Ab-MP layer while all non-target cells pass through the capture chamber. Accurate detection requires that the reduction of the cell counts between 1st and 2nd stage RPS is caused by the specific capture of pathogen (*S. cerevisiae*) by the Ab-MP layer. However, in actual experiments, the reduction could also be caused by the nonspecific attachment of non-target cells (*Chlorella*). To prove the dominance of specific capture, experiments were conducted to evaluate the capture efficiency of specific and nonspecific attachment by the Ab-MP layer using two types of Ab-functionalized MPs: 1) anti-*S. cerevisiae* Ab-functionalized MPs (Ab1-MPs) coated on the capture chamber to evaluate the specific capture of *S. cerevisiae*, and nonspecific capture of *Chlorella*, and 2) rabbit anti-mouse Ab-MPs (Ab2-MPs) coated on the capture chamber to evaluate the nonspecific capture of *S. cerevisiae* and *Chlorella*, respectively. The cell concentration and flow rate were set to be 1000 count/μL and 20 μL/hr for both experiments. For each test, only one type of cell was used. The capture efficiency is defined as the ratio of the counts of cells exiting the capture chamber over the count of cells entering the capture chamber, both counts were obtained from the counts of two RPSs. Each test was repeated five times. The measurement results for capture efficiency of *S. cerevisiae* and *Chlorella* under two chamber surface conditions are shown in Figure 6.6.

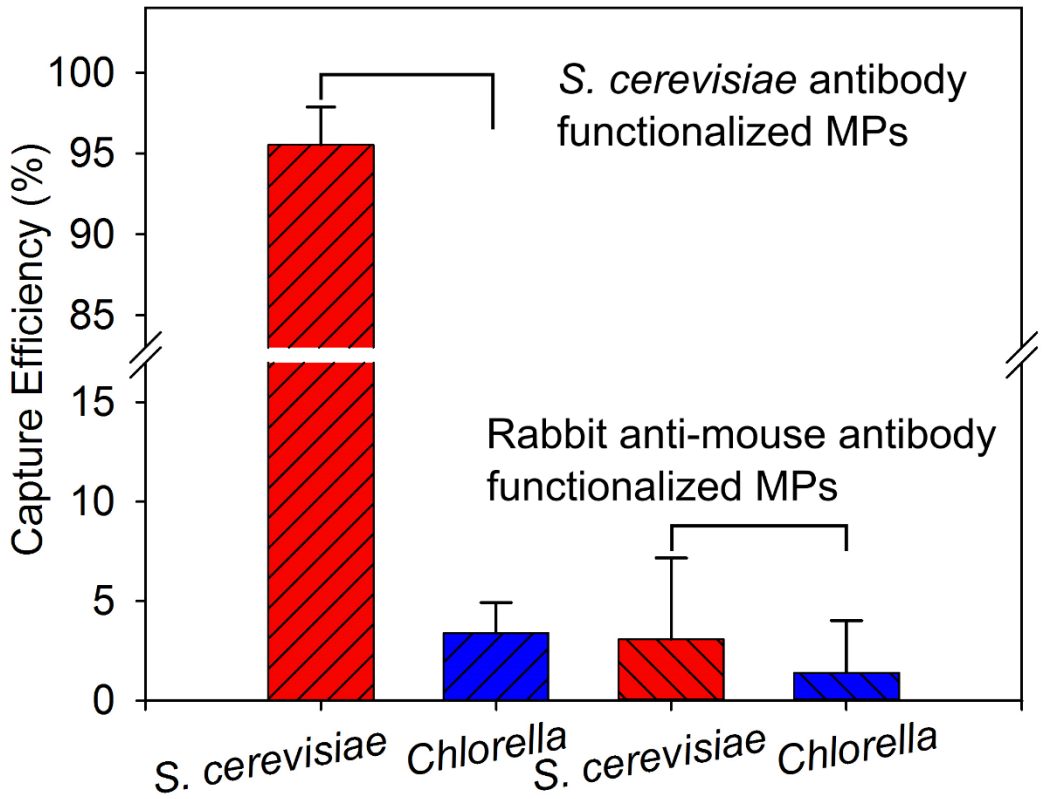

Figure 6.6 Measured capture efficiency of *S. cerevisiae* and *Chlorella*. Both *S. cerevisiae* and *Chlorella* had a concentration of 1000 count/μL

As shown in Figure 6.6, with Ab1-MPs, the capture efficiencies for *S. cerevisiae* and *Chlorella* were 95.5 ± 2.3% (specific capture efficiency) and 3.4 ± 1.5% (nonspecific capture efficiency). With the Ab2-MPs, the nonspecific capture efficiencies for *S. cerevisiae* and *Chlorella* were 3.1 ± 4.1%, and 1.4 ± 2.6%. Although the capture efficiency is highly dependent on the affinity of the antibody, the capture ligand and the contact time of the cell and the surface, the 95.5% capture efficiency is very high in this initial evaluation. Nonspecific attachment (<5%) is low, and is comparable with the nonspecific attachment reported by other studies [198] [8]. With the high specific capture efficiency and the low nonspecific capture efficiency, the proposed device is expected to differentiate and count pathogen cells accurately from a mixture with small errors.

To further reduce the nonspecific attachment, one possible solution is to use a large flow velocity and high shear stress in the capture chamber. A recent study showed that shear stresses ranging from 1.0 to 3.0 dyn/cm^2 were optimal in CD4+ T cell capture [198]. The shear stress was estimated using following equation [199].[172],

$$\tau_w = 6\mu Q/(h^2 w) \tag{6.1}$$

where τ_w is the shear stress at the walls of a rectangular channel, μ is the dynamic viscosity of the fluid, Q is the flow rate, w is the width of microfluidic channel and h is the height of the microfluidic channel. In our test, the dynamic viscosity of PBS buffer was 1×10^{-3} Pa·s [200], and the flow rate was 20 μL/hr. Hence the estimated shear stress is 0.21 dyn/cm^2. By using a large flow rate, the large shear stress at the capture chamber wall may result in a low nonspecific attachment. However, a large flow rate may also wash away the Ab-MPs later; a strong magnetic field is required for a larger flow rate. In addition, nonspecific attachment can also be reduced by: 1) increasing the antibody density on the MP surface and the Ab-MP coverage on the sensing surface, and 2) using antifouling materials to modify the MP and sensor surfaces [201].

To prove that the two-stage RPS is able to accurately detect the target cell concentrations, pure *S. cerevisiae* with concentration ranging from 5×10^2 to 5×10^3 count/μL were tested by both the two-stage RPS with Ab1-MPs coating on the capture chamber and the Accusizer. The capture chamber was coated with Ab1-MPs, which are expected to capture target cells with high efficiency. The cell counts measured by the 1st RPS indicates the target cell concentration while the cell counts measured by the 2nd RPS is used to calculate the capture efficiency at different target cell concentrations.

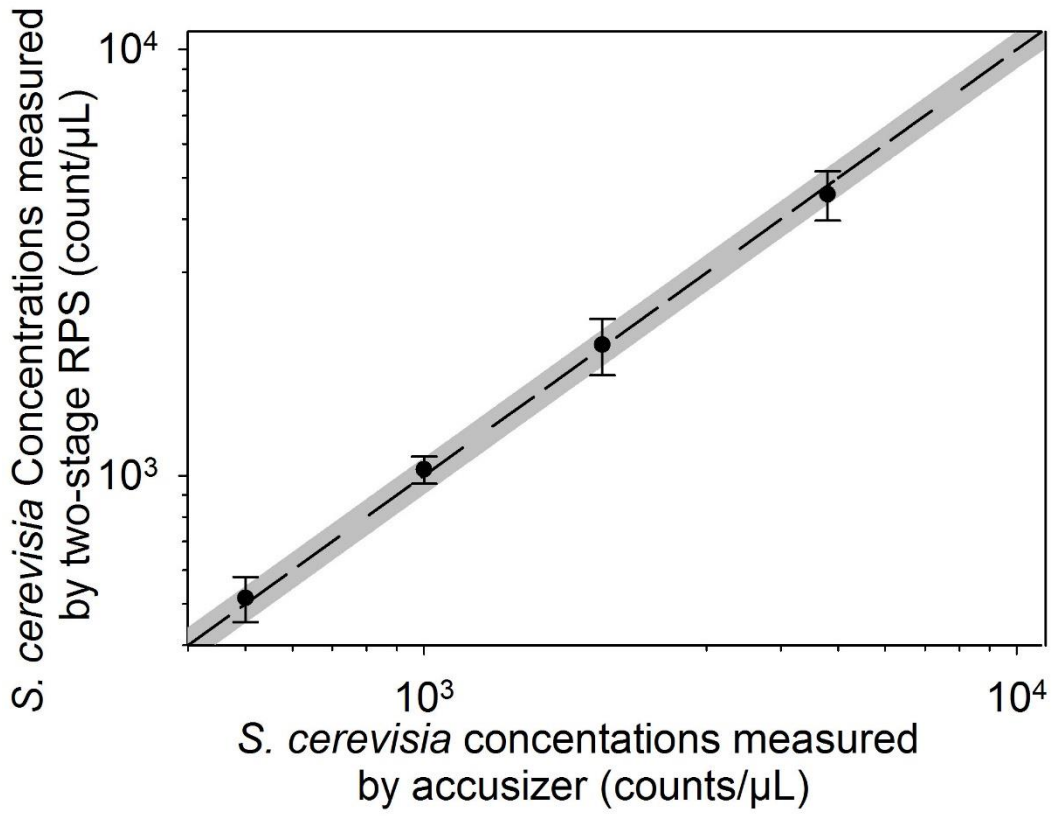

Figure 6.7 The *S. cerevisiae* concentrations measured by two-stage RPS. The gray area represents the measurement uncertainty of the Accusizer (±10%)

The *S. cerevisiae* concentrations measured by two-stage RPS are shown in Figure 6.7. The concentrations measured by the two-stage RPS (black circles) are in good agreement with those measured by the Accusizer. The measurement error ranges from 1.4 to 4.7%, which proves that the two-stage RPS is able to measure the target cell concertation with small error. According to the count reduction measured by the 1st and 2nd RPS, the capture efficiency was calculated to range from 94.8% to 95.5%, which is high and comparable to the results report by other studies [198]. Two possible solutions to further increase the capture efficiency are: 1) using a longer capture chamber to improve interaction between the cells and Ab-MPs, and 2) using antibody or aptamer with higher binding affinity [202]. Another issue that may affect the measurement accuracy is that, at

a higher concentration, the increased chance of two cells transiting through two sensing channels at the same time may cause an increase of both R_1 and R_2 (see Figure 6.1), which will lead to incorrect counts and incorrect concentration measurements. This issue can be overcome by taking two independent measurements of the two RPSs, using two pairs of electrodes.

6.4 Detection of target cells in a mixture with non-target cells

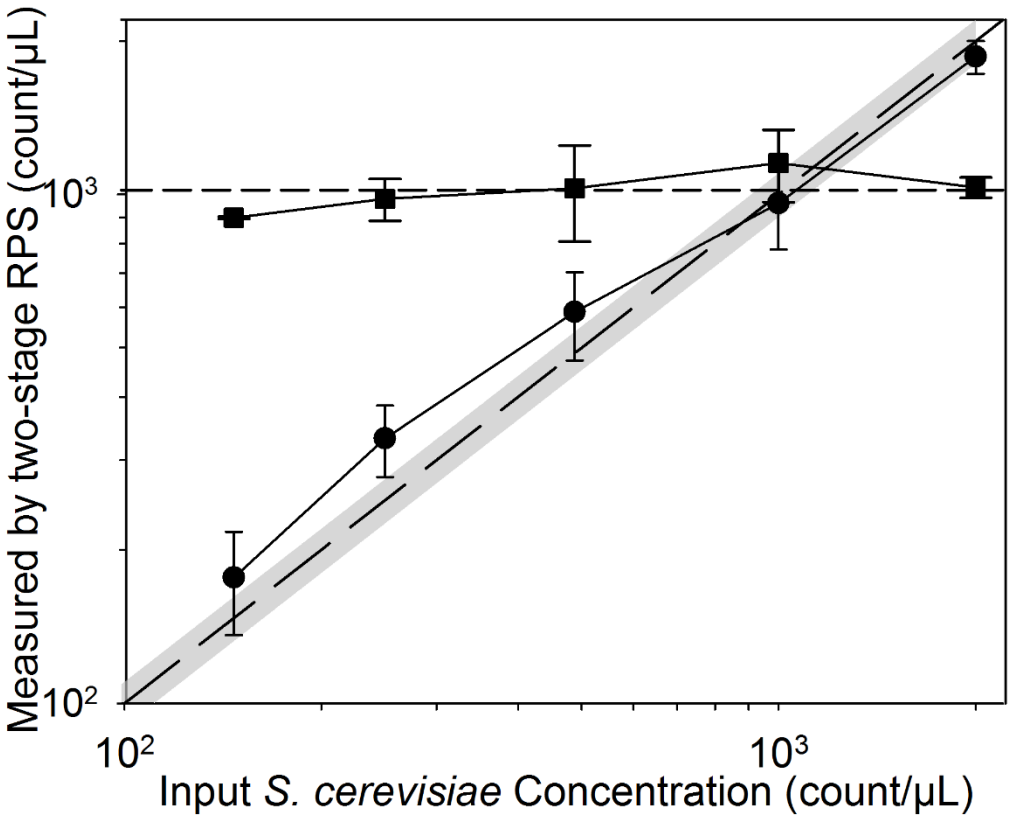

Figure 6.8 *S. cerevisiae* detection in a mixed population of *S. cerevisiae* and *Chlorella*. The gray area represents the measurement uncertainty of Accusizer

Figure 6.8 shows the *S. cerevisiae* detected in a mixed population of *S. cerevisiae* and *Chlorella*. In this experiment, the concentration of *S. cerevisiae* was varied from 5 ×

10^2 to 2×10^3 cells/μL, while the concentration of *Chlorella* was kept constant at 1.019×10^3 count/μL. The measured *S. cerevisiae* concentration vs the input concentration is plotted in Figure 6.8. For comparison, the y = x line (long dash line) and $y = 1 \times 10^3$ count/μL line (short dash line) are also plotted. The *Chlorella* concentration measured by our device and by the Accusizer at all *S. cerevisiae* concentrations was 1018 ± 92 count/μL and 1019 ± 69 count/μL, which agree with each other very well, indicating that the nonspecific capture efficiency is small. For *S. cerevisiae* measurement, the measured concentrations by the two-stage RPS device are accurate when the *S. cerevisiae*/*Chlorella* ratio (target cell to non-target cell ratio) is high (from 1.0 to 2.0). Compared to the Accusizer measurements, the measurement error ranged from 4% to 7%, which is well within the measurement uncertainty of the Accusizer. The best accuracy was achieved when *S. cerevisiae* and *Chlorella* have the same concentration. However, at lower *S. cerevisiae*/*Chlorella* ratio (0.1 to 0.5), the measurement error became higher, ranging from 20% to 32%, which is 10% to 22% higher than the measurement uncertainty of the Accusizer. Note that the detection accuracy is affected by the ratio of target/non-target cells due to the nonspecific attachment of the non-target cells. At low target cell/non-target cell ratios, the detection accuracy decreases because even a small amount of nonspecific attachment causes a large error in the detection of target cells whose concentration is low, which is a universal challenge for all cell immunoassays. For example, a previous study demonstrated that 58.2% of target *L. monocytogenes* was captured when it was mixed with non-target *S. Enteritidis* at a 1:1 ratio[203]. In our experiment, the relative error on the *S. cerevisiae* concentration measurement was 4% when the *S. cerevisiae*/*Chlorella* ratio is 1.0, indicating our method has a higher capture efficiency and higher accuracy. The

accuracy can be further improved by using a capture ligand with a higher affinity, a higher flow rate and/or antifouling surfaces [201].

The advantages of the presented pathogen cell detection method are manifold. First, it eliminates the need for on-chip surface modification, which is typically difficult and time consuming for microchannels; second, the sensing surface can be functionalized just before each test using freshly-made Ab-MPs. This greatly improves the device reliability because antibody have a limited shelf life due to irreversible denaturation [79]. Third, the Ab-MP based capture surface enables a higher capture efficiency due to increased surface roughness. Fourth, the sensing surface functionalization can be regenerated quickly by removing the magnetic field and washing away the magnetic beads for next use. With these advantages, this device can potentially be used for a range of applications in addition to microorganism identification. For example, it can potentially be used for HIV diagnosis, where a CD4/CD8 T lymphocyte ratio less than one is a possible HIV indicator [204]. The device can also be extended to detect multiple types of pathogen cells in a single test by using multiple capture chambers in series, with each chamber coated with one specific Ab-MP layer.

6.5 Summery

In this chapter, a two stage RPS was studied to detect target cell concentrations in a mixture with non-target cells. Antibody-functionalized MPs (Ab-MPs) were used to functionalize the capture chamber surface, and a two-stage resistive pulse sensor was used to detect the pathogen cells. A specific capture efficiency greater than 94.8%, and a

nonspecific capture efficiency as low as 3.4% were achieved. In the mixture measurements, for a *S. cerevisiae*/*Chlorella* ratio ranging from 1.0 to 2.0, the measurement error ranged from 4% to 7%, while the errors were 20% to 32%, for a ratio was 0.1 to 0.5. Without labelling or surface modification processes, this device enables fast and cost-effective pathogen detection and microorganism identification.

CHAPTER VI

CONCLUSIONS AND FUTURE THOUGHTS

7.1 Conclusions

In this research, I developed label-free and multiplexed immunosensor chips based on resistive pulse sensing technology for detection of macromolecular and cellular biomarkers. First, a label-free biomarker detection device based on immunoaggregation and a micro resistive pulse sensor was invented. In the detection, specific biomarkers induced the aggregation of antibody functionalized MPs; the aggregates, whose volume fraction is indicative of biomarker concentration, were detected by the resistive pulse sensor. To demonstrate the device's capability for biomarker detection, rabbit anti-goat IgG, as a model biomarker was measured and a detection range from 16 to 160 ng/mL was achieved. The volume fraction of aggregates was indicative of the biomarker concentration. The volume fraction of aggregates increases with an increase of biomarker concentration. Beyond the upper biomarker detection limit, the volume fraction of aggregates starts to drop, because the biomarkers saturate the binding sites on the MPs and prevent the formation of immunoaggregation. Human ferritin, as a biomarker to iron storage, was also tested using the immunoaggregation biomarker sensor in 10% FBS to mimic the real

disease diagnosis environment. A detection range from 0.1 to 208 ng/mL was achieved. Experiments also found that the detection range can be tuned to lower concentration or higher concentration by using a lower or higher MP concentration. Compared with commercial ELISA kits, this label-free immunoaggregation assay based on the micro resistive pulse senor has a lower limit of detection (0.1 ng/mL for human ferritin) and requires less assay steps, making it a promising technique for onsite, highly sensitive biomarker analysis. Multiplexed immunoaggregation assays based on a two-stage resistive pulse sensor were also studied in this research for detection of multiple biomarkers at the same time. Detection ranges from 5.2 to 208 ng/mL and 3.1 to 51.2×10^3 ng/mL were achieved for human ferritin and mouse anti-rabbit IgG detection, respectively. The multiplexed immunoaggregation assay further promotes the capability of the micro resistive pulse sensor, and enables multiple biomarkers detection in a single test.

For cellular biomarker detection, a two-stage resistive pulse sensor for pathogen measurement was also discovered in this research. Instead of chemical modification of the microchannel surfaces, antibody functionalized MPs were used to functionalize the capture chamber surface via an external magnetic field, and a two-stage resistive pulse sensor was used to detect the count of cells. *S. cerevisiae* was used as a model pathogen cell to test the sensor. A highly specific capture efficiency greater than 94.8%, and a nonspecific capture efficiency as low as 3.4% were achieved. The measurement of *S. cerevisiae* concentration in a mixture with *Chlorella* (control cell) was demonstrated. For a *S. cerevisiae*/*Chlorella* ratio ranging from 1.0 to 2.0, the measurement error ranged from 4% to 7%. While the error was 20% to 32%, for the ratio range from 0.1 to 0.5, which is lower than that of prior research on cell detection with a low target cell/non-target cell ratio. Without labelling or

surface modification processes, this device enables fast and cost-effective pathogen detection and microorganism identification.

The invented devices for macromolecular and cellar biomarker detections are label free, require no surface modifications for the microchannels, and hence are advantageous for developing low cost alternatives in biomarker detection analysis. It is a powerful complement to ELISA for biomarker assay. They can potentially be used for disease diagnosis/prognosis, biodefense, environmental monitoring, food and water safety and biological research.

7.2 Future thoughts

For macromolecular biomarker detection, the immunoaggregation assays based on the micro resistive pulse sensor technologies were applied for the detection of three types of macromolecule biomarkers. The micro resistive pulse sensor based immunoaggregation assay can also be applied to detect various bio-objects including bacterial, fungal and other macromolecule including hormones and proteins, DNA etc., as long as high binding affinity antibody/aptamer probes can be found. To detect additional biomarkers (>3), it is convenient to increase the multiplexed capacity using a multichannel device with a large number of detectors. In order to multiplex/encode the multichannels, one possible solution is frequency division multiplexing [191]. However, a limited number of sensing channels can be added to the multichannel devices because of the narrow frequency range in which the resistive pulse sensors have a resistive behavior [163]. Most MP multiplexing/encoding strategies are designed for optical detection, they require accurate alignment of optics,

extremely high resolution detection and a decoding algorithm which makes these methods bulky, expensive and time-consuming. It is convenient to use micro resistive pulse sensing technology for MP based multiplexing/encoding. One possible multiplexing strategy is to use MP tags (MP tags) with variable cross-section, as show in Figure 7.1.

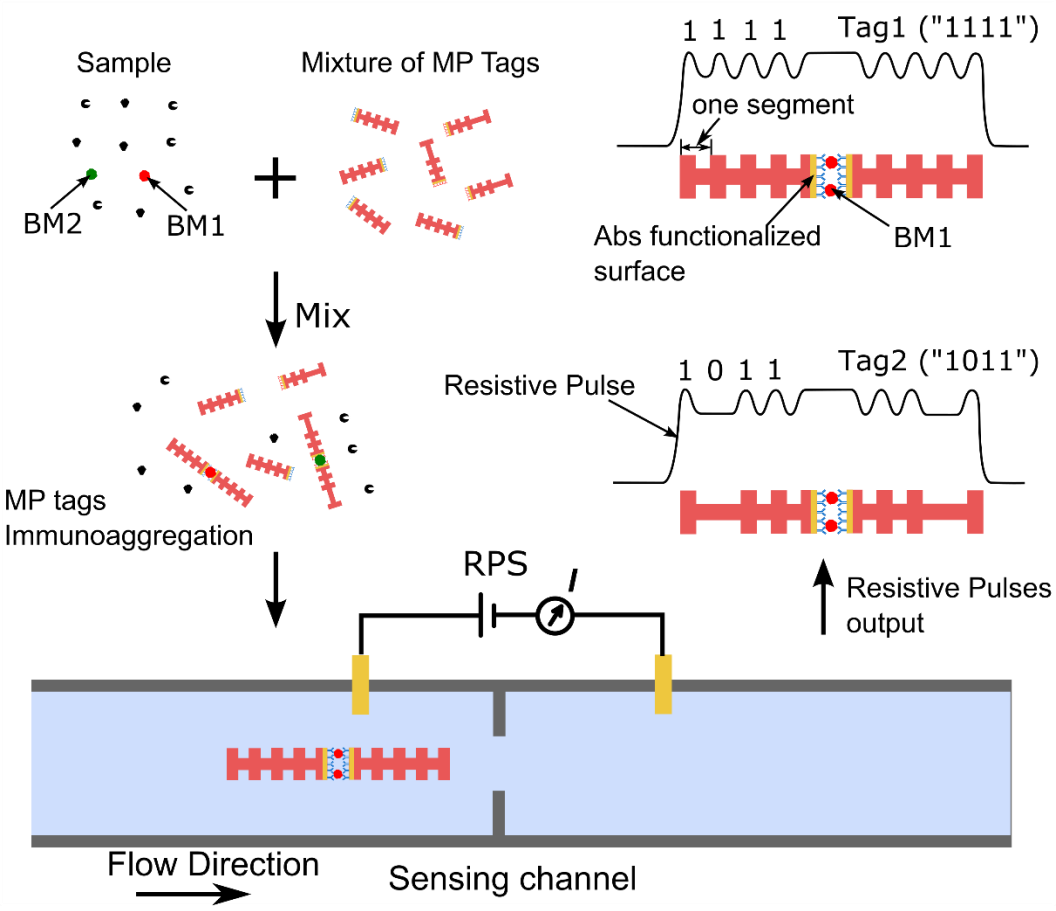

Figure 7.1 Design concept and sensing principle for the MP tags based multiplexed detection

Figure 7.1 shows the design concept and sensing principle for a multiplexed immunoaggregation assay based on MP tags. The MP tag has a variable cross-section (four segments, as shown in Figure 7.1). One end of the MP tag is immobilized with antibody.

After the MP tags are mixed with the sample, the specific binding between target biomarkers and antibody immobilized on the MP tags triggers the aggregation of MP tags. The formed MP tag aggregates are "end-to-end" type aggregates. The "end-to-end" aggregates has been proven by other studies [99]. When an MP tag aggregate passes through the sensing channel it will generate a resistive pulse and the amplitude of this resistive pulse is proportional to the cross-section of the MP tag [162]. For example, the aggregate formed by two MP-Tag1 has eight segments (each MP Tag1 has 4 segments), thus the resistive pulse generated by this aggregate will drop eight times during the transit of the aggregate, which can be marked as a digital signal "1111". In comparison, the resistive pulses generated by MP-Tag2 aggregates can be identified as "1011". The unique resistive pulse signature is used to identify the MP tags. With N segments, the maximum multiplexed capacity is 2^N. Both rod sharp [99] or thin film [30][145] particles can be used as MP tags. Two fabrication methods of MP tags are electrodeposition [126] [32] and lithography [30] [145]. The use of this type of MP tag can significantly increase the multiplexed capability of a micro resistive immunoaggregation sensor. However, several issues must be addressed before using MP tags. Firstly, in order to eliminate the rotation of MP tags, hydro-focusing is required to focus the MP tags in the center of the microchannel. Secondly the length of the sensing channel should be short enough (~10 μm) to differentiate each segment of the MP tags.

In terms of multiplexed cell detection, one possible strategy is to use a capture chamber array, as shown in Figure 7.2 (a). This device consists of a 2 × 3 capture chamber array coated with different Ab functionalized MPs, which is able to detect six types of target cells in a single test. Each capture chamber is monitored by a pair of RPSs. A total

of 8 RPSs will be integrated in this device. Each RPS is modeled as a variable resistance as shown in Figure 7.2 (b) and measured independently.

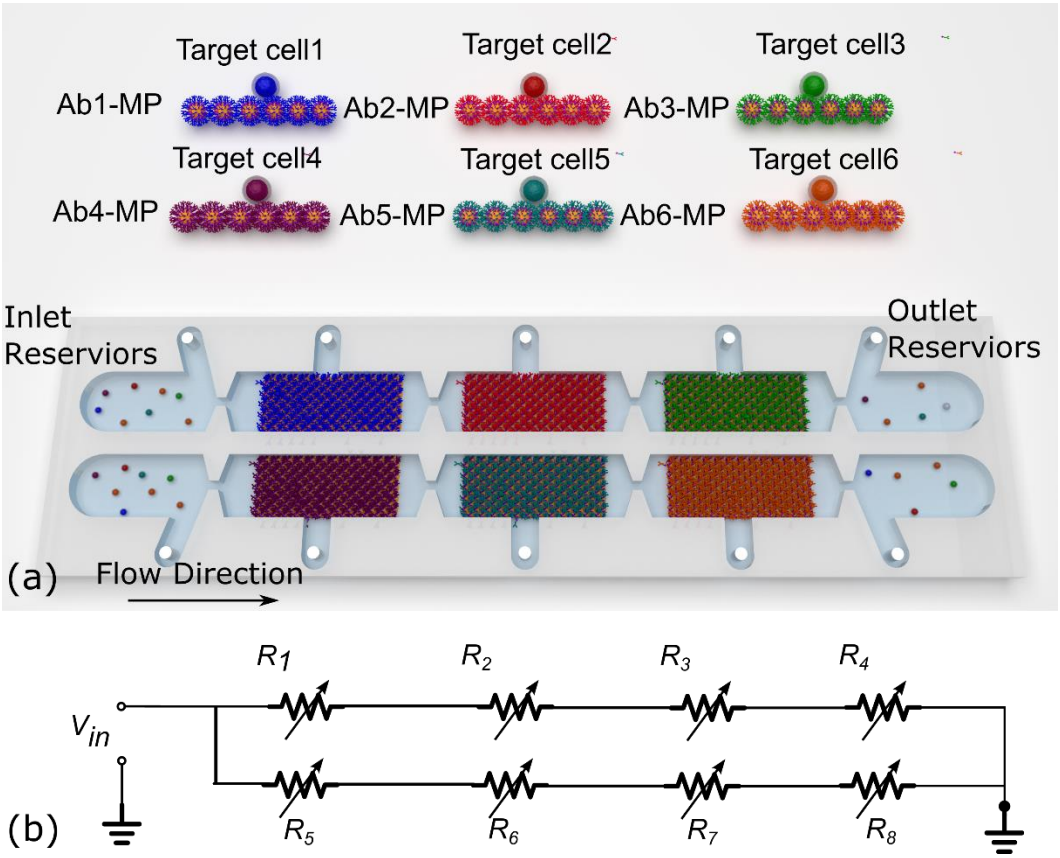

Figure 7.2 (a) Design concept of a 2 × 3 capture chamber array for multiplexed pathogen cell detection. (b) Equivalent circuit of the RPS array

Figure 7.2 shows the design concept of a 2 × 3 capture chamber array for multiplexed pathogen cell detection. For each test, cell samples are loaded into the two inlet reservoirs and driven through each capture chamber. Each chamber is coated with one type of Ab-MPs and able to capture one type of target cells. A pair of RPSs are used to monitor the counts of target cells captured by each chamber. The concentration of target cells is then calculated by using the counts of target cells captured in each chamber divided

by the volume of sample passing through each chamber (assuming the volume of each chamber is negligible comparing with the volume of cell sample).

REFERENCES

[1] Y. Han, H. Wu, F. Liu, G. Cheng, and J. Zhe, "Label-Free Biomarker Assay in a Microresistive Pulse Sensor via Immunoaggregation," *Anal. Chem.*, vol. 86, no. 19, pp. 9717–9722, 2014.

[2] X. Gao, H. J. Mathieu, and M. Schawaller, "Surface modification of polystyrene biochip for biotin-labelled protein/streptavidin or neutravidin coupling used in fluorescence assay," *Surf. Interface Anal.*, vol. 36, no. 12, pp. 1507–1512, 2004.

[3] K. Länge, G. Blaess, A. Voigt, R. Götzen, and M. Rapp, "Integration of a surface acoustic wave biosensor in a microfluidic polymer chip.," *Biosens. Bioelectron.*, vol. 22, no. 2, pp. 227–32, 2006.

[4] B. J. Hindson, A. J. Makarewicz, U. S. Setlur, B. D. Henderer, M. T. McBride, and J. M. Dzenitis, "APDS: the autonomous pathogen detection system.," *Biosens. Bioelectron.*, vol. 20, no. 10, pp. 1925–31, 2005.

[5] A. J. Baeumner, "Biosensors for environmental pollutants and food contaminants.," *Anal. Bioanal. Chem.*, vol. 377, no. 3, pp. 434–45, 2003.

[6] M. J. Jebrail and A. R. Wheeler, "Let's get digital: digitizing chemical biology with microfluidics.," *Curr. Opin. Chem. Biol.*, vol. 14, no. 5, pp. 574–81, 2010.

[7] B. Swaminathan and P. Feng, "Rapid detection of food-borne pathogenic bacteria," *Annu. Rev. Microbiol.*, vol. 48, no. 1, pp. 401–426, 1994.

[8] D. a. Boehm, P. a. Gottlieb, and S. Z. Hua, "On-chip microfluidic biosensor for bacterial detection and identification," *Sensors Actuators B Chem.*, vol. 126, no. 2, pp. 508–514, 2007.

[9] O. Lazcka, F. J. Del Campo, and F. X. Muñoz, “Pathogen detection: a perspective of traditional methods and biosensors.,” *Biosens. Bioelectron.*, vol. 22, no. 7, pp. 1205–17, Feb. 2007.

[10] R. Mayeux, “Biomarkers: potential uses and limitations.,” *NeuroRx*, vol. 1, no. 2, pp. 182–188, 2004.

[11] S. T. Sanjay, G. Fu, M. Dou, F. Xu, R. Liu, H. Qi, and X. Li, “Biomarker detection for disease diagnosis using cost-effective microfluidic platforms,” *Analyst*, 2015.

[12] K. J. Martin, M. V. Fournier, G. P. V. Reddy, and a. B. Pardee, “A Need for Basic Research on Fluid-Based Early Detection Biomarkers,” *Cancer Res.*, vol. 70, no. 13, pp. 5203–5206, 2010.

[13] U. Manne, R. Srivastava, and S. Srivastava, “Keynote review : Recent advances in biomarkers for cancer diagnosis and treatment,” vol. 10, no. 14, 2005.

[14] K. Y. Wang, S. A. Chuang, P. C. Lin, L. S. Huang, S. H. Chen, S. Ouarda, W. H. Pan, P. Y. Lee, C. C. Lin, and Y. J. Chen, “Multiplexed immunoassay: Quantitation and profiling of serum biomarkers using magnetic nanoprobes and MALDI-TOF MS,” *Anal. Chem.*, vol. 80, no. 16, pp. 6159–6167, 2008.

[15] R. Fan, O. Vermesh, A. Srivastava, B. K. H. Yen, L. Qin, H. Ahmad, G. a Kwong, C.-C. Liu, J. Gould, L. Hood, and J. R. Heath, “Integrated barcode chips for rapid, multiplexed analysis of proteins in microliter quantities of blood.,” *Nat. Biotechnol.*, vol. 26, no. 12, pp. 1373–8, 2008.

[16] M. Hossain, C. Wang, and M. Su, “Multiplexed biomarker detection using x-ray fluorescence of composition-encoded nanoparticles,” *Appl. Phys. Lett.*, vol. 97, no. 26, 2010.

[17] B. K. Van Weemen and A. H. W. M. Schuurs, “Immunoassay using antigen—enzyme conjugates,” *FEBS Lett.*, vol. 15, no. 3, pp. 232–236, 1971.

[18] E. Engvall and P. Perlmann, “Enzyme-linked immunosorbent assay (ELISA). Quantitative assay of immunoglobulin G.,” *Immunochemistry*, vol. 8, no. 9, pp. 871–4, Sep. 1971.

[19] K. Sato, M. Tokeshi, T. Odake, H. Kimura, T. Ooi, M. Nakao, and T. Kitamori,

"Integration of an Immunosorbent Assay System : Analysis of Secretory Human Immunoglobulin A on Polystyrene Beads in a Microchip," vol. 72, no. 6, pp. 1144–1147, 2000.

[20] T. Ohashi, K. Mawatari, K. Sato, M. Tokeshi, and T. Kitamori, "A micro-ELISA system for the rapid and sensitive measurement of total and specific immunoglobulin E and clinical application to allergy diagnosis.," *Lab Chip*, vol. 9, no. 7, pp. 991–5, 2009.

[21] S. Choi, M. Goryll, L. Y. M. Sin, P. K. Wong, and J. Chae, "Microfluidic-based biosensors toward point-of-care detection of nucleic acids and proteins," *Microfluid. Nanofluidics*, vol. 10, no. 2, pp. 231–247, 2010.

[22] A. H. C. Ng, U. Uddayasankar, and A. R. Wheeler, "Immunoassays in microfluidic systems.," *Anal. Bioanal. Chem.*, vol. 397, no. 3, pp. 991–1007, 2010.

[23] H. Jiang, X. Weng, and D. Li, "Microfluidic whole-blood immunoassays," *Microfluid. Nanofluidics*, vol. 10, no. 5, pp. 941–964, 2010.

[24] E. Stern, A. Vacic, N. K. Rajan, J. M. Criscione, J. Park, B. R. Ilic, D. J. Mooney, M. A. Reed, and T. M. Fahmy, "Label-free biomarker detection from whole blood," vol. 5, no. February, 2010.

[25] Y.-S. Sun, J. P. Landry, Y. Y. Fei, X. D. Zhu, J. T. Luo, X. B. Wang, and K. S. Lam, "Effect of Fluorescently Labeling Protein Probes on Kinetics of Protein−Ligand Reactions," *Langmuir*, vol. 19, no. 12, pp. 13399–13405, 2008.

[26] A. J. Qavi, A. L. Washburn, J.-Y. Byeon, and R. C. Bailey, "Label-free technologies for quantitative multiparameter biological analysis.," *Anal. Bioanal. Chem.*, vol. 394, no. 1, pp. 121–35, May 2009.

[27] R. Afshar, Y. Moser, T. Lehnert, and M. a M. Gijs, "Three-dimensional magnetic focusing of superparamagnetic beads for on-chip agglutination assays.," *Anal. Chem.*, vol. 83, no. 3, pp. 1022–9, Feb. 2011.

[28] Y. Moser, T. Lehnert, and M. a M. Gijs, "On-chip immuno-agglutination assay with analyte capture by dynamic manipulation of superparamagnetic beads.," *Lab Chip*, vol. 9, no. 22, pp. 3261–7, 2009.

[29] M. Wiklund, O. Nord, R. Gothäll, A. V Chernyshev, P.-A. Nygren, and H. M. Hertz, "Fluorescence-microscopy-based image analysis for analyte-dependent particle doublet detection in a single-step immunoagglutination assay.," *Anal. Biochem.*, vol. 338, no. 1, pp. 90–101, 2005.

[30] D. C. Pregibon, M. Toner, and P. S. Doyle, "Multifunctional encoded particles for high-throughput biomolecule analysis.," *Science*, vol. 315, no. 5817, pp. 1393–1396, 2007.

[31] S. Solé, "New materials for electrochemical sensing III. Beads," *TrAC Trends Anal. Chem.*, vol. 20, no. 2, pp. 102–110, 2001.

[32] S. R. Nicewarner-Pena, R. G. Freeman, B. D. Reiss, L. He, D. J. Pena, I. D. Walton, R. Cromer, C. D. Keating, and M. J. Natan, "Submicrometer metallic barcodes.," *Science*, vol. 294, no. 5540, pp. 137–141, 2001.

[33] J. Canning, K. Sommer, M. Englund, and S. Huntington, "Novel colloidal materials for high-throughput screening applications in drug discovery and genomics," *Adv. Mater.*, vol. 13, no. 12–13, pp. 975–979, 2001.

[34] J. Dasso, J. Lee, H. Bach, and R. G. Mage, "A comparison of ELISA and flow microsphere-based assays for quantification of immunoglobulins.," *J. Immunol. Methods*, vol. 263, no. 1–2, pp. 23–33, May 2002.

[35] C. T. Lim and Y. Zhang, "Bead-based microfluidic immunoassays: the next generation.," *Biosens. Bioelectron.*, vol. 22, no. 7, pp. 1197–204, Feb. 2007.

[36] E. Moran and S. Sarshar, "Radio frequency tag encoded combinatorial library method for the discovery of tripeptide-substituted cinnamic acid inhibitors of the protein tyrosine phosphatase," *J. Am. Chem. Soc.*, no. 6, pp. 10787–10788, 1995.

[37] P. D. Skottrup, M. Nicolaisen, and A. F. Justesen, "Towards on-site pathogen detection using antibody-based sensors.," *Biosens. Bioelectron.*, vol. 24, no. 3, pp. 339–48, 2008.

[38] L. C. Waters, S. C. Jacobson, N. Kroutchinina, J. Khandurina, R. S. Foote, and J. M. Ramsey, "Microchip device for cell lysis, multiplex PCR amplification, and electrophoretic sizing.," *Anal. Chem.*, vol. 70, no. 1, pp. 158–162, 1998.

[39] A. M. Foudeh, T. Fatanat Didar, T. Veres, and M. Tabrizian, “Microfluidic designs and techniques using lab-on-a-chip devices for pathogen detection for point-of-care diagnostics.,” *Lab Chip*, vol. 12, no. 18, pp. 3249–66, Sep. 2012.

[40] T. G. Henares, F. Mizutani, and H. Hisamoto, “Current development in microfluidic immunosensing chip.,” *Anal. Chim. Acta*, vol. 611, no. 1, pp. 17–30, 2008.

[41] B. Y. R. S. Yalow, S. A. Berson, R. Service, V. A. Hospital, and N. York, “Immunoassay of endogenous plasma insulin in man,” *Obes. Res.*, vol. 4, no. 6, pp. 583–600, 1996.

[42] A. E. Bolton and W. M. Hunter, “The labelling of proteins to high specific radioactivities by conjugation to a 125I-containing acylating agent.,” *Biochem. J.*, vol. 133, no. 3, pp. 529–39, 1973.

[43] S. A. Berson and R. S. Yalow, “General principles of radioimmunoassay,” *Clin. Chim. acta*, vol. 369, no. 2, pp. 125–143, 2006.

[44] S. D. Gan and K. R. Patel, “Enzyme immunoassay and enzyme-linked immunosorbent assay.,” *J. Invest. Dermatol.*, vol. 133, no. 9, p. e12, Sep. 2013.

[45] H. V Webster, a J. Bone, K. a Webster, and T. J. Wilkin, “Comparison of an enzyme-linked immunosorbent assay (ELISA) with a radioimmunoassay (RIA) for the measurement of rat insulin.,” *J. Immunol. Methods*, vol. 134, no. 1, pp. 95–100, 1990.

[46] A. Voller, A. Bartlett, and D. E. Bidwell, “Enzyme immunoassays with special reference to ELISA techniques,” pp. 507–520, 1978.

[47] E. Ishikawa, “Development and clinical application of sensitive enzyme immunoassay for macromolecular antigens--a review.,” *Clin. Biochem.*, vol. 20, no. 6, pp. 375–85, 1987.

[48] J. C. Booth, G. Hannington, T. M. Bakir, H. Stern, H. Kangro, P. D. Griffiths, and R. B. Heath, “Comparison of enzyme-linked immunosorbent assay, radioimmunoassay, complement fixation, anticomplement immunofluorescence and passive haemagglutination techniques for detecting cytomegalovirus IgG antibody.,” *J. Clin. Pathol.*, vol. 35, no. 12, pp. 1345–8, 1982.

[49] R. M. Lequin, “Enzyme immunoassay (EIA)/enzyme-linked immunosorbent assay (ELISA).,” *Clin. Chem.*, vol. 51, no. 12, pp. 2415–8, 2005.

[50] M. Y. Liu, A. M. Xydakis, R. C. Hoogeveen, P. H. Jones, E. O. B. Smith, K. W. Nelson, and C. M. Ballantyne, “Multiplexed analysis of biomarkers related to obesity and the metabolic syndrome in human plasma, using the Luminex-100 system,” *Clin. Chem.*, vol. 51, no. 7, pp. 1102–1109, 2005.

[51] L. J. Lucas, J.-H. Han, J. Chesler, and J.-Y. Yoon, “Latex immunoagglutination assay for a vasculitis marker in a microfluidic device using static light scattering detection.,” *Biosens. Bioelectron.*, vol. 22, no. 9–10, pp. 2216–22, 2007.

[52] J. S. Daniels and N. Pourmand, “Label-free impedance biosensors: Opportunities and challenges,” *Electroanalysis*, vol. 19, no. 12, pp. 1239–1257, 2007.

[53] S. Ray, G. Mehta, and S. Srivastava, “Label-free detection techniques for protein microarrays: prospects, merits and challenges.,” *Proteomics*, vol. 10, no. 4, pp. 731–48, Feb. 2010.

[54] L. Gervais and E. Delamarche, “Toward one-step point-of-care immunodiagnostics using capillary-driven microfluidics and PDMS substrates.,” *Lab Chip*, vol. 9, no. 23, pp. 3330–7, 2009.

[55] C. Jönsson, M. Aronsson, G. Rundström, C. Pettersson, I. Mendel-Hartvig, J. Bakker, E. Martinsson, B. Liedberg, B. MacCraith, O. Ohman, and J. Melin, “Silane-dextran chemistry on lateral flow polymer chips for immunoassays.,” *Lab Chip*, vol. 8, no. 7, pp. 1191–7, 2008.

[56] R. S. Sista, A. E. Eckhardt, V. Srinivasan, M. G. Pollack, S. Palanki, and V. K. Pamula, “Heterogeneous immunoassays using magnetic beads on a digital microfluidic platform.,” *Lab Chip*, vol. 8, no. 12, pp. 2188–96, 2008.

[57] H. Liu and R. M. Crooks, “Three-Dimensional Paper Microfluidic Devices Assembled Using the Principles of Origami,” 2011.

[58] P. Novo, D. M. F. Prazeres, V. Chu, and J. P. Conde, “Microspot-based ELISA in microfluidics: chemiluminescence and colorimetry detection using integrated thin-film hydrogenated amorphous silicon photodiodes.,” *Lab Chip*, vol. 11, no. 23, pp. 4063–71, 2011.

[59] J. M. Klostranec, Q. Xiang, G. A. Farcas, J. A. Lee, A. Rhee, E. I. Lafferty, S. D. Perrault, K. C. Kain, and W. C. W. Chan, "Convergence of Quantum Dot Barcodes with Microfluidics and Signal Processing for Multiplexed High-Throughput Infectious Disease Diagnostics," 2007.

[60] Q. D. Microfluidic, M. Hu, J. Yan, Y. He, H. Lu, L. Weng, S. Song, C. Fan, and L. Wang, "Ultrasensitive , Multiplexed Detection of Cancer Biomarkers Directly in Serum by Protein Chip," vol. 4, no. 1.

[61] K. N. Han, C. A. Li, and G. H. Seong, "Microfluidic chips for immunoassays.," *Annu. Rev. Anal. Chem. (Palo Alto. Calif).*, vol. 6, pp. 119–41, 2013.

[62] P. Liu, T. S. Seo, N. Beyor, K. Shin, J. R. Scherer, and R. A. Mathies, "Integrated Portable Polymerase Chain Reaction-Capillary Electrophoresis Microsystem for Rapid Forensic Short Tandem Repeat Typing," vol. 79, no. 5, pp. 1881–1889, 2007.

[63] F. Xu, P. Datta, H. Wang, S. Gurung, M. Hashimoto, S. Wei, J. Goettert, R. L. Mccarley, and S. A. Soper, "Polymer Microfluidic Chips with Integrated Waveguides for Reading Microarrays," vol. 79, no. 23, pp. 9007–9013, 2007.

[64] W. Du, Q. Fang, Q. He, and Z. Fang, "High-Throughput Nanoliter Sample Introduction Microfluidic Chip-Based Flow Injection Analysis System with Gravity-Driven Flows," vol. 77, no. 5, pp. 1330–1337, 2005.

[65] J. Seo and L. P. Lee, "Disposable integrated microfluidics with self-aligned planar microlenses," *Sensors Actuators B Chem.*, vol. 99, no. 2–3, pp. 615–622, May 2004.

[66] W.-T. Liu, L. Zhu, Q.-W. Qin, Q. Zhang, H. Feng, and S. Ang, "Microfluidic device as a new platform for immunofluorescent detection of viruses.," *Lab Chip*, vol. 5, no. 11, pp. 1327–30, 2005.

[67] L. J. Lucas, J. N. Chesler, and J.-Y. Yoon, "Lab-on-a-chip immunoassay for multiple antibodies using microsphere light scattering and quantum dot emission.," *Biosens. Bioelectron.*, vol. 23, no. 5, pp. 675–81, 2007.

[68] F. B. Myers and L. P. Lee, "Innovations in optical microfluidic technologies for point-of-care diagnostics.," *Lab Chip*, vol. 8, no. 12, pp. 2015–31, 2008.

[69] O. Hofmann, X. Wang, A. Cornwell, S. Beecher, A. Raja, D. D. C. Bradley, A. J. Demello, and J. C. Demello, "Monolithically integrated dye-doped PDMS long-pass filters for disposable on-chip fluorescence detection.," *Lab Chip*, vol. 6, no. 8, pp. 981–7, 2006.

[70] D. V. Vezenov, B. T. Mayers, D. B. Wolfe, and G. M. Whitesides, "Integrated fluorescent light source for optofluidic applications," *Appl. Phys. Lett.*, vol. 86, no. 4, p. 041104, 2005.

[71] L. Novak, P. Neuzil, J. Pipper, Y. Zhang, and S. Lee, "An integrated fluorescence detection system for lab-on-a-chip applications.," *Lab Chip*, vol. 7, no. 1, pp. 27–9, 2007.

[72] B. V Chikkaveeraiah, A. A. Bhirde, N. Y. Morgan, H. S. Eden, and X. Chen, "Electrochemical Immunosensors for Detection of Cancer Protein Biomarkers," no. 8, pp. 6546–6561, 2012.

[73] M. Dequaire, C. Degrand, B. P. De Clermont-ferrand, and A. Landais, "An Electrochemical Metalloimmunoassay Based on a Colloidal Gold Label," vol. 72, no. 22, pp. 5521–5528, 2000.

[74] J. F. Rusling, C. V Kumar, J. S. Gutkind, and V. Patel, "Measurement of biomarker proteins for point-of-care early detection and monitoring of cancer.," *Analyst*, vol. 135, no. 10, pp. 2496–511, 2010.

[75] J. Wang, "Carbon-Nanotube Based Electrochemical Biosensors: A Review," *Electroanalysis*, vol. 17, no. 1, pp. 7–14, 2005.

[76] S. N. Kim, J. F. Rusling, and F. Papadimitrakopoulos, "Carbon Nanotubes for Electronic and Electrochemical Detection of Biomolecules.," *Adv. Mater.*, vol. 19, no. 20, pp. 3214–3228, 2007.

[77] X. Li, R. Wang, and X. Zhang, "Electrochemiluminescence immunoassay at a nanoporous gold leaf electrode and using CdTe quantun dots as labels," *Microchim. Acta*, vol. 172, no. 3–4, pp. 285–290, 2010.

[78] B. N. Tags, "Ultrasensitive Immunoassay of Protein Biomarker Based," *Anal. Chem.*, vol. 83, no. 13, pp. 5214–5221, 2011.

[79] S. D. Jayasena, “Aptamers: An emerging class of molecules that rival antibodies in diagnostics,” *Clin. Chem.*, vol. 45, no. 9, pp. 1628–1650, 1999.

[80] B. O. Liedberg, “Surface plasmon resonance for gas detection and biosensing,” *Sensors and Actuators*, vol. 4, pp. 299–304, 1983.

[81] M. Fleischmann, “Raman spectra of pyridine adsorbed at a silver electrode,” *Chem. Phys. Lett.*, vol. 26, no. 2, pp. 2–5, 1974.

[82] A. Bromberg and R. a Mathies, “Multichannel homogeneous immunoassay for detection of 2,4,6-trinitrotoluene (TNT) using a microfabricated capillary array electrophoresis chip.,” *Electrophoresis*, vol. 25, no. 12, pp. 1895–900, 2004.

[83] A. Bromberg, R. A. Mathies, J. B. I. Trans, and E. Devices, “Homogeneous Immunoassay for Detection of TNT and Its Analogues on a Microfabricated Capillary Electrophoresis Chip is developed using a microfabricated capillary electro-,” vol. 75, no. 5, pp. 1188–1195, 2003.

[84] P. C. Mathias, N. Ganesh, and B. T. Cunningham, “Application of Photonic Crystal Enhanced Fluorescence to a Cytokine Immunoassay,” vol. 80, no. 23, pp. 9013–9020, 2008.

[85] A. L. Washburn, M. S. Luchansky, A. L. Bowman, and R. C. Bailey, “Letters to Analytical Chemistry Quantitative , Label-Free Detection of Five Protein Biomarkers Using Multiplexed Arrays of Silicon Photonic Microring Resonators,” vol. 82, no. 1, pp. 69–72, 2010.

[86] A. Ymeti, J. Greve, P. V Lambeck, T. Wink, T. A. M. Beumer, and R. R. Wijn, “Fast , Ultrasensitive Virus Detection Using a Young Interferometer Sensor,” pp. 12–15, 2007.

[87] X. Zhu, J. P. Landry, Y. Sun, J. P. Gregg, K. S. Lam, and X. Guo, “Oblique-incidence reflectivity difference microscope for label-free high-throughput detection of biochemical reactions in a microarray format,” vol. 12, pp. 8–11, 2007.

[88] Y. Tang, X. Zeng, and J. Liang, “Surface plasmon resonance: An Introduction to a surface spectroscopy technique,” *J. Chem. Educ.*, vol. 87, no. 7, pp. 742–746, 2010.

[89] M. S. Chiriacò, E. Primiceri, E. D'Amone, R. E. Ionescu, R. Rinaldi, and G. Maruccio, "EIS microfluidic chips for flow immunoassay and ultrasensitive cholera toxin detection.," *Lab Chip*, vol. 11, no. 4, pp. 658–63, Feb. 2011.

[90] M. Lee, K. Y. Baik, M. Noah, Y.-K. Kwon, J.-O. Lee, and S. Hong, "Nanowire and nanotube transistors for lab-on-a-chip applications.," *Lab Chip*, vol. 9, no. 16, pp. 2267–80, 2009.

[91] H. Lang, N. Backmann, C. Zahnd, F. Huber, A. Bietsch, A. Plu, M. Hegner, C. Gerber, and H. Gu, "A label-free immunosensor array using single-chain," vol. 102, no. 41, pp. 5–10, 2005.

[92] K. S. Hwang, H. Lee, J. Park, S. Yoon, and H. Park, "In-situ quantitative analysis of a prostate-specific antigen (PSA) using a nanomechanical PZT cantilever," pp. 547–552, 2004.

[93] V. S. . Craig and M. Plunkett, "Determination of coupled solvent mass in quartz crystal microbalance measurements using deuterated solvents," *J. Colloid Interface Sci.*, vol. 262, no. 1, pp. 126–129, 2003.

[94] J. a. Molina-Bolívar and F. Galisteo-González, "Latex Immunoagglutination Assays," *J. Macromol. Sci. Part C Polym. Rev.*, vol. 45, no. 1, pp. 59–98, 2005.

[95] M. Wiklund and H. M. Hertz, "Ultrasonic enhancement of bead-based bioaffinity assays.," *Lab Chip*, vol. 6, no. 10, pp. 1279–92, 2006.

[96] K. S. Kim and J.-K. Park, "Magnetic force-based multiplexed immunoassay using superparamagnetic nanoparticles in microfluidic channel.," *Lab Chip*, vol. 5, no. 6, pp. 657–64, 2005.

[97] J. M. Singer and C. M. Plotz, "The latex fixation test: I. Application to the serologic diagnosis of rheumatoid arthritis," *Am. J. Med.*, vol. 21, no. 6, pp. 888–892, 1956.

[98] V. S. Garcia, V. D. G. Gonzalez, I. S. Marcipar, J. R. Vega, and L. M. Gugliotta, "Optimisation and standardisation of an immunoagglutination assay for the diagnosis of Trypanosoma cruzi infection based on latex-(recombinant antigen) complexes," *Trop. Med. Int. Heal.*, vol. 19, no. 1, pp. 37–46, 2014.

[99] M. Platt, G. R. Willmott, and G. U. Lee, "Resistive pulse sensing of analyte-induced multicomponent rod aggregation using tunable pores," *Small*, vol. 8, no. 15, pp. 2436–2444, 2012.

[100] J. Knight, A. Vishwanath, J. Brody, and R. Austin, "Hydrodynamic Focusing on a Silicon Chip: Mixing Nanoliters in Microseconds," *Phys. Rev. Lett.*, vol. 80, no. 17, pp. 3863–3866, 1998.

[101] N. Pamme, R. Koyama, and A. Manz, "Counting and sizing of particles and particle agglomerates in a microfluidic device using laser light scattering: application to a particle-enhanced immunoassay.," *Lab Chip*, vol. 3, no. 3, pp. 187–92, 2003.

[102] M. Wiklund, O. Nord, R. Gothäll, A. V Chernyshev, P.-A. Nygren, and H. M. Hertz, "Fluorescence-microscopy-based image analysis for analyte-dependent particle doublet detection in a single-step immunoagglutination assay.," *Anal. Biochem.*, vol. 338, no. 1, pp. 90–101, 2005.

[103] H. Wu, Y. Han, X. Yang, G. G. Chase, Q. Tang, C.-J. Lee, B. Cao, J. Zhe, and G. Cheng, "A Versatile Microparticle-Based Immunoaggregation Assay for Macromolecular Biomarker Detection and Quantification," *PLoS One*, vol. 10, no. 2, p. e0115046, 2015.

[104] S. J. Gray, M. A. Sobanski, E. B. Kaczmarski, M. Guiver, W. J. Marsh, R. Borrow, R. A. Barnes, and W. T. Coakley, "Ultrasound-enhanced latex immunoagglutination and PCR as complementary methods for non-culture-based confirmation of meningococcal disease.," *J. Clin. Microbiol.*, vol. 37, no. 6, pp. 1797–801, 1999.

[105] H. Nilsson, M. Wiklund, T. Johansson, H. M. Hertz, and S. Nilsson, "Microparticles for selective protein determination in capillary electrophoresis," *Electrophoresis*, vol. 22, no. 12, pp. 2384–2390, 2001.

[106] M. Wiklund and H. M. Hertz, "Ultrasonic enhancement of bead-based bioaffinity assays.," *Lab Chip*, vol. 6, no. 10, pp. 1279–92, 2006.

[107] N. E. Thomas and W. T. Coakley, "Measurement of antigen concentration by an ultrasound-enhanced latex immunoagglutination assay," *Ultrasound Med. Biol.*, vol. 22, no. 9, pp. 1277–1284, 1996.

[108] X. Xuan, J. Zhu, and C. Church, “Particle focusing in microfluidic devices,” *Microfluid. Nanofluidics*, vol. 9, no. 1, pp. 1–16, 2010.

[109] R. W. DeBlois, “Counting and Sizing of Submicron Particles by the Resistive Pulse Technique,” *Rev. Sci. Instrum.*, vol. 41, no. 7, p. 909, 1970.

[110] C. C. Harrell, Y. Choi, L. P. Horne, L. A. Baker, Z. S. Siwy, C. R. Martin, V. Gaines, R. V May, I. Final, and F. July, “Resistive-Pulse DNA Detection with a Conical Nanopore Sensor,” no. 31, pp. 10837–10843, 2006.

[111] J. Sha, T. Hasan, S. Milana, C. Bertulli, N. a W. Bell, G. Privitera, Z. Ni, Y. Chen, F. Bonaccorso, A. C. Ferrari, U. F. Keyser, and Y. Y. S. Huang, “Nanotubes complexed with DNA and proteins for resistive-pulse sensing.,” *ACS Nano*, vol. 7, no. 10, pp. 8857–69, 2013.

[112] H. Bayley and C. R. Martin, “Resistive-pulse sensing-from microbes to molecules,” *Chem. Rev.*, vol. 100, no. 7, pp. 2575–2594, 2000.

[113] Z. D. Harms, K. B. Mogensen, P. S. Nunes, K. Zhou, B. W. Hildenbrand, I. Mitra, Z. Tan, A. Zlotnick, J. P. Kutter, and S. C. Jacobson, “Nanofluidic devices with two pores in series for resistive-pulse sensing of single virus capsids.,” *Anal. Chem.*, vol. 83, no. 24, pp. 9573–8, 2011.

[114] D. J. Niedzwiecki, R. Iyer, P. N. Borer, and L. Movileanu, “Sampling a Biomarker of the Human Immunode fi ciency Virus across a Synthetic Nanopore,” no. 4, pp. 3341–3350, 2013.

[115] A. Carbonaro and L. L. Sohn, “A resistive-pulse sensor chip for multianalyte immunoassays.,” *Lab Chip*, vol. 5, no. 10, pp. 1155–60, 2005.

[116] K. J. Freedman, A. R. Bastian, I. Chaiken, and M. J. Kim, “Solid-state nanopore detection of protein complexes: applications in healthcare and protein kinetics.,” *Small*, vol. 9, no. 5, pp. 750–9, 2013.

[117] L. T. Sexton, L. P. Horne, S. a Sherrill, G. W. Bishop, L. a Baker, and C. R. Martin, “Resistive-pulse studies of proteins and protein/antibody complexes using a conical nanotube sensor.,” *J. Am. Chem. Soc.*, vol. 129, no. 43, pp. 13144–52, 2007.

[118] J. J. Kasianowicz, E. Brandin, D. Branton, and D. W. Deamer, "Characterization of individual polynucleotide molecules using a membrane channel.," *Proc. Natl. Acad. Sci. U. S. A.*, vol. 93, no. 24, pp. 13770–3, 1996.

[119] S. Nanopore, A. J. Storm, C. Storm, J. Chen, and H. Zandbergen, "Fast DNA Translocation through a," pp. 1–5, 2005.

[120] M. Wanunu, "Nanopores: A journey towards DNA sequencing," *Phys. Life Rev.*, vol. 9, no. 2, pp. 125–158, 2012.

[121] S. Harrer, S. C. Kim, C. Schieber, S. Kannam, N. Gunn, S. Moore, D. Scott, R. Bathgate, S. Skafidas, and J. M. Wagner, "Label-free screening of single biomolecules through resistive pulse sensing technology for precision medicine applications," *Nanotechnology*, vol. 26, no. 18, p. 182502, 2015.

[122] Z. R. Yurkovetsky, F. Y. Linkov, D. E Malehorn, and A. E. Lokshin, "Multiple biomarker panels for early detection of ovarian cancer.," *Future Oncol.*, vol. 2, no. 6, pp. 733–741, 2006.

[123] R. G. Moore, A. K. Brown, M. C. Miller, S. Skates, W. J. Allard, T. Verch, M. Steinhoff, G. Messerlian, P. DiSilvestro, C. O. Granai, and R. C. Bast, "The use of multiple novel tumor biomarkers for the detection of ovarian carcinoma in patients with a pelvic mass," *Gynecol. Oncol.*, vol. 108, no. 2, pp. 402–408, 2008.

[124] P. Bahrmann, a. Bahrmann, B. Hofner, M. Christ, S. Achenbach, C. C. Sieber, and T. Bertsch, "Multiple biomarker strategy for improved diagnosis of acute heart failure in older patients presenting to the emergency department," *Eur. Hear. J. Acute Cardiovasc. Care*, vol. 4, no. 2, pp. 137–147, 2015.

[125] F. Wei, P. Patel, W. Liao, K. Chaudhry, L. Zhang, M. Arellano-Garcia, S. Hu, D. Elashoff, H. Zhou, S. Shukla, F. Shah, C. M. Ho, and D. T. Wong, "Electrochemical sensor for multiplex biomarkers detection," *Clin. Cancer Res.*, vol. 15, no. 13, pp. 4446–4452, 2009.

[126] K. Braeckmans, S. C. De Smedt, M. Leblans, R. Pauwels, and J. Demeester, "Encoding microcarriers: present and future technologies.," *Nat. Rev. Drug Discov.*, vol. 1, no. 6, pp. 447–456, 2002.

[127] a. Kumar, G. Goel, E. Fehrenbach, a. K. Puniya, and K. Singh, "Microarrays: The technology, analysis and application," *Eng. Life Sci.*, vol. 5, no. 3, pp. 215–222,

2005.

[128] M. F. Templin, D. Stoll, J. M. Schwenk, O. Pötz, S. Kramer, and T. O. Joos, "Protein microarrays: Promising tools for proteomic research," *Proteomics*, vol. 3, no. 11, pp. 2155–2166, 2003.

[129] B. M. Murphy, X. He, D. Dandy, and C. S. Henry, "Competitive Immunoassays for Simultaneous Detection of Metabolites and Proteins Using Micromosaic Patterning," vol. 80, no. 2, pp. 444–450, 2008.

[130] S. Wang, L. Ge, X. Song, J. Yu, S. Ge, J. Huang, and F. Zeng, "Paper-based chemiluminescence ELISA: lab-on-paper based on chitosan modified paper device and wax-screen-printing.," *Biosens. Bioelectron.*, vol. 31, no. 1, pp. 212–8, 2012.

[131] L. Ge, J. Yan, X. Song, M. Yan, S. Ge, and J. Yu, "Three-dimensional paper-based electrochemiluminescence immunodevice for multiplexed measurement of biomarkers and point-of-care testing.," *Biomaterials*, vol. 33, no. 4, pp. 1024–31, Feb. 2012.

[132] H. Kong, D. Liu, S. Zhang, and X. Zhang, "Protein sensing and cell discrimination using a sensor array based on nanomaterial-assisted chemiluminescence," *Anal. Chem.*, vol. 83, no. 6, pp. 1867–1870, 2011.

[133] Y. Lu, W. Shi, J. Qin, and B. Lin, "Low cost, portable detection of gold nanoparticle-labeled microfluidic immunoassay with camera cell phone.," *Electrophoresis*, vol. 30, no. 4, pp. 579–82, Feb. 2009.

[134] H. Schroeder, M. Adler, K. Gerigk, B. Mu, and F. Go, "User Configurable Microfluidic Device for Multiplexed Immunoassays Based on DNA-Directed Assembly," vol. 81, no. 3, pp. 1275–1279, 2009.

[135] F. Zhou, M. Lu, W. Wang, Z.-P. Bian, J.-R. Zhang, and J.-J. Zhu, "Electrochemical immunosensor for simultaneous detection of dual cardiac markers based on a poly(dimethylsiloxane)-gold nanoparticles composite microfluidic chip: a proof of principle.," *Clin. Chem.*, vol. 56, no. 11, pp. 1701–7, 2010.

[136] V. Romanov, S. N. Davidoff, A. R. Miles, D. W. Grainger, B. K. Gale, and B. D. Brooks, "A critical comparison of protein microarray fabrication technologies," *Analyst*, vol. 139, no. 6, p. 1303, 2014.

[137] T. Endo, K. Kerman, N. Nagatani, H. M. Hiepa, D. Kim, Y. Yonezawa, K. Nakano, and E. Tamiya, “Multiple Label-Free Detection of Antigen - Antibody Reaction Using Localized Surface Plasmon Resonance-Based Core - Shell Structured Nanoparticle Layer Nanochip,” vol. 78, no. 18, pp. 6465–6475, 2006.

[138] H. Huang, C. He, Y. Zeng, X. Xia, X. Yu, P. Yi, and Z. Chen, “A novel label-free multi-throughput optical biosensor based on localized surface plasmon resonance.,” *Biosens. Bioelectron.*, vol. 24, no. 7, pp. 2255–9, 2009.

[139] Z. Wang, S. Zong, W. Li, C. Wang, S. Xu, H. Chen, and Y. Cui, “SERS-fluorescence joint spectral encoding using organic–metal–QD hybrid nanoparticles with a huge encoding capacity for high-throughput biodetection: putting theory into practice,” *J. Am. Chem. Soc.*, vol. 134, no. 6, pp. 2993–3000, 2012.

[140] G. Zheng, F. Patolsky, Y. Cui, W. U. Wang, and C. M. Lieber, “Multiplexed electrical detection of cancer markers with nanowire sensor arrays.,” *Nat. Biotechnol.*, vol. 23, no. 10, pp. 1294–301, 2005.

[141] E. Zampetti, S. Pantalei, A. Macagnano, E. Proietti, C. Di Natale, and A. D’Amico, “Use of a multiplexed oscillator in a miniaturized electronic nose based on a multichannel quartz crystal microbalance,” *Sensors Actuators B Chem.*, vol. 131, no. 1, pp. 159–166, 2008.

[142] M. Yue, J. C. Stachowiak, H. Lin, R. Datar, and R. Cote, “Label-Free Protein Recognition Two-Dimensional Array Using Nanomechanical Sensors,” no. Ccd, pp. 2–6, 2008.

[143] G. Shekhawat, S. Tark, V. P. Dravid, and Q. A. Turchette, “MOSFET-Embedded for in Measuring Deflection Sensors Biomolecular,” vol. 311, no. 5767, pp. 1592–1595, 2014.

[144] J. Villaseñor-Park and A. G. Ortega-Loayza, “Microarray technique, analysis, and applications in dermatology.,” *J. Invest. Dermatol.*, vol. 133, no. 4, p. e7, 2013.

[145] K. W. Bong, S. C. Chapin, and P. S. Doyle, “Magnetic barcoded hydrogel microparticles for multiplexed detection.,” *Langmuir*, vol. 26, no. 11, pp. 8008–14, 2010.

[146] J. Park, V. Sunkara, T. Kim, H. Hwang, and Y. Cho, “Lab-on-a-disc for Fully Integrated Multiplex Immunoassays,” *Anal. Chem.*, vol. 84, pp. 2133–2140, 2012.

[147] Z. Gao, M. Xu, L. Hou, G. Chen, and D. Tang, "Magnetic bead-based reverse colorimetric immunoassay strategy for sensing biomolecules," *Anal. Chem.*, vol. 85, no. 14, pp. 6945–6952, 2013.

[148] J. M. Nam, A. R. Wise, and J. T. Groves, "Colorimetric bio-barcode amplification assay for cytokines," *Anal. Chem.*, vol. 77, no. 21, pp. 6985–6988, 2005.

[149] C. I. Brady, N. H. Mack, L. O. Brown, and S. K. Doorn, "Self-assembly approach to multiplexed surface-enhanced Raman spectral-encoder beads.," *Anal. Chem.*, vol. 81, no. 17, pp. 7181–8, 2009.

[150] X. Su, J. Zhang, L. Sun, T. W. Koo, S. Chan, N. Sundararajan, M. Yamakawa, and A. a. Berlin, "Composite Organic-Inorganic Nanoparticles (COINs) with chemically encoded optical signatures," *Nano Lett.*, vol. 5, no. 1, pp. 49–54, 2005.

[151] M. Han, X. Gao, J. Z. Su, and S. Nie, "Quantum-dot-tagged microbeads for multiplexed optical coding of biomolecules," vol. 19, 2001.

[152] K. Nicolaou and X. Xiao, "Radiofrequency Encoded Combinatorial Chemistry," *Angew. Chem. Int. Ed. Engl.*, vol. 92037, no. 619, pp. 0–2, 1995.

[153] S. I. Stoeva, J. S. Lee, C. S. Thaxton, and C. a. Mirkin, "Multiplexed DNA detection with biobarcoded nanoparticle probes," *Angew. Chemie - Int. Ed.*, vol. 45, no. 20, pp. 3303–3306, 2006.

[154] T. M. McHugh, R. C. Miner, L. H. Logan, and D. P. Stites, "Simultaneous detection of antibodies to cytomegalovirus and herpes simplex virus by using flow cytometry and a microsphere-based fluorescence immunoassay," *J Clin Microbiol*, vol. 26, no. 10, pp. 1957–1961, 1988.

[155] J. J. Scillian, T. M. McHugh, M. P. Busch, M. Tam, M. J. Fulwyler, D. Y. Chien, and G. N. Vyas., "Early detection of antibodies against rDNA-produced HIV proteins with a flow cytometric assay," *Blood*, vol. 73, no. 7, pp. 2041–2048, 1989.

[156] M. Geysen, "Encoding scheme for solid phase chemical libraries," WO Patent 00/61281, 2000.

[157] M. S. Wang and L. Li, "Rapid screening assay methods and devices," U.S. Patent No. 5,922,617. 13 1999.

[158] D. Kozak, W. Anderson, R. Vogel, and M. Trau, “Advances in Resistive Pulse Sensors: Devices bridging the void between molecular and microscopic detection.,” *Nano Today*, vol. 6, no. 5, pp. 531–545, 2011.

[159] T. Osaki, H. Suzuki, B. Le Pioufle, and S. Takeuchi, “Multichannel simultaneous measurements of single-molecule translocation in α-hemolysin nanopore array,” *Anal. Chem.*, vol. 81, no. 24, pp. 9866–9870, 2009.

[160] N. A. W. Bell, V. V Thacker, S. Hernández-Ainsa, M. E. Fuentes-Perez, F. Moreno-Herrero, T. Liedl, and U. F. Keyser, “Multiplexed ionic current sensing with glass nanopores.,” *Lab Chip*, vol. 13, no. 10, pp. 1859–62, 2013.

[161] J. Zhe, A. Jagtiani, P. Dutta, J. Hu, and J. Carletta, “A micromachined high throughput Coulter counter for bioparticle detection and counting,” *J. Micromechanics Microengineering*, vol. 17, no. 2, pp. 304–313, Feb. 2007.

[162] K. R. Balakrishnan, G. Anwar, M. R. Chapman, T. Nguyen, A. Kesavaraju, and L. L. Sohn, “Node-pore sensing: a robust, high-dynamic range method for detecting biological species.,” *Lab Chip*, vol. 13, no. 7, pp. 1302–7, 2013.

[163] A. V Jagtiani, J. Carletta, and J. Zhe, “An impedimetric approach for accurate particle sizing using a microfluidic Coulter counter,” *J. Micromechanics Microengineering*, vol. 21, no. 4, p. 045036, 2011.

[164] E. R. Billinge and M. Platt, “Multiplexed, label-free detection of biomarkers using aptamers and Tunable Resistive Pulse Sensing (AptaTRPS),” *Biosens. Bioelectron.*, vol. 68, pp. 741–748, 2015.

[165] E. R. Billinge, M. Broom, and M. Platt, “Monitoring aptamer-protein interactions using tunable resistive pulse sensing,” *Anal. Chem.*, vol. 86, no. 2, pp. 1030–1037, 2014.

[166] J. H. Jung, D. S. Cheon, F. Liu, K. B. Lee, and T. S. Seo, “A graphene oxide based immuno-biosensor for pathogen detection.,” *Angew. Chem. Int. Ed. Engl.*, vol. 49, no. 33, pp. 5708–11, 2010.

[167] E. Yacoub-George, W. Hell, L. Meixner, F. Wenninger, K. Bock, P. Lindner, H. Wolf, T. Kloth, and K. a Feller, “Automated 10-channel capillary chip immunodetector for biological agents detection,” *Biosens. Bioelectron.*, vol. 22, no. 7, pp. 1368–75, 2007.

[168] J. C. Jokerst, J. a Adkins, B. Bisha, M. M. Mentele, L. D. Goodridge, and C. S. Henry, “a Paper-Based Analytical Device for the Colorimetric Detection of Foodborne Pathogenic Bacteria,” pp. 2116–2118, 2011.

[169] D. Issadore, J. Chung, H. Shao, M. Liong, A. A. Ghazani, C. M. Castro, R. Weissleder, and H. Lee., “Ultrasensitive clinical enumeration of rare cells ex vivo using a micro-hall detector,” *Sci. Transl. Med.*, vol. 4, no. 141, pp. 141ra92–141ra92, 2012.

[170] O. Torun, I. Hakkı Boyacı, E. Temür, and U. Tamer, “Comparison of sensing strategies in SPR biosensor for rapid and sensitive enumeration of bacteria.,” *Biosens. Bioelectron.*, vol. 37, no. 1, pp. 53–60, 2012.

[171] A. Carbonaro, S. K. Mohanty, H. Huang, L. a Godley, and L. L. Sohn, “Cell characterization using a protein-functionalized pore.,” *Lab Chip*, vol. 8, no. 9, pp. 1478–85, 2008.

[172] N. N. Watkins, S. Sridhar, X. Cheng, G. D. Chen, M. Toner, W. Rodriguez, and R. Bashir, “A microfabricated electrical differential counter for the selective enumeration of CD4+ T lymphocytes.,” *Lab Chip*, vol. 11, no. 8, pp. 1437–47, 2011.

[173] Z. Qin, J. Zhe, and G.-X. Wang, “Effects of particle’s off-axis position, shape, orientation and entry position on resistance changes of micro Coulter counting devices,” *Meas. Sci. Technol.*, vol. 22, no. 4, p. 045804, 2011.

[174] K. R. Balakrishnan, J. C. Whang, R. Hwang, J. H. Hack, L. a. Godley, and L. L. Sohn, “Node-Pore Sensing Enables Label-Free Surface-Marker Profiling of Single Cells,” *Anal. Chem.*, p. 150212080100008, 2015.

[175] F. C. Dudak and I. H. Boyaci, “Rapid and label-free bacteria detection by surface plasmon resonance (SPR) biosensors,” *Biotechnol. J.*, vol. 4, no. 7, pp. 1003–1011, 2009.

[176] J. G. Kralj, C. Arya, A. Tona, T. P. Forbes, M. S. Munson, L. Sorbara, S. Srivastava, and S. P. Forry, “A simple packed bed device for antibody labelled rare cell capture from whole blood,” *Lab Chip*, vol. 12, no. 23, p. 4972, 2012.

[177] J. Riordon, M. Nash, M. Calderini, and M. Godin, “Microelectronic Engineering Using active microfluidic flow focusing to sort particles and cells based on high-

resolution volume measurements," *Microelectron. Eng.*, vol. 118, pp. 35–40, 2014.

[178] J. D. Uram, K. Ke, A. J. Hunt, and M. Mayer, "Label-free affinity assays by rapid detection of immune complexes in submicrometer pores.," *Angew. Chem. Int. Ed.*, vol. 45, no. 14, pp. 2281–5, 2006.

[179] J. Zhe, A. Jagtiani, P. Dutta, J. Hu, and J. Carletta, "A micromachined high throughput Coulter counter for bioparticle detection and counting," *J. Micromechanics Microengineering*, vol. 17, no. 2, pp. 304–313, 2007.

[180] H. Song, Y. Wang, J. M. Rosano, B. Prabhakarpandian, C. Garson, K. Pant, and E. Lai, "A microfluidic impedance flow cytometer for identification of differentiation state of stem cells.," *Lab Chip*, vol. 13, no. 12, pp. 2300–10, 2013.

[181] T. Sun and H. Morgan, "Single-cell microfluidic impedance cytometry: a review," *Microfluid. Nanofluidics*, vol. 8, no. 4, pp. 423–443, 2010.

[182] D. Holmes and H. Morgan, "Single cell impedance cytometry for identification and counting of CD4 T-cells in human blood using impedance labels.," *Anal. Chem.*, vol. 82, no. 4, pp. 1455–61, 2010.

[183] M. Javanmard, A. H. Talasaz, M. Nemat-Gorgani, D. E. Huber, F. Pease, M. Ronaghi, and R. W. Davis, "A microfluidic platform for characterization of proteinprotein interactions," *IEEE Sens. J.*, vol. 9, no. 8, pp. 883–891, 2009.

[184] Y. Zheng, J. Chen, T. Cui, N. Shehata, C. Wang, and Y. Sun, "Characterization of red blood cell deformability change during blood storage.," *Lab Chip*, vol. 14, no. 3, pp. 577–83, 2014.

[185] J. Chen, Y. Zheng, Q. Tan, E. Shojaei-Baghini, Y. L. Zhang, J. Li, P. Prasad, L. You, X. Y. Wu, and Y. Sun, "Classification of cell types using a microfluidic device for mechanical and electrical measurement on single cells.," *Lab Chip*, vol. 11, no. 18, pp. 3174–81, 2011.

[186] Y. Zheng, E. Shojaei-Baghini, A. Azad, C. Wang, and Y. Sun, "High-throughput biophysical measurement of human red blood cells.," *Lab Chip*, vol. 12, no. 14, pp. 2560–7, 2012.

[187] Y. Wu, J. D. Benson, J. K. Critser, and M. Almasri, "MEMS-based Coulter

counter for cell counting and sizing using multiple electrodes," *J. Micromechanics Microengineering*, vol. 20, no. 8, p. 085035, 2010.

[188] A. M. Dondorp, B. J. Angus, K. Chotivanich, K. Silamut, R. Ruangveerayuth, M. R. Hardeman, P. a Kager, J. Vreeken, and N. J. White, "Red blood cell deformability as a predictor of anemia in severe falciparum malaria," *Am. J. Trop. Med. Hyg.*, vol. 60, no. 5, pp. 733–7, 1999.

[189] Y. Zheng, J. Nguyen, C. Wang, and Y. Sun, "Electrical measurement of red blood cell deformability on a microfluidic device.," *Lab Chip*, vol. 13, no. 16, pp. 3275–83, 2013.

[190] P. K. Ang, A. Li, M. Jaiswal, Y. Wang, H. W. Hou, J. T. L. Thong, C. T. Lim, and K. P. Loh, "Flow sensing of single cell by graphene transistor in a microfluidic channel.," *Nano Lett.*, vol. 11, no. 12, pp. 5240–6, 2011.

[191] A. V Jagtiani, J. Carletta, and J. Zhe, "A microfluidic multichannel resistive pulse sensor using frequency division multiplexing for high throughput counting of micro particles," *J. Micromechanics Microengineering*, vol. 21, no. 6, p. 065004, 2011.

[192] O. A. Saleh and L. L. Sohn, "An Artificial Nanopore for Molecular Sensing," *Nano Lett.*, vol. 3, no. 1, pp. 10–11, 2003.

[193] X. Yang and D. Chasteen, "Ferroxidase activity of ferritin: effects of pH, buffer and Fe (II) and Fe (III) concentrations on Fe (II) autoxidation and ferroxidation," *Biochem. J.*, vol. 338, pp. 615–618, 1999.

[194] D. Botstein, S. a Chervitz, and J. M. Cherry, "Yeast as a model organism.," *Science*, vol. 277, no. 5330, pp. 1259–1260, 1997.

[195] M. J. McCullough, B. C. Ross, and P. C. Reade, "Candida albicans: a review of its history, taxonomy, epidemiology, virulence attributes, and methods of strain differentiation.," *Int. J. Oral Maxillofac. Surg.*, vol. 25, no. 2, pp. 136–144, 1996.

[196] J. N. Aucott, J. Fayen, H. Grossnicklas, a Morrissey, M. M. Lederman, and R. a Salata, "Invasive infection with Saccharomyces cerevisiae: report of three cases and review.," *Rev. Infect. Dis.*, vol. 12, no. 3, pp. 406–411, 2015.

[197] P. Muñoz, E. Bouza, M. Cuenca-Estrella, J. M. Eiros, M. J. Pérez, M. Sánchez-Somolinos, C. Rincón, J. Hortal, and T. Peláez, "Saccharomyces cerevisiae fungemia: an emerging infectious disease.," *Clin. Infect. Dis.*, vol. 40, no. 11, pp. 1625–1634, 2005.

[198] X. Cheng, D. Irimia, M. Dixon, K. Sekine, U. Demirci, L. Zamir, R. G. Tompkins, W. Rodriguez, and M. Toner, "A microfluidic device for practical label-free CD4(+) T cell counting of HIV-infected subjects.," *Lab Chip*, vol. 7, no. 2, pp. 170–8, 2007.

[199] S. Usami, H. H. Chen, Y. H. Zhao, S. Chien, and R. Skalak, "Design and Construction of a Linear Shear-Stress Flow Chamber," *Ann. Biomed. Eng.*, vol. 21, no. 1, pp. 77–83, 1993.

[200] F. Momen-Heravi, L. Balaj, S. Alian, A. J. Trachtenberg, F. H. Hochberg, J. Skog, and W. P. Kuo, "Impact of biofluid viscosity on size and sedimentation efficiency of the isolated microvesicles," *Front. Physiol.*, vol. 3, pp. 1–6, 2012.

[201] B. Cao, L. Li, H. Wu, Q. Tang, B. Sun, H. Dong, J. Zhe, and G. Cheng, "Zwitteration of dextran: a facile route to integrate antifouling, switchability and optical transparency into natural polymers.," *Chem. Commun. (Camb).*, vol. 50, no. 24, pp. 3234–7, 2014.

[202] J. Zhang, W. Sheng, and Z. H. Fan, "An ensemble of aptamers and antibodies for multivalent capture of cancer cells.," *Chem. Commun. (Camb).*, vol. 50, no. 51, pp. 6722–5, 2014.

[203] A. Foddai, C. T. Elliott, and I. R. Grant, "Maximizing capture efficiency and specificity of magnetic separation for mycobacterium avium subsp. paratuberculosis cells," *Appl. Environ. Microbiol.*, vol. 76, no. 22, pp. 7550–7558, 2010.

[204] J. M. Taylor, J. L. Fahey, R. Detels, and J. V. Giorgi, "CD4 percentage, CD4 number, and CD4: CD8 ratio in HIV infection: which to choose and how to use," *AIDS J. Acquir. Immune Defic. Syndr. 2*, vol. 2, no. 2, pp. 114–124, 1989.